Mud Column Characteristics and Conditions

APPENDIX 4

MUD COLUMN CHARACTERISTICS AND CONDITIONS

TABLE OF CONTENTS

LIST OF FIGURES

1.0 EFFICACY OF MUD PLUGS IN ABANDONED WELLS

1.1 SUMMARY

Common drilling mud is largely composed of clays and water, forming a colloidal base. Typically, bentonite (sodium montmorillonite) is added to the drilling mud as the clay and is used to obtain viscosity in the slurry and promoting the formation of wall cake (the low-permeability layer of clay lining the borehole). Bentonite is hydrophilic (it readily absorbs water), and its flat platy shape is the primary reason it is desired for use in common drilling fluids. The development of gel strength in a drilling mud is due to the tendency of the clay platelets to align in a configuration where positively charged edges are adjacent to negatively charged surfaces, resulting in a medium with thixotropic properties. Thixotropy is the characteristic whereby certain gels evolve to a semi-solid state when allowed to stand undisturbed but liquefy upon shock disturbance. The gel phase is desirable because it assists in suspending cuttings released by the drilling procedure, producing the required viscosity and mud cake properties in the circulating mud system.

The physical characteristics that make clay-based drilling mud useful during active drilling operations also make it an effective barrier to vertical fluid movement within abandoned boreholes. In thixotropic behavior, under static conditions the clay platelets aggregate (flocculate) in three ways: 1) face-to-face, 2) edge-to-edge, or 3) edge-to-face, because the platelets are electrically charged. This thixotropic or gelling property of a clay-based bentonite slurry is what gives drilling mud its gel strength. In clay-based mud systems, gel structures build with time (progressive gel) as the positive edge of one particle or plate moves toward the negative surface of another; that is, when the platelets are layered (Gray et al., 1980). Laboratory studies have shown that although the exact relationship between gel strength and time varies, depending on specific mud composition and additives, the gel strength always increases with time. Additionally, this orientation of the clay plates reduces the vertical permeability of the mud column significantly because tortuosity through the mud is increased.

Clay-based drilling fluids that contain bentonite or natural clays provide adequate long-term protection against vertical fluid movement into and within in abandoned wellbores. Field studies of mud conditions in decades old abandoned wellbores confirm expectations gained from laboratory testing data and can be used to predict the long-term behavior of relevant mud properties.

1.2 INTRODUCTION

Whenever effluent is injected into a subsurface geologic formation, the pressure within the injection interval will increase. This pressure increase will be greatest at the injection well(s) and will decrease with distance away from the injection site. Because of the driving force supplied by the increase in formation pressure within the injection intervals, artificial penetrations within the radius of the effluent plume have the potential to convey effluent out of the injection zone, and artificial penetrations within the Area of Review have the potential to convey formation brines into an Underground Source of Drinking Water (USDW). This is especially so in the specific case where a well is abandoned with brine in the open spaces of the wellbore and/or annulus. However, in rotary drilled wells this is exceedingly rare and only occurs where a formerly productive well is "walked away" from without abandonment.

In a rotary drilled well, the driving force due to injection is opposed by the flow resistance of the material (drilling mud and /or drilling mud and cement plugs) residing in the borehole or the borehole by casing annulus. In order to pose a potential threat to a USDW (*i.e.*, pressure buildup from injection sufficient to drive fluids into a USDW), the pressure increase in the injection interval must be greater than the pressure necessary to displace the material residing within the open spaces in the borehole. This pressure necessary to displace the material residing within the borehole is defined as the allowable buildup pressure.

A mud column exerts pressure. For a well to provide a pathway for fluid movement, the pressures acting on the mud column (pressure due to injection plus original formation pressure) must be greater than the mud column pressure (Davis, 1986). Exploration and production wells are commonly drilled at a mud weight that provides 200 psi or more overbalance to the formations encountered during the drilling activity (Pearce, 1989). In a static fluid column of drilling mud, such as exists upon abandonment of the well, the gel strength of the mud must also be considered. Gel strength refers to the shear stress required to initiate flow after static periods of time (*i.e.*, without mud circulation) and is a measure of the degree of gelation that occurs due to the attractive forces between particles in the mud over time. The gel strength adds to the flow resistance in the well and fluid movement cannot begin until the pressure in the injection interval has increased beyond this critical threshold value necessary to overcome the flow resistance of the borehole material (weight and gel strength).

As long as the pressure buildup in the injection interval is less than the threshold value, the artificial penetration cannot serve as a conduit for either effluent or formation brines (Davis, 1986; Collins

1986). Therefore, as long as the threshold value is not exceeded, the artificial penetration is safe, and corrective action tore-enter and plug the well is not necessary.

1.3 PROPERTIES OF CLAY-BASED DRILLING MUD

The physical characteristics which make drilling muds useful during drilling also make them effective barriers against formation fluid entry into a wellbore and mud-column displacement into a wellbore. This is particularly true of a commonly used base for mud, bentonite, which is predominantly sodium montmorillonite clay. Bentonite-based mud types are used the Cheney Ranch field wells. The platy electrically charged clay particles comprising bentonite strongly attract water, a polar molecule. This causes the clay to swell, thereby increasing the borehole fluid viscosity (Davis, 1986). Of the clays, montmorillonite has the greatest hydration potential and effects the greatest viscosity enhancement for a given amount of solids. This accounts for its long-standing popularity of bentonite as an additive.

A second important property, the gel strength of clay-based drilling muds comes from the tendency of the plate-like clay particles to align so that positively charged edges are adjacent to negatively charged flat surfaces. The gel is "a disheveled yet interconnected network of parallel clay particles separated by an average distance" (Jahnke, 1987). If the mud is agitated, then the gel breaks down. If, on the other hand, the mud sits at rest, then gel strength increases with time as the additional clay particles come into alignment. This is documented by studies conducted by both Garrison (1939) and Gray, et al. (1980). If the drilling fluid is at rest for a long time, high pump pressures are sometimes necessary to restore circulation in the borehole (see example from Cheney Ranch field below). This strong resistive force in a mud column would also need to be overcome during injection.

For many years, alternating cement and mud plugs have been advocated for properly abandoning well bores because they provide an effective barrier to vertical fluid flow. The “balanced method” is the most common method used for the placement of cement plugs during well abandonment procedures. Mud plugs have been shown to have a very low permeability and provide great resistance to fluid movement. In addition, mud plugs have been shown to plug an artificial penetration through time and under the various conditions encountered within a wellbore. A mud plug, with its inherent low permeability, in combination with the hydrostatic head of an overbalanced mud column, is sufficient to counterbalance increased formation pressure due to injection effects, thereby creating an effective barrier to fluid flow. These sealing and fluid barrier characteristics of mud plugs, combined with hydrostatic pressures and natural borehole closure processes, minimize the chance of encountering a truly open conduit in an artificial penetration that was drilled in unconsolidated sediments.

Drilling mud is largely composed of clays and water. Commonly, bentonite-type clays (sodium

montmorillonite) is added to the drilling mud to obtain viscosity in the slurry, in addition to promoting the formation of wall cake (the low-permeability layer of clay lining the borehole). Bentonite is hydrophilic (it readily absorbs water), and its flat platy shape is the primary reason it is desired for use in drilling mud fluids. Clay platelets aggregate (flocculate) in three ways:

1) face-to-face,

2) edge-to-edge, or

3) edge-to-face

Because the platelets are electrically charged. This thixotropic or gelling property of a bentonite slurry is what gives drilling mud its gel strength, as discussed below. Gel structures build with time as the positive edge of one particle or plate moves toward the negative surface of another; that is, when the platelets are layered (Gray et al., 1980). This orientation reduces the vertical permeability of the mud column significantly because tortuosity is increased.

The gel strength and wall cake of bentonite clay mud systems provide an effective barrier against both vertical fluid migration within the wellbore, and migration of fluids into overlying formations. The following subsections examine various aspects of mud plugs and their ability to effectively prevent migration of fluids.

The permeability of drilling mud in abandoned wells depends on the amount and size of the clay particles and other colloids available in the mud slurry, as well as the time the mud has been left in the hole. Although the permeability of mud in deep boreholes has not been measured directly, the permeability of other similar clay mixtures, such as those used in slurry wall construction and bentonite grout slurry mixtures used to plug shallow borings, has been measured and quantified. Alther (1982), while investigating the use of bentonite for clay caps and slurry wall containment, found that a mixture of bentonite and high-permeability soils reduced the coefficient of permeability to 10^{-9} cm/sec. Alther (1982) used a falling head permeameter to measure the permeability of a mixture of 8 percent bentonite and 92 percent Lake Michigan sand.

Polk and Gray (1984) investigated the adequacy of mud as a sealing agent in abandoned boreholes related to mineral exploration. Their focus was on the ability of a bentonite mud to form a filter cake with a low enough permeability to ensure that there would not be fluid flow between aquifers penetrated during drilling. Polk and Gray (1984) directly measured filter cake permeabilities using the cake formed in a standard American Petroleum Institute (API) filter press filtration test run for 30 minutes at a differential pressure of 100 psi. The cake that formed on the filter paper was then

tested with water to determine the cake's permeability. The cake had measured permeabilities ranging from 2 x 10^{-8} to 8 x 10^{-9} cm/sec, which are regarded as low enough permeability values to prevent fluid flow from one aquifer to another through an open borehole. The filter cake essentially keeps all the solid particles within the mud column. The formation of these low permeability filter cakes is one of the most desirable properties of clay-based mud systems. Experiments show the filter cake to have permeability below microdarcy values (Kelessidis, et al, 2007; Elkatatny et al., 2012). This mud filter cake acts as a membrane "skin" or barrier that effectively seal off formations and prevent fluid loss from the mud column to the formation or loss of fluid from the formation when the well was drilled.

Because the EPA defines "low permeability" for soil as 1 x 10^{-7} cm/sec, the minimum required permeability of the three feet of compacted clay beneath a landfill or surface impoundment, then it is reasonable to believe that the permeability of a column or mud plug (1x10^{-7} cm/sec or less) is more than sufficient to prevent movement of fluids within an "open" unplugged well bore.

1.3.1 Long-term Properties of Drilling Mud

The functions of the drilling mud result from its physical properties. The primary functions of drilling mud are to prevent the inflow of formation fluids and prevent the collapse of formation materials into the wellbore. These are primarily accomplished by altering the mud weight during drilling. Mud weight can be increased by increasing the salinity of the mud or adding insoluble solids, typically barite ($BaSO_4$). In general, mud weight is increased with depth so that the mud column will overbalance the encountered formation pressures by 200 to 400 psi (Pierce, 1989). The physical characteristics that make the mud useful during drilling also make it an effective barrier to vertical fluid movement over the long-term.

1.3.1.1 Static Mud Column Height

In general, the top of the mud column is found at, or very near, ground level for re-entered boreholes. Documentation offered from several field examples are:

- In the Nora Schulze wellbore, located in Nueces County, Texas, was reentered by K. E. Davis Associates during 1988. The top of the mud plug was encountered immediately below the cement plug at the top of the wellbore (top cement plug), with no fallback in the mud column.

- Subsurface, Inc. (1976) reentered and replugged the Brewster Bartle Drilling Company (British American Oil Production Company), University of Texas No. 1B well located in Galveston County, Texas, during 1976, at the request of Amoco and Monsanto. During the re-entry operation, drilling mud was found immediately below the surface cement plug with its properties relatively intact. This confirms that mud properties maintain their plugging capabilities and offer major resistance as fluid barriers.

- AIC (1988), in a study of well reentries originally plugged 20 to 30 years prior, found that in the Texas Gulf Coast and West Texas, most operators reported finding the top of the mud just below the surface plug.

- Mr. John Luttig, PE, stated in a letter that he has never encountered voids in e a wellbore devoid of mud in any well reentry in his more than 30 years in the oil fields of East Texas (Luttig, 1990: Pers.Com.). This includes wells that had been plugged for more than 50 years following plugging. He also indicated that he confirmed this statement with his contemporaries.

It is not possible to force significant quantities of mud out of the borehole and out into a permeable formation because of the effect of nearly impermeable residual mud cake that forms along the formation wall.

1.3.1.2 Mud Column Properties

The long-term properties of mud can be determined from a theoretical standpoint. Mud weight should not vary significantly from that at abandonment because virtually all the weighting (barite) particles will remain in suspension due to mud gel strength, which quickly develops. Pearce (1989) found that gravitational settling of barite or other mud additives has been overestimated. Even though settling of the largest drill cuttings particles may occur, overall, this effect does not diminish mud density, or more importantly, affect the plugging and sealing characteristics of a column of mud in an abandoned borehole. The higher the gel strength of a mud column, the larger the particle that can remain in indefinite suspension. This is completely analogous to a solid mechanics problem where a sphere is suspended in an elastic solid. Only when the maximum shear stress on the surface of the particle exceeds the gel strength of the mud will the particle have the potential to settle out of the mud column. For mud-based barite weighting particles, with a density of 4.2 gm/cm^3, the critical diameter (in centimeters) for settling is approximately equal to

the gel strength of the mud (lb./100 ft^2) divided by 100. For a reasonable low-end gel strength of 20 lb./100 ft^2 (typically required at 30 minutes measurement time) all barite particles smaller than 0.2 cm will remain in indefinite suspension. In a typical weighted drilling mud, barite particles are generally an order of magnitude less than 0.2 cm in diameter (NL Baroid, 1988). The maximum diameter of the largest 3 percent of the barite particles in standard API weighted mud systems can be no greater than 0.00635 cm (Gray et al., 1980), or 31 times smaller than the theoretical settling size. A gel strength of only 6 lb./100 ft^2 is needed to suspend 97 percent of the barite in the mud column and the larger drilled solids in the well (Pearce, 1989). Even if these larger drilled solids settle out of the mud, this will not readily affect the weight of the mud as these larger drilled particles are routinely screened out of the mud at surface during active drilling and circulation of the mud system (Pearce, 1989).

Since the solids remain in the mud column, the only way to relieve formation stresses imposed on the static mud column is by compaction and the consequent movement of water from the mud out into the formation. However, this process is self-limiting, any water movement from the mud column will increase the average density of the mud due to the loss of low density water, increase the gel strength and the solids are brought closer together and decrease the effective permeability of the mud column (Pearce, 1989).

1.3.1.3 Mud Column Gel Strength

The relationship between gel strength and time varies with the mud type, depending on such variables as composition, pH, temperature, pressure, solids, and degree of flocculation (Figure 1). Srini-Vasan (1957) investigated the affect of temperature (up to 220 ^{o}F) on water-based muds with drilling weights like the wells in the Cheney Ranch Field. Annis (1967) showed that the gelling process is depends on both time and temperature, with 18 parts per billion (ppb) bentonite solution at any temperature having a gel strength six times that of the initial gel strength of the mud. Vryzas et al. (2016) found that the gel-like structure of water/bentonite suspensions proved to be rheologically stable after an aging period of 30 and 60 days.

As shown in Davis and Pearce (1989), Chevron conducted laboratory experiments to determine the expected condition of mud left in wellbores. Chevron formulated muds like those used in Mississippi and “aged” the mud samples at temperature and pressure for a two-week period. The testing showed that the muds developed significant compressive strength and was described as a “plug”, with a gel strength too high to measure with standard equipment (Davis and Pearce, 1989).

Field evidence of the longevity of mud as a plugging material has been demonstrated during well reentries. The Nora Schulze No. 2, located in Nueces County, Texas, was reentered by Envirocorp in the late 1980's. The well was plugged with 10.6 to 11.0 lb./gal mud when abandoned in 1959 (Pearce, 1989). Mud samples were taken upon reentry to a depth of approximately 754 feet using tubing pushed into the mud column from a depth of 120 feet. Below a depth of 754 feet, the mud could only be displaced from the well by breaking circulation (Pearce, 1989). Results of measured mud characteristics are presented in Figure 2. The average mud weight of the recovered samples was 11.1 lb./gal, showing that the mud did not appreciably change over the intervening 29 years following abandonment. The gel strengths of the samples ranged between 217 lb./100 ft^2 to greater than 320 lb./100 ft^2. These values are over an order of magnitude greater than the 20 lb./100 ft^2 value required in California plugging rules and commonly used for modeling purposes (Pearce, 1989). In addition, shear strengths of the mud samples ranged from 170 lb./100 ft^2 to 7,000 lb./100 ft^2, increasing with depth (Pearce, 1989).

Additional information on mud characteristics from well reentries are:

- Subsurface, Inc. (1976) reentered and replugged the Brewster Bartle Drilling Company (British American Oil Production Company), University of Texas No. 1B well located in Galveston County, Texas, during 1976, at the request of Amoco and Monsanto. Cement plugs were placed from 11,000 to 11,200 feet, and from 130 to 180 feet, and near the surface (top cement plug) with mud-laden fluid filling the remainder of the wellbore (conforming to Texas Railroad Commission plugging and abandonment requirements of 1961). During the re-entry operation, drilling mud was found immediately below the surface cement plug with its properties relatively intact. The mud had to be circulated out using 12-lb/gal mud.

- AIC (1988), in a study of well reentries originally plugged 20 to 30 years prior, found that in the Texas Gulf Coast, most operators reported that the mud was generally hard, with the following comments reflecting the condition of the drilling mud and/or borehole fluids encountered in the Gulf Coast:

    - mud set up like cement;
    - mud set up firm after about five years; and
    - mud encountered is hard and firm

1.4 CONCLUSIONS

The long-term properties of clay-based drilling mud can be determined from a theoretical standpoint. Mud weight is not expected to vary significantly from that at abandonment (start of static conditions) because virtually all of the weighting barite particles (97%) will remain in indefinite suspension due to gel strength of the mud. Gel strength in clay-based muds generally increases with time due to the electrical attraction of the clay platelets in the mud to continually align.

Field investigations from well reentries have found that measured mud properties support the expectations associated with extrapolating laboratory studies over an extended period of time. In the reentry of the Nora Schulte wellbore, mud density remained essentially unaltered, gel strength exceeded 100 lbs./l00 ft^2, and, even for the most highly gelled samples, the mud remained a fluid. All evidence gathered to date indicates clay, water-based drilling fluids provide adequate protection against vertical fluid migration over short and long time periods.

REFERENCES

Agency Information Consultants, Inc., 1988, Mud conditions of re-entered wells: Prepared for E. I. du Pont de Nemours.

Akpan, E. U., 2019, Water-Based Drilling Fluids for High Temperature and Dispersible Shale Formation Applications: Ph.D. Thesis, Petroleum and gas Engineering Division, School of Computing, Science and Engineering, University of Salford, United Kingdom

Ali, M. S. and Al-Marhoun, M. A., 1990, The Effect Of High Temp., High pressure and aging on water-base drilling fluids: Society of Petroleum Engineers, 21613-MS SPE.

Alther, G. R., 1982, The role of bentonite in soil sealing applications: Association of Engineering Geologists Bulletin, v. 19, no. 4, p. 401-409.

Annis, M. R., 1967, High temperature properties of water-based drilling fluids: Journal of Petroleum Technology, n. 19, pp. 1074-1080.

Collins, R. E., 1986, Technical basis for area of review, an engineering study prepared for Chemical Manufacturers Association: Chemical Manufacturers Association Reference Number 80-160-000-4.

Collins, R. E. and Kortum, D., 1989, Drilling mud as a hydraulic seal in abandoned wellbores: Underground Injection Practices Council, 1989 Winter Meeting, San Antonio, Texas.

Davis, K. E., 1986, Factors effecting the area of review for hazardous waste disposal wells: Proceedings of the International Symposium on Subsurface Injection of Liquid Wastes, New Orleans, National Water Well Association, Dublin, Ohio, p. 148-194.

Davis, K. E., and Pearce, M.S., 1989, Draft Report-A Review of Literature and Laboratory Data Concerning Mud Filled Holes: prepared for Chemical Manufacturing Association, Washington DC, Envirocorp Project No. 10-1302.

Elkatatny, S., Mahmound, M. A., Nase-El_Din, H. A., 2012, Characteristics of filter cake generated by water-based drilling fluids using CT scan; SPE Drilling and Completion, SPE-144098-PA, v. 27, n. 2.

Garrison, A. D., 1939, Surface chemistry of shales and clays: Transaction American Institute of Mechanical Engineers, v. 132, pp. 423-436.

Gray, G. D., Darley, H. C., and Rodgers, W. F., 1980, Composition and Properties of Oil Well Drilling mud fluids: Gulf Publishing Company, Houston, Texas.

IADC, 2014, IADC Drilling Manual.

Jahnke, F. M., 1987, Diffusion of ion-exchanging electrolytes in montmorillonite gels: Ph. D. Dissertation, University of California, Berkeley.

Kelessidis, V. C., Tsamantake, C., Pasadakis, N., Repouskou, E, and Hamilaki, E., 2007, Permeability, porosity and surface characteristics of filter cakes from water-bentonite suspensions: Fourth International Conference on Computational Methods in Multiphase Flow, Multiphase Flow IV, WIT Transactions on Engineering Sciences, v. 56, p. 173 – 182.

Luttig, J., 1990, Wellbore Communication in Abandoned Oil and Gas Wells, Harrison County, Texas (personal communication).

NL Baroid, 1988, Particle size distribution curve for standard API calibration barite sample: Letter to DuPont.

Ochoa, M. V., 2006, Analysis of drilling fluid rheology and tool joint effect to reduce errors in hydraulics calculations: Ph.D. Dissertation, Texas A&M University.

Pearce, M. S., 1989, Long-term properties of clay, water-based drilling mud fluids: Proceedings of the International Symposium on Class I & II Injection Well Technology, Dallas, Texas, Underground Injection Practices Council Research Foundation, p. 115-132.

Polk, G. and Gray, G. R., 1984, Plugging mineral exploration holes with a drilling fluid conditioner, *in* Proceedings of the First National Conference on Abandoned Wells: Problems and Solutions, May 20-21, 1984, p. 295-300.

Subsurface, Inc., 1976, Plugging and abandonment of British-American, University of Texas B-1, Prepared for Amoco/Monsanto.

Srini-Vasan, S., 1957, A study of temperature on flow properties of non-Newtonian drilling fluids: MS Thesis University of Tulsa.

Tehrani, A., 2008, Thixotropy in water-based drilling fluids: Annual Transactions of the Nordic Rheology Society, vol. 16.

Vryzas, Z., Wubulikasimu1, Y., Gerogiorgis, D., and Kelessidis, V. C., 2016, Understanding the temperature effect on the rheology of water-bentonite suspensions: Annual Transactions of the Nordic Rheology Society, vol. 24, pp. 199-208.

Weintritt, D. J., and Hughes, R. G., 1965, Factors involved in high temperature drilling mud fluids: Journal of Petroleum Technology, Transaction American Institute of Mechanical Engineers, v. 234, pp. 707-716.

FIGURES

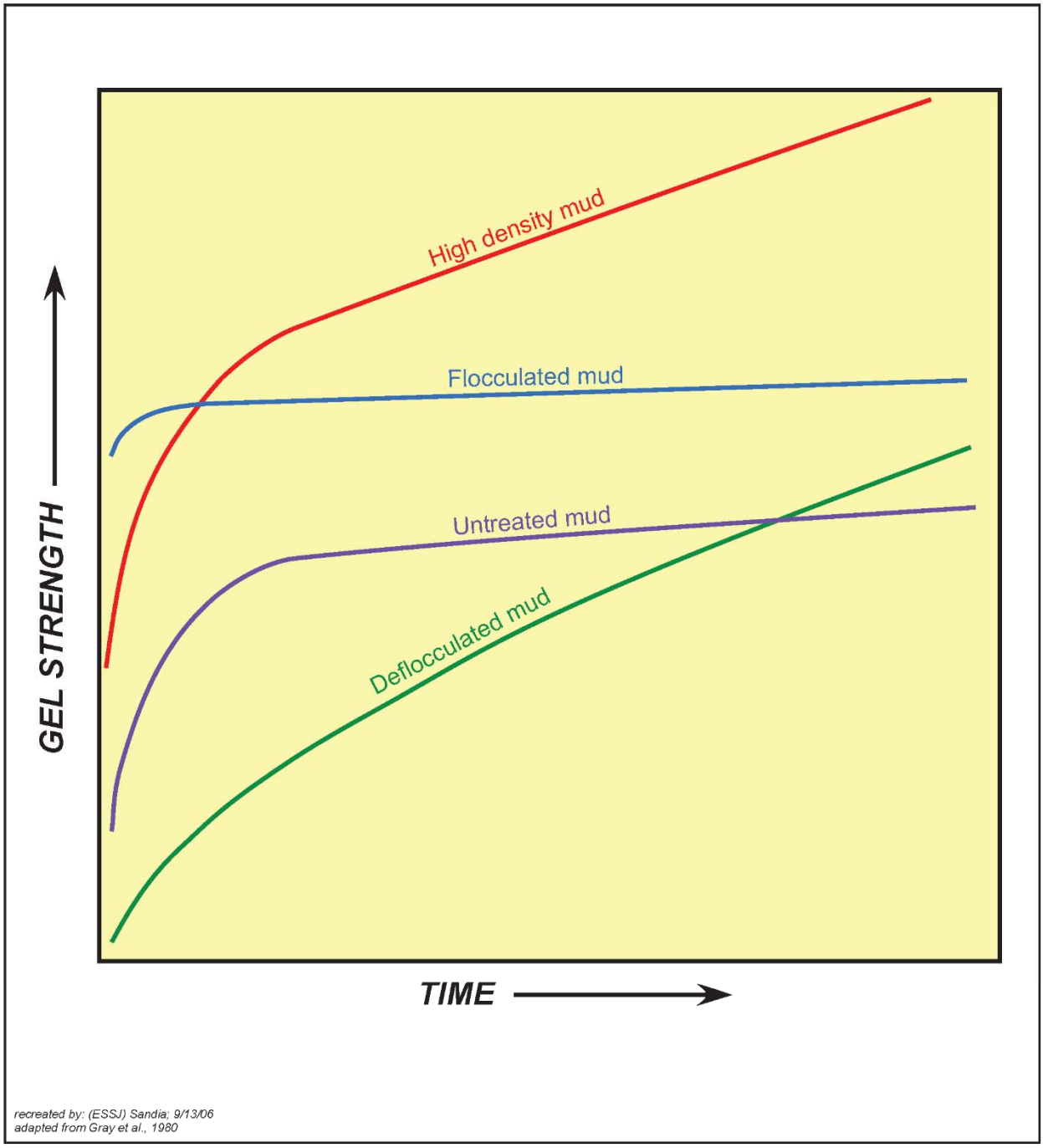

Figure 1 Gel Strength Increase Through Time (Adapted from: Gray et al., 1980)

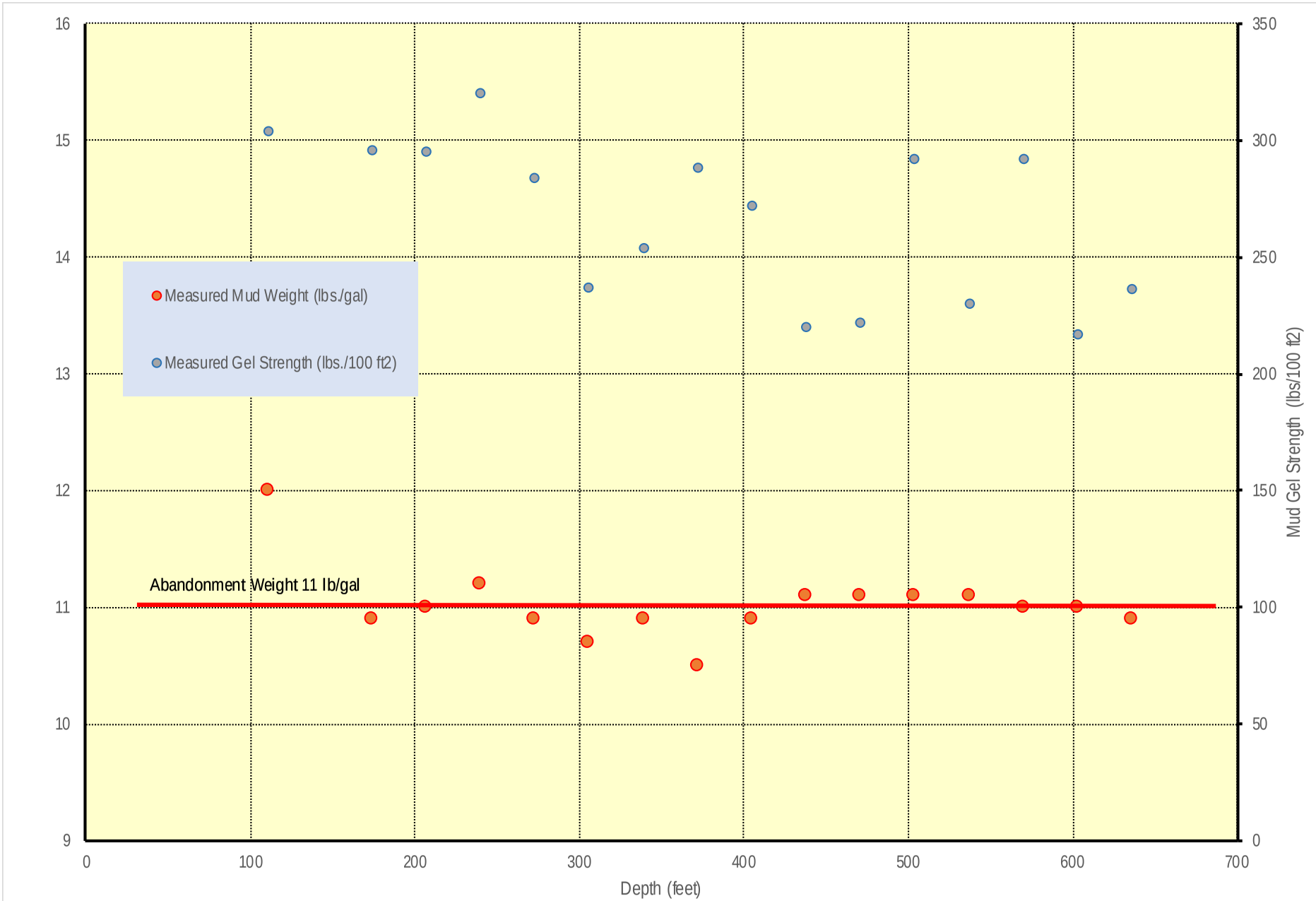

Figure 2 Measured Mud Properties in the Nora Schultze No. 1 well upon reentry in 1988

Drilling Mud as a Hydraulic Seal in Abandoned Wellbores

DRILLING MUD AS A HYDRAULIC SEAL IN ABANDONED WELLBORES

R. E. Collins and D. Kortum
Research & Engineering Consultants, Inc., Englewood, Colorado 80111

Abstract

Results of a series of laboratory experiments are presented which exhibit the contribution of mud gel strength to the hydraulic sealing characteristics of mud filling an abandoned well. The apparatus consisted of a small scale, simulated wellbore fitted with a sandstone core plug at the lower end. Mud filling this wellbore was allowed to gel for a fixed time, then the brine pressure required for initiation of brine entry through the brine saturated core plug was measured. These data, together with measured properties of the mud, and geometry of the simulated wellbore constituted the experimental data.

These data indicate that in most circumstances the gel character of the mud contributes as much to the minimum fluid entry pressure as does the hydrostatic head of the mud. In fact, in many cases the gel might contribute more to sealing pressure than hydrostatic head by a factor of three or more. Furthermore it has been found that non-uniformities in hole diameter appear to cause an even greater contribution of mud gel to hole sealing by mud.

This study lends support to the viewpoint that abandoned wells pose very little threat as a path for contamination of any USDW in deep well injection operations if these wells are filled with gelled mud. However, these experiments are not truly scaled and it is proposed that properly scaled experiments are needed. A parallel study is also called for to characterize the properties of old muds in abandoned wells.

DRILLING MUD AS A HYDRAULIC SEAL IN ABANDONED WELLBORES

R. E. Collins and D. Kortum
Research & Engineering Consultants, Inc., Englewood, Colorado 80111

Introduction

That a column of drilling mud remaining in an uncased well at abandonment provides a hydrostatic pressure against fluid entry from penetrated strata is generally accepted, but it has not been generally accepted that the gel property of the mud contributes an increment to this pressure that may be significant. Barker (1981) was evidently the first investigator to propose that both hydrostatic and gel contributions be included when estimating the threshold of aquifer pressure at which fluid from the aquifer could enter a mud-filled abandoned well. Specifically Barker estimated this threshold pressure from a balance of forces as in Figure 1.

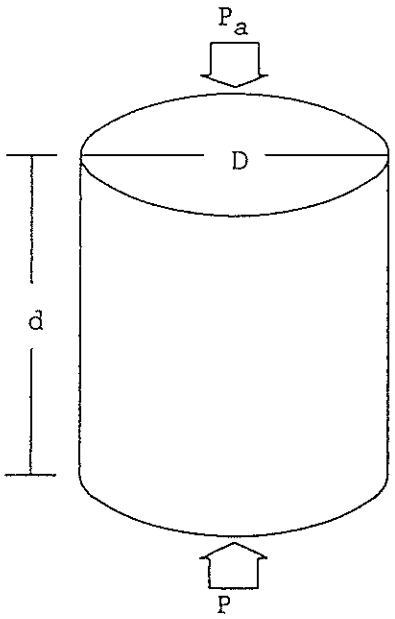

$$\text{Net Pressure force, up} = \frac{\pi D^2}{4}(P - P_a)$$

$$\text{Weight force, down} = \frac{\pi D^2}{4} d\rho_m$$

$$\text{Shear force at wall, down} = \pi DdG$$

FIGURE 1

Here a straight, cylindrical well of diameter D and depth d to an aquifer is filled with mud of weight density ρ_m and gel strength G. At depth d a uniform pressure P exists over the cross-section of the well. If the upward

force of this pressure exceeds the sum of the downward forces due to the atmosphere, weight of the mud, and the shear force at the wall of the hole then the column could be displaced upward by this pressure. Since pressure must be uniform in any horizontal plane within continuous fluid at rest, P is also the pressure of the brine in the aquifer at depth d. Thus Barker's criterion for no brine entry into the mud-filled well is

$$(1) \qquad \frac{\pi D^2}{4} P < \frac{\pi D^2}{4} d\rho_m + \pi DdG + P_a$$

where P_a is atmospheric pressure. This explicitly assigns the shear force per unit area on the wall of the hole as the gel strength G.

If the original, pre-injection pressure of the injection interval, $P_a + \rho_B gd$, is subtracted there results the criterion for admissible pressure increase in the aquifer, ΔP, with no brine entry into the abandoned well. Here ρ_B is the depth-averaged brine density from surface to the aquifer at depth d. In oil field units this gives the criterion as

$$(2) \qquad \Delta P \leq 0.052\ (\rho_m - \rho_B)d + 3.33 \times 10^{-3} \frac{Gd}{D}$$

For a minimum mud weight, about 9.0 lb./gal. for Bentonite mud, having a gel strength of 50 lb./(100 ft.^{2}) for a fresh water mix, and an average ρ_B of 8.4 lb./gal. this yields for a 5000 ft., 9-5/8" diameter hole

$$(3) \qquad \Delta P < 130 + 86.5 = 216.5 \text{ psi}$$

Thus gel contributes about 40% of the hole-sealing pressure of the mud in the hole. Clearly then it is important that this entry pressure criterion be validated.
Although this threshold pressure assignment is plausible it has not been confirmed experimentally. Thus we undertook a few simple experiments directed to such a demonstration. These are described here together with the rather surprising results that were obtained.

General Description of Apparatus and Procedure

This study actually included nine different experiments using the same basic apparatus with only minor alterations. Figure 2 shows the general configuration of laboratory equipment. A core was epoxied into a nipple and then attached to a pipe joint below the core which in turn was attached to a line carrying brine from a salt water reservoir. The pressure at this reservoir was recorded using a gauge or mercury manometer. Pressure was supplied to the brine using compressed nitrogen and a pressure regulator. Brine was pushed through the brine delivery system until no air existed in the lines and the rock was saturated with the brine. At this point, a pipe was attached to the core nipple and a column of bentonite mud (20 ppb bentonite with 3 ppb salt in Experiment No. 1 and 30 ppb bentonite in all other experiments)* was placed in the pipe over the core.

*ppb = pounds per barrel

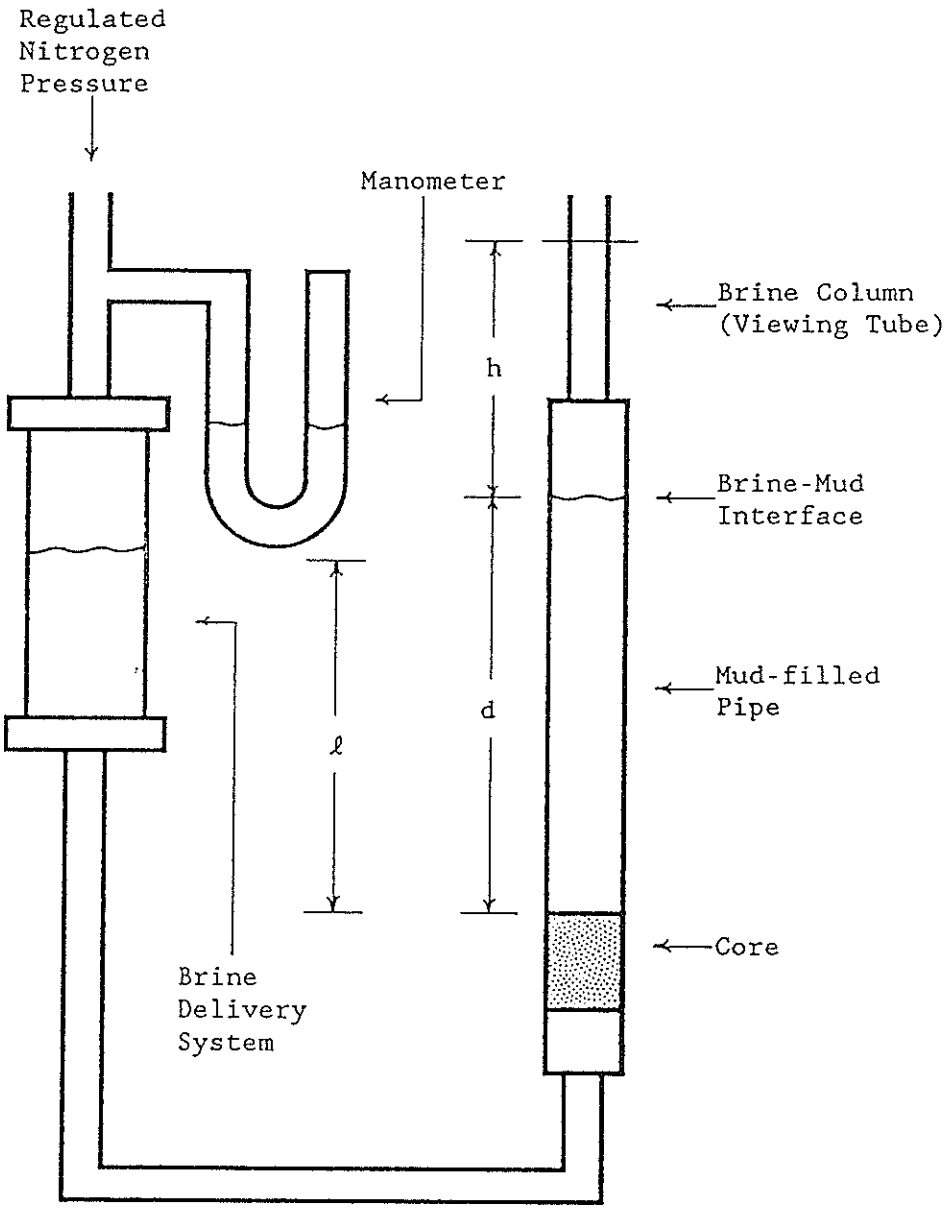

(not to scale)

GENERAL DESCRIPTION OF EQUIPMENT

FIGURE 2

A sample of this mud was also placed in a Fann viscometer cup to remain quiescent. A small diameter transparent tube was attached to the top of the mud column and filled with brine to provide a volumetrically sensitive detection for movement of the mud column. The mud was allowed to gel for approximately 12 hours, at which time pressure was slowly applied to the brine delivery system until fluid movement was noted in the viewing tube at the top of the column. Concurrently, the gel strength of the mud sample in the viscometer cup was measured using a Fann V-G meter. Note that the relevant distances to calculate pressures are indicated by ℓ, h, and d in Figure 1. All physical dimensions of this apparatus are given in the appendix together with physical properties of the fluids used.

Data Reduction

The data reduction scheme in these experiments required calculation of the brine pressure, P_c, at the face of the core contacting the mud column. From Figure 1 this is (gauge value)

$$P_c = P_m + \rho_B g \ell \tag{4}$$

where P_m is the pressure read on the manometer of the brine chamber. Also the hydrostatic pressure at the core face (gauge value), P_h, due to the brine column in the sight tube and the mud column is

$$P_h = \rho_m g d + \rho_B g h \tag{5}$$

Thus the difference in these two pressures, $P_c - P_h$, is the measured excess brine pressure in the core plug required solely to "break the gel" and initiate fluid entry. Specifically our Eq.(1) is now expressed in terms of these pressures as

$$\frac{\pi D^2}{4} (P_c - P_h) \geq \pi D d G \tag{6}$$

Now the first experiment indicated that a significant discrepancy existed between the measured pressure difference, $P_c - P_h$, as obtained using Eqs.(4) and (5) and the value implied by the equality in Eq.(6). That is, a value for $P_c - P_h$ can be computed from the measured value for G in the Fann instrument using Eq.(6). Specifically the measured value of $P_c - P_h$ was more than five times as large as that computed in this way. Thus these data implied that mud gel was contributing much more to the threshold brine entry pressure than one computes from the Fann measured value for G.

After some deliberation a hypothesis was formed to account for this discrepancy and this guided the design of subsequent experiments. It was conjectured that the excess pressure required to break the gel arose from the non-uniform diameter of the simulated wellbore. Specifically there was a narrowing of the diameter immediately above the core and abrupt "shoulders" of about 1/16" at the coupling. Also there was a "shoulder" of about 1/4" at the sight tube connection. It was believed that stress concentrations at these sharp corners caused a much greater applied stress to be required to shear the mud in the column.

Subsequent experiments were designed to test this hypothesis by introducing specific shape irregularities in the simulated wellbore. Then in each experiment an apparent gel strength was computed from measured pressures, P_c and P_h, using Eq.(6) as

$$(7) \qquad G' = \frac{D}{4d} (P_c - P_h)$$

This is then compared to G determined in the Fann instrument as the ratio

$$(8) \qquad R = \frac{G'}{G}$$

Following is a description of specific experiments in which R was determined for various geometries.

Description of Experiments

Exps. 1 & 2
The geometries for the various experimental runs are shown in Figure 3. In the first two runs, the pipe size was small (refer to Appendix). Two 1/16" shoulders were located along the length of the pipe, one just above the core and one midway up the length of the pipe. In addition, a fairly severe constriction occurred at the top of the column where the viewing tube was substantially smaller (diameter = 1/8") than the pipe itself and mud actually extended into this tube. Therefore, three constrictions existed along the mud column. The 1/16" shoulders were fairly large relative to the total diameter of the pipe.

Exp. 3
A large pipe was substituted for the small pipe (see Appendix). The pipe contained only one 1/8" shoulder located above the core. The adapter with brine viewing tube on top was used as shown in inset of Figure 3.

Exp. 4
The same set-up as Exp. 3 was used; however, the pipe had an oily film over its entire inner surface. No specific data were collected since fluid movement occurred immediately and no apparent gel strength was observed. i.e. $P_c - P_h$ was zero.

Exp. 5
Exp. 5 was similar to Exp. 3 except that an additional constriction was placed on the mud column and the mud column extended into the smaller pipe on top and into the brine viewing tube (see Figure 3 inset).

Exps. 6 & 7
Experiments 6 and 7 were identical. These were identical to Exp. 3 but instead of a smooth pipe being used, a series of five joints and nipples (in addition to the one located above the core mentioned in Exp. 3) were located along the length of the pipe (see Figure 3).

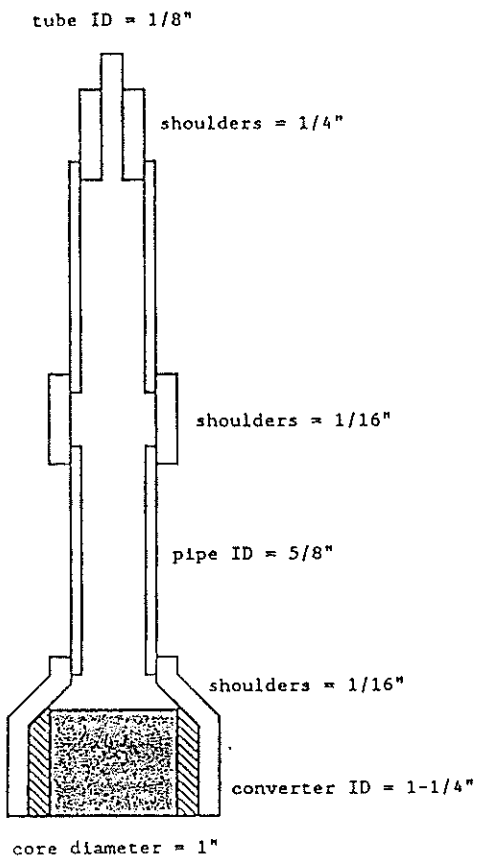

Experiments 1, 2
and modified for
Experiment 8

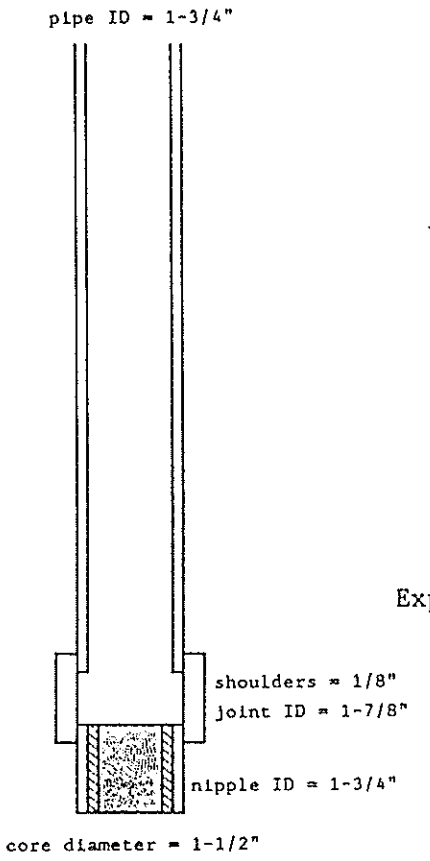

Experiments 3, 4
and modified for
Experiments 5, 9

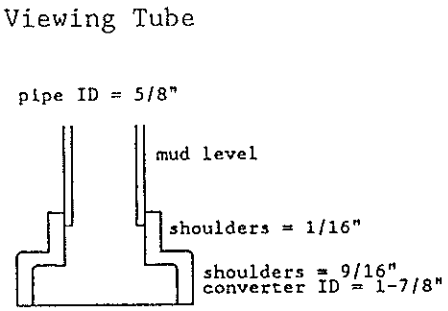

Experiments 3 - 9

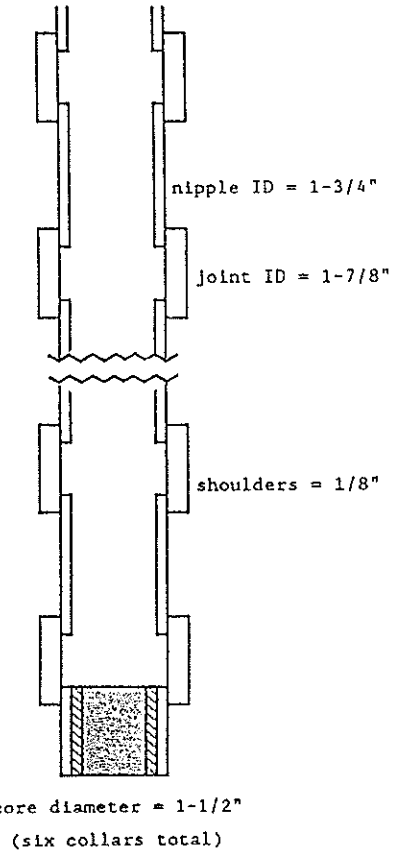

Experiments 6, 7

(not to scale)

FIGURE 3

Exp. 8
This experiment employed the small pipe as in Exps. 1 and 2 but in this case the mud did not extend into the small viewing tube initially. The mud level was in the 5/8" ID pipe.

Exp. 9
This experiment was intended to test behavior in a pipe of uniform dimensions with no constrictions anywhere. A PVC pipe was mounted into the nipple containing the core used in Exps. 3 and 4 with the pipe inserted flush to the core plug face. Thus no "shoulders" were present in the mud-filled pipe. The adapter with the brine-filled viewing tube was mounted on top but the mud level was in the uniform diameter pipe.

Results and Discussion

Values for all parameters and data collected in these experiments are listed in the appendix and here we summarize values determined for R, the ratio of apparent to actual gel strength in Table I.

TABLE I

Exp. No.	1	2	3	4	5	6	7	8	9
R	5.11	5.05	1.68	0.00	2.77	3.83	3.61	5.76	1.99

The results of Exps. 1 and 2 indicate non-uniform geometry profoundly influences the apparent gel strength. Apparently the relative size of diameter constrictions in relation to the cylinder in which the mud stands produced the larger increases in apparent gel strength observed in Exps. 1 and 2 as compared to other experiments.

In Exp. 3, the one shoulder in the large pipe produced, approximately, a 68% increase in apparent gel strength over the Fann measured value. In Exps. 6 and 7, it would be reasonable to assume that the increase in apparent gel strength should be about six times the 68% value observed in Exp. 3 since 6 shoulders are present. This would produce an R value of 1 + (0.68 x 6) or 5.08 which is larger than the apparent values actually observed in Exps. 6 and 7.

Exp. 5 provides further evidence that geometric irregularities produce increases in apparent gel strength. With the constriction on the top of the pipe (along with the shoulder of Exp. 3), the apparent gel strength is increased by nearly three-fold over the Fann measured value.

Exp. 4 demonstrates that when the mud column is detached from the pipe structure by an oily film, either the brine flows up the pipe around the mud column or the column provides little or no gel strength since it is, in effect, not bonded to the pipe.

Exp. 8 was to test whether the very large value of G observed in Exps. 1 and 2 was due in part to the fact that mud extended into the small diameter viewing tube at the top of the 5/8" ID pipe. Since the observed value of R in Exp. 8 was even larger, this is not the case.

The objective in Exp. 9 was to determine whether a tube free of any non-uniformities in diameter of the mud column would yield a G value comparable to that measured in the Fann viscometer. Since the apparent G value in this case was almost double the Fann determined value, this is not the case. Thus, there are other factors involved besides non-uniform diameter of hole which cause the high apparent G values.

We can speculate on the implications of the data obtained in the above experiments:

(1) There is clearly an increase in the contribution of mud gel strength to the threshold pressure for brine entry arising from constrictions or non-uniformities in pipe (simulated bore-hole) diameter. A factor of about 2 - 5 was observed.

(2) There is another contribution to threshold brine entry pressure not associated with hole geometry. We speculate that this may be due to gelled mud in the pores of the core plug. Also it is possible that upon standing with mud pressure on the core plug, some particulates could enter the larger pores of the core plug. This might account for the results in Exps. 8 and 9.

Regardless of the ultimate resolution of these questions one fact is certain and this is that the gel strength of mud in an abandoned well does indeed contribute significantly to the threshold pressure for fluid entry to the well.

Conclusions

The experiments described here confirm that the gel characteristics of drilling mud do contribute substantially to the threshold pressure required for brine entry from an aquifer into a mud-filled wellbore. Specifically the threshold pressure for fluid entry computed by Eq.(1) above, using an average hole diameter D and a laboratory measured G value, will always be significantly conservative. The data presented have suggested that irregularities in hole diameter can cause the true gel contribution to be four to five times greater than that calculated for a uniform diameter. However, since these experiments were not properly scaled direct application of this result to actual wells should be used with caution. Further experiments and analysis could resolve this issue of effects of hole diameter irregularities. Other questions raised in these experiments might be explained in part by prior studies on particulate transport in porous media [Gruesbeck and Collins (1982)] but the effect of gelling of colloidal clay which invades the porous rock calls also for additional experiments.

Appendix

Data and Results
(see Nomenclature at end)

Experiment 1

Geometry	in.	cm.
Core Diameter	1.0	2.54
Pipe I.D.	0.625	1.488
Length, ℓ	24.409	62.0
Length, d	11.5	29.2
Length, h	4.53	11.5

Pressures	psi	in. Hg
P_m	3.0	
P_s	+0.8937	+1.8
P_h	0.5966	1.2
P_c	3.89	7.9

Gel Strength	psi	lbs./100 ft.^{2} (12 hrs.)
G		125.0
G'	0.04475	644.0

$G'/G = R = 5.11$

Experiment 2

Geometry	in.	cm.
Core Diameter	1.0	2.54
Pipe I.D.	0.625	1.488
Length, ℓ	14.6	37.0
Length, d	12.0	30.5
Length, h	3.94	10.0

Pressures	psi	in. Hg
P_m	7.859	16.0
P_s	-0.533	-1.1
P_h	0.5966	1.2
P_c	7.326	14.9

Gel Strength	psi	lbs./100 ft.^{2} (12 hrs.)
G		250.0
G'	0.08763	1262.0

$G'/G = R = 5.05$

Experiment 3

Geometry	in.	cm.
Core Diameter	1.5	3.82
Pipe I.D.	1.625	4.12
Length, ℓ	11.4	29.0
Length, d	26.0	66.0
Length, h	6.5	16.5

Pressures	psi	in. Hg
P_m	3.438	7.0
P_s	-0.418	-0.851
P_h	1.218	2.48
P_c	3.02	6.15

Gel Strength	psi	lbs./100 ft.^{2} (12 hrs.)
G		250.0
G'	0.02816	405.0

$G'/G = R = 1.68$

Experiment 5

Geometry	in.	cm.	
Core Diameter	1.5	3.82	
Pipe I.D.	1.625	4.12	small pipe
Length, ℓ	12.2	31.0	radius =
Length, d	33.9	86.0	0.3125 in.
Length, h	3.54	9.0	(see sketch)

Pressures	psi	in. Hg
P_m	4.91	10.0
P_s	-0.4476	-0.91
P_h	1.4059	2.86
P_c	4.4643	9.1

Gel Strength	psi	lbs./100 ft.^{2} (12 hrs.)
G		210.0
G'	0.04042	582.0

$G'/G = R = 2.77$

Experiment 6

Geometry	in.	cm.
Core Diameter	1.5	3.82
Pipe I.D.	1.625	4.12
Length, ℓ	13.8	35.0
Length, d	26.0	66.0
Length, h	6.3	16.0

Pressures	psi	in. Hg
P_m	3.93	8.0
P_s	-0.5044	-1.28
P_h	1.21	2.46
P_c	3.425	6.97

Gel Strength	psi	lbs./100 ft.^{2} (12 hrs.)
G		130.0
G'	0.03460	498.0

$G'/G = R = 3.83$

Experiment 7

Geometry	in.	cm.
Core Diameter	1.5	3.82
Pipe I.D.	1.625	4.12
Length, ℓ	13.8	35.0
Length, d	26.0	66.0
Length, h	6.3	16.0

Pressures	psi	in. Hg
P_m	4.13	8.4
P_s	-0.5044	-1.28
P_h	1.21	2.46
P_c	3.6214	7.373

Gel Strength	psi	lbs./100 ft.^{2} (12 hrs.)
G		150.0
G'	0.03768	542.0

$G'/G = R = 3.61$

Experiment 8
(small pipe - no top constriction)

Geometry	in.	cm.
Core Diameter	1.0	2.54
Pipe I.D.	0.625	1.876
Length, ℓ	21.65	55.0
Length, d	9.84	25.0
Length, h	3.05	7.75

Pressures	psi	in. Hg
P_m	6.1886	12.6
P_s	-0.7925	-1.6135
P_h	0.4827	0.9828
P_c	5.396	10.98

Gel Strength	psi	lbs./100 ft.^{2} (12 hrs.)
G		195.0
G'	0.078	1123.0

$G'/G = R = 5.76$

Experiment 9
(large pipe, PVC - no shoulders)

Geometry	in.	cm.
Core Diameter	1.5	3.82
Pipe I.D.	1.5	3.82
Length, ℓ	20.866	53.0
Length, d	22.441	57.0
Length, h	5.906	15.0

Pressures	psi	in. Hg
P_m	3.438	7.0
P_s	-0.7637	-1.555
P_h	1.062	2.162
P_c	2.674	5.444

Gel Strength	psi	lbs./100 ft.^{2} (12 hrs.)
G		195.0
G'	0.02694	388.0

$G'/G = R = 1.99$

Fluid Properties

	Density (g/cc)	lb./gal.	psi/ft.	psi/in.	psi/cm.
Salt	1.0147	8.45	0.4394	0.0366	0.01441
Mud (Exp. 1)	1.0396	8.65	0.4498	0.0375	0.01476
Mud (Exps. 2 - 9)	1.0444	8.70	0.4520	0.0377	0.01484

Mud Composition:

Exp. 1: 20 ppb bentonite, 3 ppb salt
Exps. 2 - 9: 30 ppb bentonite

Nomenclature

ℓ, d, h	Vertical Dimensions of Experimental Set-Up
r_c	Core Radius
r_p	Pipe Radius
h_p	Pipe Length
P_m	Manometer Pressure
P_s	Hydrostatic Pressure of Brine Reservoir
P_h	Hydrostatic Head of Mud/Brine Over Core
P_c	Pressure at Core Face

Bibliography

Barker, S. E.; "Determining the Area of Review for Industrial Waste Disposal Wells", M.S. Thesis (supervised by R. E. Collins), University of Texas at Austin, (1981)

Davis, K. E. and G. D. Sengelmann; "Factors Affecting the Area of Review for Hazardous Waste Disposal Wells", Proc. Int. Conf. Underground Injection, New Orleans, Louisiana, March (1986)

Gray, G. R. and H. C. H. Darley; Composition and Properties of Oil Well Drilling Fluids, 4th Ed., Gulf Pub. Co., Houston, Texas, (1981)

Gruesbeck, C. and R. E. Collins; "Entrainment and Deposition of Fine Particles in Porous Media", Soc. Pet. Engr. J., p. 847 - 856, December (1982)

Johnston, O. C. and Ben K. Knape; Pressure Effects of the Static Mud Column in Abandoned Wells, Texas Water Commission Report LP86-06, September (1986)

Weintritt, P. J. and R. G. Hughes; "Factors Involved in High Temperature Drilling Fluids", J. Pet. Tech., p. 707, June (1965)

Draft Report a Review of Literature and Laboratory Data Concerning Mud Filled Holes

0113265

DRAFT

DRAFT REPORT
A REVIEW OF LITERATURE AND LABORATORY DATA CONCERNING MUD FILLED HOLES

CHEMICAL MANUFACTURING ASSOCIATION
WASHINGTON, DC

ENVIROCORP PROJECT NO. 10-1302

FOR ADDITIONAL INFORMATION CONTACT

KEN E. DAVIS OR MARK S. PEARCE
(713) 880-4640 OR (713) 334-6437

OCTOBER 1989

PREPARED BY

ENVIROCORP SERVICES & TECHNOLOGY, INC.
HOUSTON, TEXAS

TABLE OF CONTENTS

TABLES

FIGURES

1.0 INTRODUCTION

0113265

The purpose of the Underground Injection Control (UIC) Regulations are to prevent the possible contamination of underground sources of drinking water (USDW). One possible avenue of contamination is through manmade wellbores. Native or other injected fluids may migrate up these wellbores and contaminate a USDW.

Several factors must be considered to determine the probability of upward fluid migration and thus the potential for USDW contamination. These include but are not limited to the following:

- The subsurface lithology penetrated.
- Drilling method used.
- Location and condition of casing.
- Location of mechanical and/or cement plugs.
- Type of fluid left in the well.

The static mud column or drilling fluid left in the hole will provide substantial resistance to upward migration or flow. Most mud systems develop a gel structure when allowed to remain quiescent. This gel strength provides resistance to migration or flow and helps maintain the density of the fluid by suspending barite, clay, and other drilled solids. The density of the mud column provides hydrostatic head or a pressure along the wellbore that also provides resistance to upward fluid flow or migration. These properties are additive, therefore the sum of these forces must be exceeded for flow and/or migration to occur. Additionally, other related factors, such as wellbore closure from collapse or other natural events, must also be considered.

2.0 PURPOSE OF THE REPORT

Some doubt has been expressed by the regulators, concerned citizen groups, and the owner/operators related to the conditions of abandoned wellbores and annular spaces and their ability to contain injected and native fluids. This concern is a result of a deficiency in the literature specifically addressing the factors related to wellbore closure and the effect on the prevention of fluid migration. This report provides data on the factors effecting the static mud column, in the wellbore or behind the casing in the casing/wellbore annulus, to provide significant resistance to upward fluid migration along these potential pathways. The area within the zone of endangering influence from nearby injection wells is the area of greatest concern.

The zone of endangering influence is defined as that area, the radius of which is the lateral distance in which pressures in the injection zone may cause the migration of the injection and/or formation fluid into an underground source of drinking water (USDW). In some cases, this zone may also include the area of potential

plume migration. There are numerous factors that must be considered when determining the potential for USDW contamination, however, the purpose of this report is to only address those factors that are relevant to the properties of drilling and other fluids remaining in abandoned wellbores and those left in the casing/wellbore annulus of both abandoned and active wells.

3.0 SUMMARY

4.0 SUMMARY OF KNOWN MUD PROPERTIES

The wellbore and annulus space are rarely empty and are filled with native water, brine, or drilling fluid. In the case of native waters or brine the fluids may have seeped into the wellbore or been left there by the original driller. If the well was originally drilled with a cable tool rig or rotary drilling rig using compressed air, the fluid in the hole is probably native water or brine. However, the vast majority of artificial penetrations are made exploring for oil, gas and other minerals. Virtually all the wells drilled along the Gulf Coast used drilling fluids. In other areas it is logical to conclude that most wellbores are mud filled since rotary drilling techniques using drilling fluid are predominately used when drilling oil and gas exploration and development wells and other mineral extraction wells. Upon completion of the drilling operation, if the well is not completed for production, the drillpipe is removed from the wellbore and the drilling mud used to drill the well will remain in the wellbore indefinitely. If the well is completed or casing is run and partially cemented across a portion of the wellbore, drilling mud would have been displaced ahead of the cement from the annular space between the casing and open hole. If cement was not circulated to the surface, then the annular space above the cemented section will be filled with drilling mud.

A fluid filled wellbore or annular space provides resistance to upwards fluid migration because of two opposing forces. Barker (1981) was evidently the first investigation to propose the effects of these forces on fluid migration. The first would be the hydrostatic head or downward force caused by the weight of the fluid column. This can be described as psi/foot of depth by taking the weight of one cubic foot of water and dividing it into 144 square inches one-foot high. A cubic foot of water weighs approximately 62.3 pounds, dividing by 144 square inches, we find that a column of water one-foot high exerts a downward pressure of 0.433 psi. Therefore a column of water 1000 feet deep would provide a downward force of 433 psi. If fluid were migrating upward, it would have to have a driving force in excess of 433 psi. This example used fresh water having a density of 8.33 lbs/gal. Rogers, (1963) prepared a graph (Figure 1) showing the relationship of hydrostatic pressure with depth for mud fluids of various densities ranging from 8.33 to 20 ppg.

Drilling fluid density is the only short-term property of a drilling mud which can prevent reservoir fluids from entering the wellbore. Fluid density is also the only mud property that can prevent formation collapse due to tectonic stresses or unconsolidation of the formation. In general, as indicated by Mitchell, Goodman, and Wood (1987), and by Gray and Darley (1980, p. 355) drillers commonly use a mud weight that will overbalance the highest formation fluid pressure encountered by a "safe margin" which will commonly range between 200 to 400 psi. The overbalanced mud weight is used to provide a conservative margin of error to prevent fluid flow into the wellbore.

Along the Gulf Coast, increased mud weight is also used to prevent the unconsolidated formation from sloughing into the well. As an example, a well recently drilled in the Upper Texas Coast under the supervision of

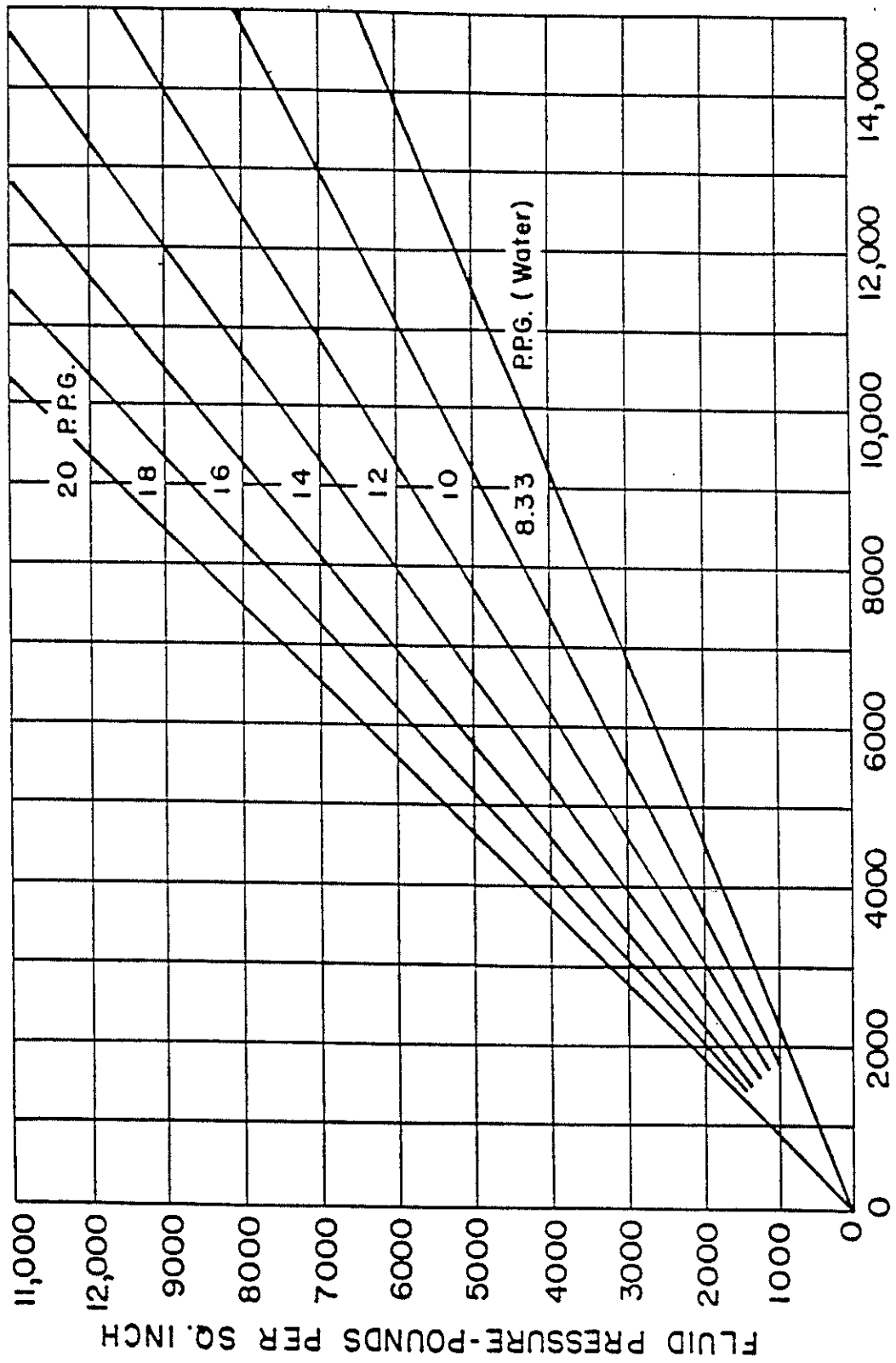

Hydrostatic pressure of mud fluids.

FIGURE 1

Envirocorp required an 8.8 pound/gallon (lb/gal) mud to balance the formation fluid pressure during a gravel pack operation. However, the mud weight needed to be increased above 9.4 lb/gal to prevent the sides of the open hole from sloughing into the wellbore.

The above example, and the data provided by Mitchell, Goodman, and Wood (1987) demonstrates that the original mud column will commonly overbalance the highest static reservoir pressure encountered by 100 psi or more. The average overbalance pressure indicated by the data provided by the above authors is approximately 350 psi. One should remember that this overbalance pressure or "safe margin" will eventually press the mud filtrate into the shale formations and increase the shale hydration force. This will increase the probability of wellbore closures across shale sections.

Dissolved and suspended solids are the reason mud fluids have densities higher than their base fluid. For example, the density of water can be increased from 8.33 ppg to 10.0 ppg by making a solution of common salt (sodium chloride). Likewise, mixtures of bentonite clay and barite (barium sulfate) can attain weights in excess of 20 ppg.

Mined barium sulfate, or simply barite, is the most common material used to increase the density of drilling mud. API barite (See Table 1) is specified to have a specific gravity of no less than 4.20. The average specific gravity for drilled solids is approximately 2.65.

TABLE 1
TYPICAL API BARITE PARTICLE SIZE DISTRIBUTION

VOLUME, %	SIZE PARTICLE, MICRONS
10	2.22
20	4.51
25	6.58
30	8.71
35	10.98
40	13.88
45	16.79
50	19.82
55	22.84
60	28.97
65	31.19
70	35.65
75	40.64
80	46.03
85	51.43
90	62.96

Gray, Darley, and Rogers, (1980) divided the particles suspended in mud into three groups according to size: (1) colloids, from about 0.005 to 1 micron (1 micron = 0.001 mm), which impart viscous and filtration properties; (2) silt and barite (sometimes called "inert solids"), 1 to 50 microns, which provide density; and, (3) sand, 50 to 420 microns, which generally does not significantly benefit the properties of the mud. NL Baroid, (1979) classified these same particles as follows: API sand, more than 74 microns, silt, 2-74 microns, barite 2-60 microns, and clays, less than 1 micron.

The relationship of particle size distribution to filtration rate is well known. Generally, muds with low filtration rates have a higher concentration of small particles than those with high filtration rates. Gates and Bowie, (1942) illustrated this relationship (Figure 2) by plotting the particle size distribution for both a low filter rate (0-20 ml/hr) mud and high filter rate (40-75 ml/hr) mud.

This relationship indicates that muds having low filtration rates would be more stable. The suspended solids would have less tendency to settle and therefore the density or mud weight would generally remain constant throughout the mud column in a wellbore or annular space.

The ability for the mud column to support its mixture of suspended solids is extremely important to maintain the integrity of the columns hydrostatic head. Pearce, (1989) showed that less than 3% of the barite has any potential to settle out of the mixture if minimal gel strengths (5.616/100 ft^2) are present.

The second opposing force that would act as a deterrent to fluid migration along a wellbore would be present only if the fluid filling the wellbore had gel strength. Most drilling fluids contain this characteristic. Collins and Kortum (1988) suggest gel strength contributes 40% of the hole-sealing pressure of the mud in the hole.

One of the primary functions of the drilling mud is the removal of drilled cuttings from the wellbore. The mud carries the cuttings from beneath the bit, transports them up the wellbore/drillpipe annulus and releases them at the surface. Since normal drilling operations require that mud circulation be stopped periodically to add another joint of drillpipe, the mud must have a property which acts to suspend the drilled cuttings in the static mud column. This property is known as gel strength. Gel strength is time dependent and increases as the mud column remains quiescent. Most drilling fluids are thixotropic and develop a gel structure like "Jello" when allowed to stand quiescent but become fluid when disturbed.

To determine the combined effect of both hydrostatic head and gel strength acting as a deterrent to fluid migration along a mud filled wellbore or annulus, we must first identify the forces acting on a wellbore and/or annulus existing in a static state. Figure 3 represents a vertical force diagram of a static mud column in an abandoned well that contains no uncemented casing. Figure 4 represents the forces acting on the static mud column in the annulus between the casing and open hole above the cemented interval.

The equation for the force balance in Figure 3 takes the following form,

$$w + GS_w 2\pi r_w h = Pf \pi r^2_w - P_t \pi r^2_w \quad (1)$$

where

$$w = r^2_w \rho h$$

and

- w = weight of mud column
- GS_w = gel strength of mud column acting on circumference area of wellbore
- P_t = pressure at top of well
- P_f = pressure at formation being contained
- r_w = radius of wellbore
- h = height of mud column in wellbore
- ρ = density of mud

Simplifying the force balance and adjusting for standard units, we obtain the following pressure equation,

$$P_f = P_t + 0.052\rho h + 3.33 \times 10^{-3} GSh/D \quad (2)$$

where

- P_f = pressure at the contained formation in psi
- P_t = pressure at the top of well in psi
- ρ = density of mud in lb/gal
- h = height of mud column in feet
- GS = gel strength in lb/100 ft^2
- D = diameter of wellbore in inches

The force balance equation for Figure 4 takes the form

$$w + GS_c(2\pi r_c h) + GS_w(2\pi r_w h) = \quad (3)$$

$$P_f \pi (r^2_w - r^2_c) - P_t \pi (r^2_w - r^2_c)$$

where

$$w = \rho h (r^2_w - r^2_c)$$

ANNULUS STATIC MUD COLUMN FORCE BALANCE DIAGRAM

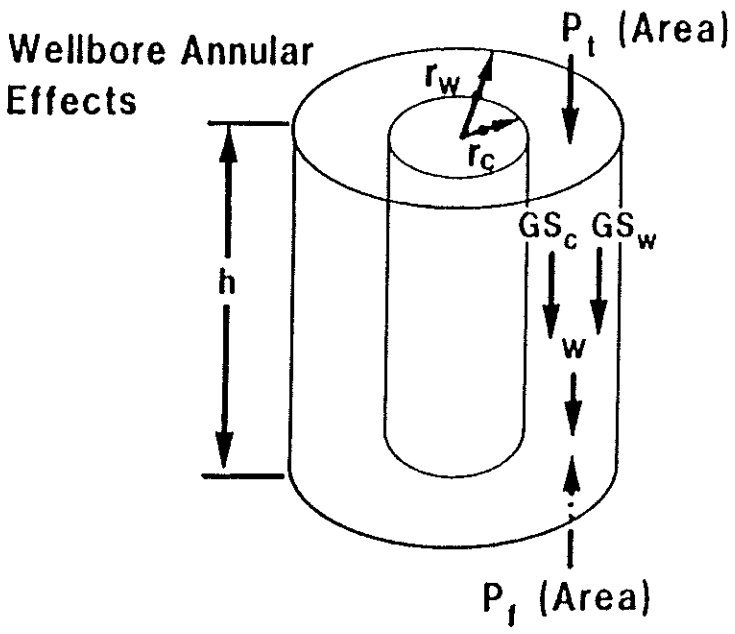

P_t (Area) = Pressure at the Top of Well = $P_t \pi (r_w^2 - r_c^2)$

W = Weight of Fluid Column = $\rho h \pi (r_w^2 - r_c^2)$

GS_w = Gel Stength of Mud Acting on Circumference Area of Well Bore = $GS_w (2 \pi r_w h)$

GS_c = Gel Stength of Mud Acting on Circumference Area Casing = $GS_c (2 \pi r_c h)$

P_f (Area) = Pressure at the Formation Being Contained = $P_f \pi (r_w^2 - r_c^2)$

Forces From Mud Column = Sum of Pressure Forces

$$w + GS_s (2 \pi r_c h) + GS_w (2 \pi r_w h) = P_f \pi (r_w^2 - r_c^2) - P_t \pi (r_w^2 - r_c^2)$$

0113265

Ken E. Davis Associates

FIGURE 4

and

w = weight of mud column in annulus

GS = gel strength of mud acting on circumference area of both the wellbore (GS_w) and casing wall (GS_c) and $GS_w = GS_c$

P_t = pressure at top of well

P_f = pressure at formation being contained

r_w = radius of wellbore

r_c = outside radius casing

h = height of mud column in annulus

ρ = density of mud

Simplifying the force balance and adjusting for standard units, we obtain the following pressure equation,

$$P_f = P_t + 0.052\rho h + \frac{3.33 \times 10\text{-}3^{GSh}}{D_w - D_c} \quad (4)$$

where:

P_f = pressure at the contained formation in psi

P_t = pressure at top of well in psi

ρ = density of mud in lb/gal

h = height of mud column in feet

GS = gel strength of mud in lb/100 ft2

D_w = diameter of wellbore in lb/100 ft^2

D_c = outside diameter of casing in inches

It is generally recommended that the values required to calculate the flow resistance of a mud filled wellbore or annular space be obtained from the well records. The physical configuration of the well can usually be obtained from many sources. These include but are not limited to state libraries, geological surveys and other public information sources. The density of the drilling fluid used to drill the well is normally recorded on the geophysical log heading. The gel strength values may be more difficult to obtain. Mud properties are generally run while conditioning the mud to run casing and cement. These values are normally determined by the drilling fluid supplier or service company and are reported on standardized forms. These data are normally available from the owner/operator's well files or the service company. Also, it is frequently not necessary to find the well records of each well since wells drilled adjacent to each other frequently use the same or similar mud systems. Historical records are also a good source of obtaining conservative values for gel strengths of specific types of drilling fluid systems.

Since the gel strength of different types of mud systems varies, it is difficult to determine the exact gel strength of the mud in a particular wellbore. Collins and Kortum (1988) suggest that the configuration of the wellbore can increase the apparent gel strength six times the observed values. A review of the gel strength characteristics of various types of muds was made to evaluate the factors that effect the gel strength structure. No consideration was given to the hole configuration. The aim of this review was to provide sufficient information to determine the minimum gel strength structure that could be anticipated for any combination of formation, wellbore, and mud type.

Thixotropy is the property, exhibited by certain gels, of liquefying when stirred or shaken and then returning to their gelled state when allowed to stand quiescent. This property in drilling fluids is the result of various clay minerals being used as additives in drilling fluids. Generally, clay particles fall into the colloidal particle range. Colloidal systems used in drilling fluids include solids dispersed in liquids and liquid droplets dispersed in other liquids. These highly active colloidal particles comprise a small percentage of the total solids in drilling muds but act to form the dispersed gel forming phase of the mud that provides the desired viscosity, thixotropy, and wall cake properties.

Thixotropy is essentially a surface phenomenon which is characterized by gel strength measurements. The gel strength indicates the attractive forces between particles under static conditions. The strength of the gel structure which forms under static conditions is a function of the amount and type of clays in suspension, time, temperature, pressure, Ph, and the chemical treating agents used in the mud. Those factors which promote, the edge-to-edge and face-to-edge association of the clay particles defined as flocculation increase the gelling tendency of the mud and those factors which prevent the association decrease the gelling tendency.

Due to their size, colloidal particles remain indefinitely in suspension. When suspended in pure water the clay particles will not flocculate. When flocculation occurs the particles form clumps or flocs. These loosely associated flocs contain large volumes of water. If the clay concentration in the mud is sufficiently high, flocculation will cause formation of a continuous gel structure instead of individual flocs.

Gel strength is measured by a multispeed direct indicating viscometer by slowly turning the driving shaft by hand and observing the maximum deflections before the gel structure breaks. The gel strength is normally measured after quiescent periods of 10 seconds (initial gel strength) and 10 minutes. The measurements are taken at surface conditions of standard temperature and pressure. To determine the gel strength of the static mud column in an abandoned well it is necessary to determine the gel strength of the mud under the influence of borehole conditions. The initial and 10 minute gel strengths bear no direct relation to the ultimate gel strength of the mud at borehole conditions. To determine the ultimate gel strength of a mud it is necessary to discuss the factors which act to influence the initial gel strength at borehole conditions.

Once the drilling operation is completed and the well is abandoned the mud is subjected to conditions vastly different from those encountered at the surface. In the range of formation depths utilized for disposal of industrial wastes the temperature would be expected to range from 80 to 300°F, the pressure from 1500 to 5000 psi and time from days to several years. Several studies have been conducted to determine the impact of conditions. The information obtained from this research should provide a means of determining a reasonable minimum gel strength value for the abandoned wells which exist in the range of formations described above.

It is observed that common used water-base muds develop high gel strengths after prolonged periods of quiescence. The relationship between gel strength and time varies widely from mud to mud, depending on the composition, degree of flocculation, temperature, pH, solids, and pressure. Figure 5 (Gray, Darley, and Rogers, 1980) indicates the increase in gel strength with time for various mud types and reveals that there is no well established means of predicting long-term gel strengths with time. It is noted in all cases that the gel strength is observed to increase.

Annis (1976) noted that when a bentonite mud is quiescent, the gelling process depends on both temperature and time. Annis compared the effect of temperature on the initial and 30 minute gel strength of an 18 ppb bentonite suspension. Figure 6 indicates that the 30 minute gel strength of the 18 ppb suspension is at any temperature approximately six times the initial gel strength. The dependence of gel strength on time at different temperatures, as noted by Annis, is shown in Figure 7. Based on these and other tests of up to 18 hours Annis concluded that there is a strong indication that gel strength increases indefinitely with time.

The above works indicate that the ultimate gel strength of water-base muds is considerably higher than the values recorded for the initial and 10 minute gel strength. Although there is no direct relationship between gel strength and time, it is possible, based on available information, to conclude that the ultimate gel strength of a mud will be several times larger than the initial or 10 minute gel strength of the mud. In reference to the work by Garrison (1939), it is possible to consider the ultimate gel strength of a treated mud to be equivalent to that of a similar mud that was not treated, since the effect of the thinner is to decrease the rate of gelling and not the ultimate gel strength obtained.

In addition to time, temperature can have a major effect on the gel strength of water-based drilling fluids. Stini-Vasan (1957) studied the effects of temperature on the gel strength of several water-based drilling muds. In most of the cases investigated by Stini-Vasan it was noted that the gel strength leveled off after 160°F. The emulsion and lime treated muds showed no change in gel strength with increase of temperature. It was found that each mud had its own characteristic curve and no quantitative interpretation was possible. The work of Weintritt and Hughes (1965) on Table 2, indicates that emulsion Mud G experienced no change in gel strength in going from 75 to 180°F over a wide range of times. It is noted that although the gel strength did not vary with temperature, it went from an initial gel strength of 0 to a gel strength of 25 after 16 hours. These values are displayed graphically on Figure 8.

INCREASE IN GEL STRENGTH OF VARIOUS MUD TYPES WITH TIME

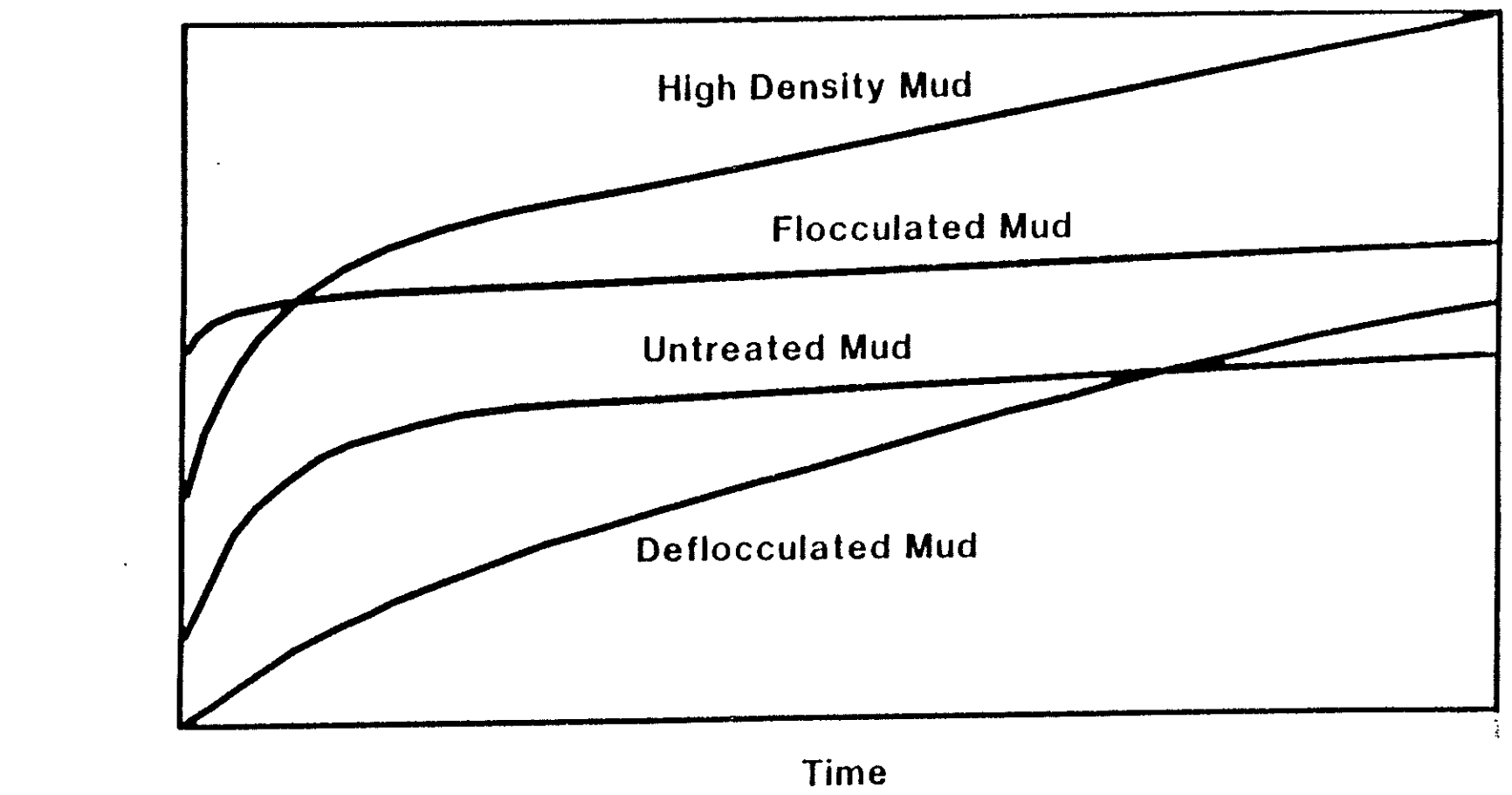

(From Gray, Darley, and Rogers)

Ken E. Davis Associates

FIGURE 5

EFFECT OF TEMPERATURE ON INITIAL AND 30-MINUTE GEL STRENGTH

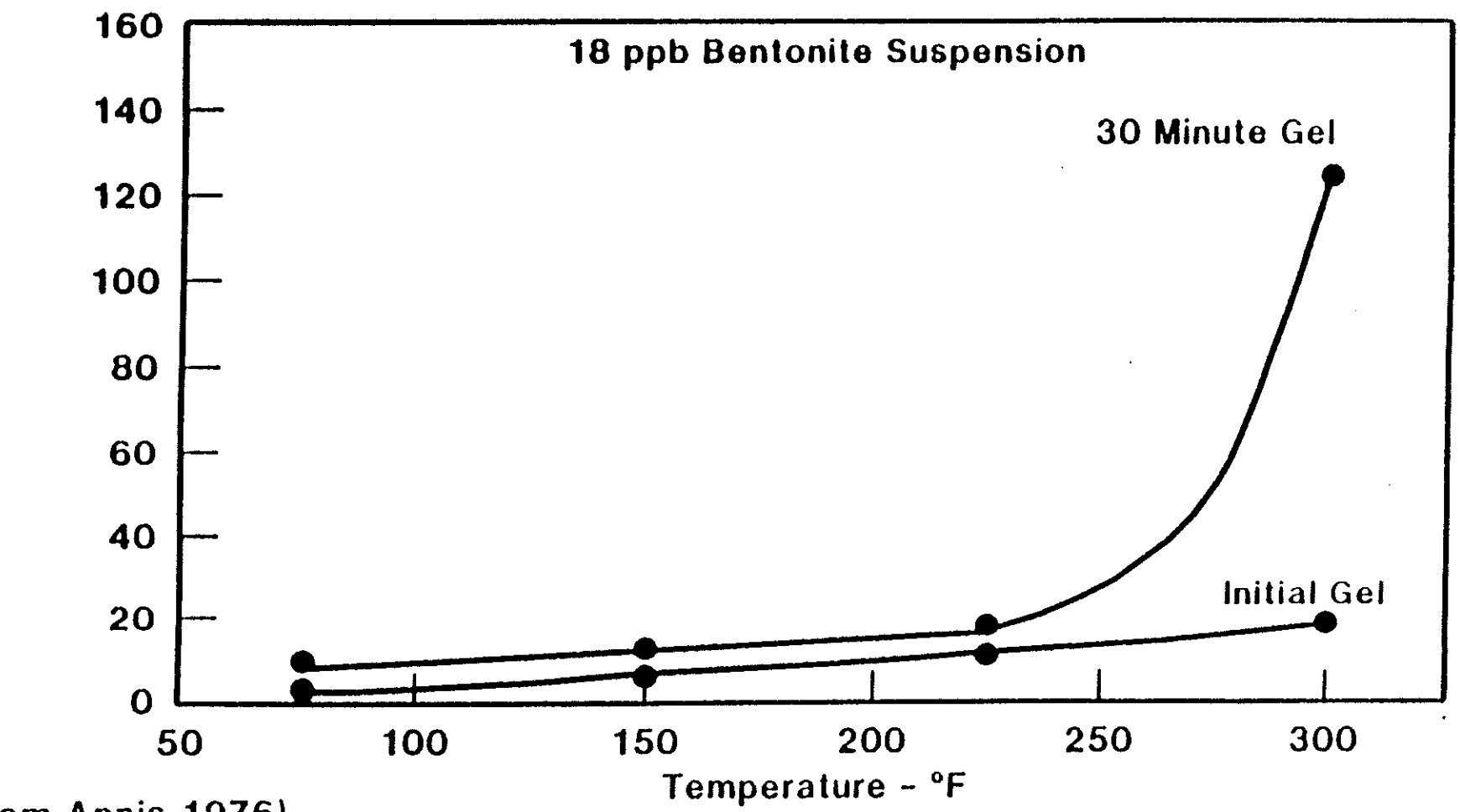

(From Annis 1976)

Ken E. Davis Associates

FIGURE 6

EFFECTS OF TIME AND TEMPERATURE ON GEL STRENGTH

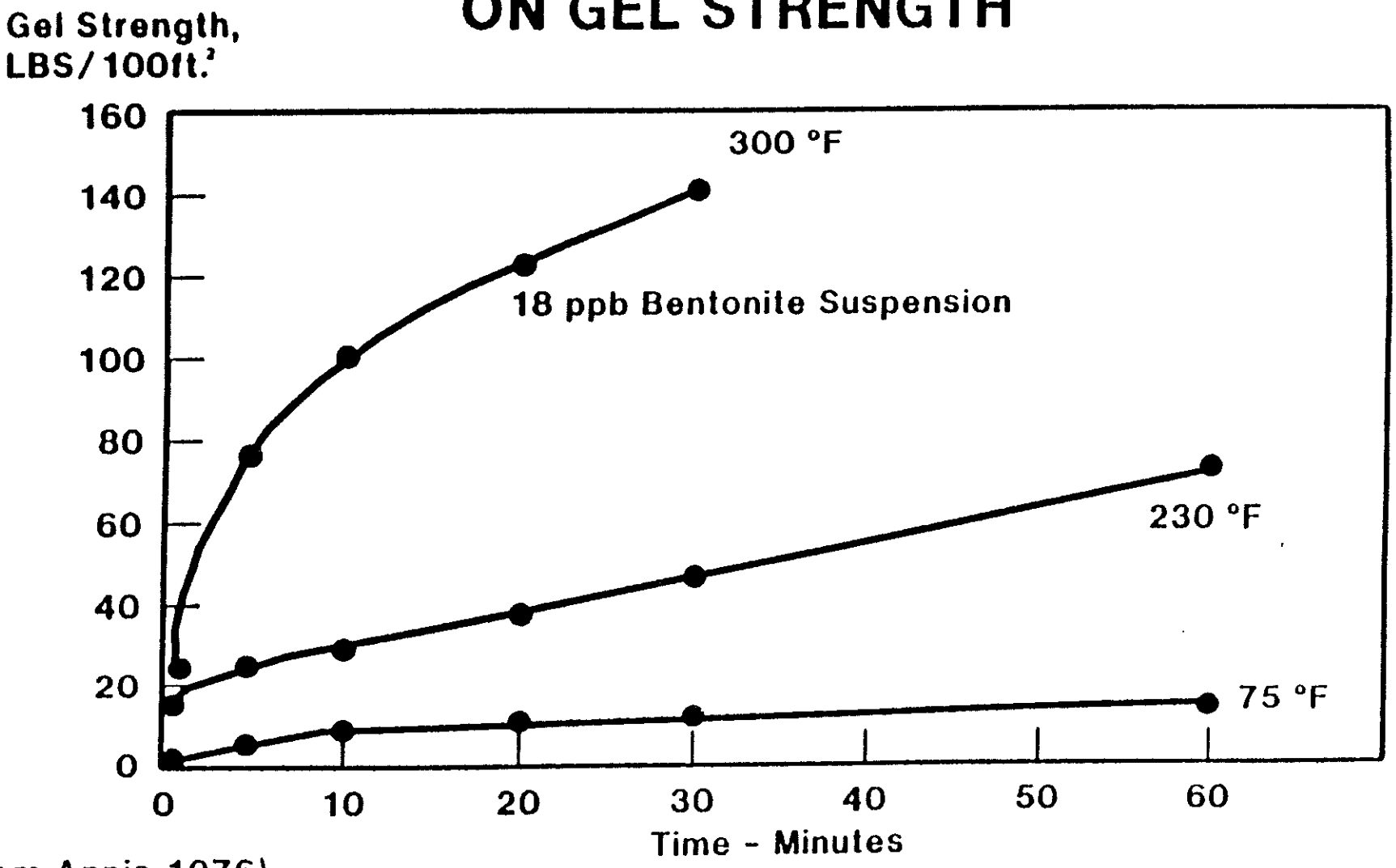

(From Annis 1976)

Ken E. Davis Associates

FIGURE 7

TABLE 2

COMPARISON OF MUD PROPERTIES WITH PROGRESSIVE GEL-STRENGTH TESTS
GYP-FERROCHROME LIGNOSULFONATE EMULSION MUDS

	SAMPLE			
	Mud E	Mud F	Mud G	
			No Treatment	3 lb/bbl
Weight, unstirred, lb/gal	11.0	10.7	10.6	
Weight, stirred, lb/gal	11.0	10.3	10.7	
Plastic Viscosity, cp	14	23	16	15
Yield Point, lb/100 sq ft	3	6	2	1
10-sec gel, lb/100 sq ft	1	2	1	0
10-min gel, lb/100 sq ft	8	8	7	3
API filtrate,	6.2	3.3	5.2	2.9
pH	10.9	10.6	10.5	10.4
Composition:				
Water % by vol	76	63	75	
Oil, % by vol	5	11	9	
Solids, % by vol	19	16	16	
Solids, % by vol	39	36	37	
Solids, SG	2.7	2.9	3.0	
Filtrate Ion Analysis:				
Chlorides, ppm	3500	400	3000	
Sulfates, epm	250	300	130	
Carbonate, epm	24	28	12	
Bicarbonate, epm	12	160	12	
Calcium, epm	44	52	44	

Progressive Gel Strengths
lb/100 sq ft

Temperature (°F)								
Time	75°	180°	75°	180°	75°	180°	75°	180°
0 minutes	1	1	2	2	1	1	0	0
3 minutes	2	3	2	5	3	8	1	1
10 minutes	8	18	8	12	7	26	3	3
30 minutes	15	40	11	18	17	58	5	5
60 minutes	27	90	18	16	29	91	6	6
2 hours	31	145	22	22	29	104	7	7
4 hours	37	190	29	42	46	172	10	10
8 hours	46	190	33	42				
16 hours	80	320	40	57	95	320	25	25

(From Weintritt and Hughes, 1965)

FIGURE 8
EFFECT OF TIME ON
GEL STRENGTH OF THREE
FIELD MUDS AT 75°F
(FROM WEINTRITT AND HUGHES, 1965)

SEE TABLE 2

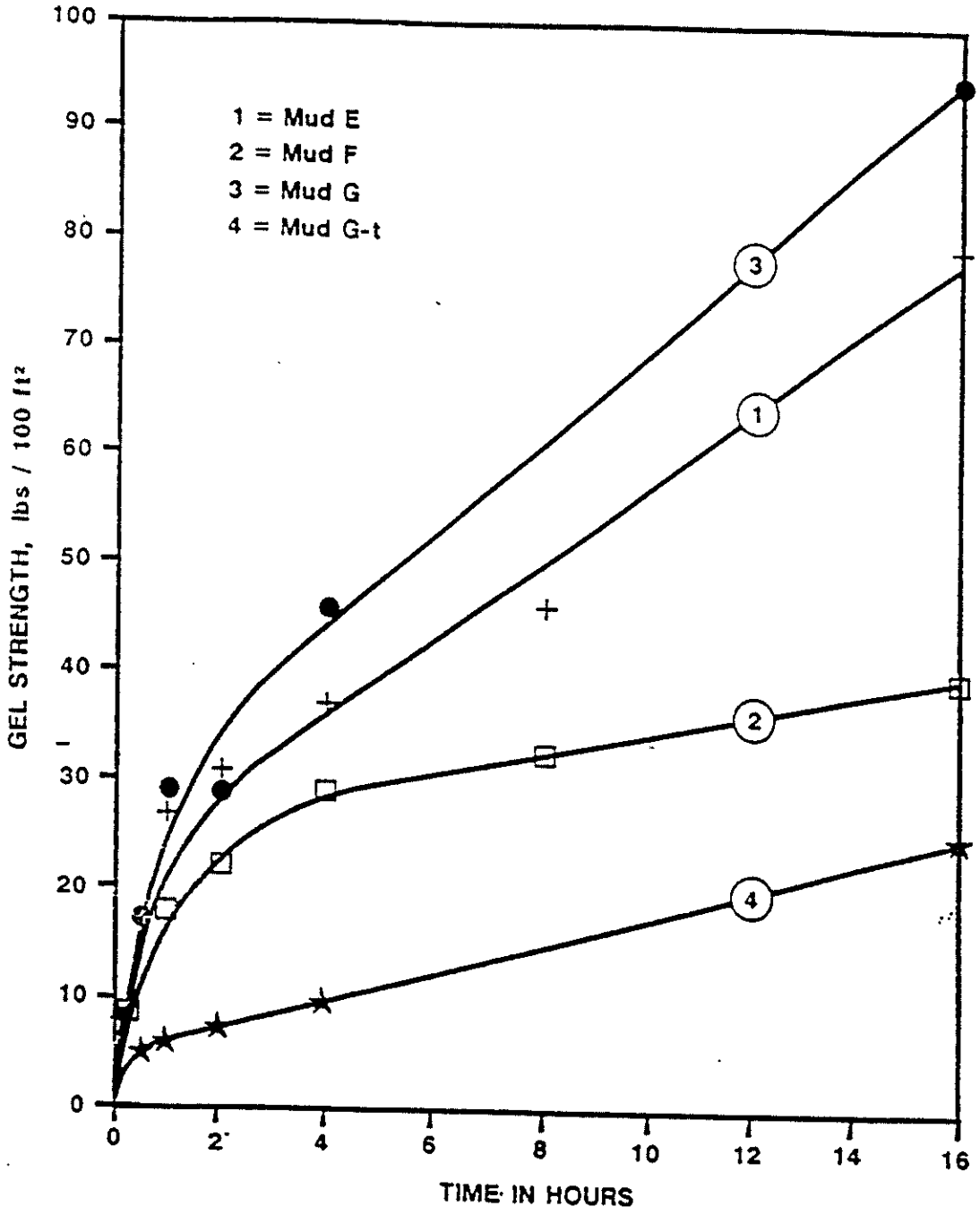

Annis (1976) was capable of investigating the gel strength up to temperatures of 350°F. Stini-Vasan (1957) observed that the gel strengths leveled off after 160°F but Annis noted that at higher temperatures a rapid increase in the gel strength was noted. Thus increased temperature, like increased bentonite concentration promotes flocculation. The temperature at which a rapid increase in gel strength occurs, represents the onset of flocculation. Therefore it is possible to expect the gel strength to increase significantly at some elevated temperature. However, Hiller (1963) noted that some clay suspensions display a decrease in gel strength with increased pressure, especially at high temperatures. He noted that the gel strength was reduced to 1/4 of its original value for a pressure increase form 300 to 8000 psi at a temperature of 302°F.

Although no direct means exists to determine the ultimate gel strength of a drilling mud at borehole conditions, it is possible to safely say that the gel strength developed in the borehole is considerably greater than that indicated by the initial and 10 minute gel strengths recorded for a given mud. These conclusions are substantially supported with subsequent lab tests run on the Fann 70 Consistometer under actual well conditions. Futher confirmation was obtained from the evaluation of a mud system taken from an abandoned well after 29 years. These data are presented in section 6.0.

Pearce (1989) made an estimation of the minimum gel strength required to suspend solid weighting material indefinitely in the drilling fluid. He said the gel strength required to prevent a spherical solid of radius r from settling can be estimated using the following equation:

$$(\rho_b - \rho_f)\, g\, (4\pi r^3/3) = G\, (\pi r^2) \qquad (5)$$

or

$$G = 4\,(\rho_b - \rho_f)\, gr/3$$

where:

P_b = density of barite (4.2 g/cm^3)
P_f = density of water (1.0 g/cm^3)
r = radius of barite particle (cm)
G = Gel Strength (dynes/cm^2)

If the maximum radius of barite is assumed to be 0.00635 cm (0.0025 inches) or larger, the largest 3% of the solids allowed in standard API barite (Gray, Darley, and Rogers, 1980, p. 533), the gel strength is calculated to be 26.6 dynes/cm^2 or 5.6 lbs/100 ft^2. This calculation shows that only minimal gel strength is required to keep over 97% of the barite weighting material suspended. Since barite density is 4.2 g/cm^3, bentonite density is 2.6 g/cm^3, and the density of sandstone is 2.65 g/cm^3, it is clear that the gel strength in the field muds will reach a value in excess of the gel strength required to maintain mud density in less than an hour. Only the larger drilled solids and the largest 3% of the barite have any potential for settling during this time period.

As indicated by the above calculation, a gel strength of 5.6 lbs/100 ft^2 is adequate to suspend the largest 3% of the barite particles in the mud. It should be noted that the development of sufficient gel strength to prevent barite from settling does not mean that drilled solids do not settle from the mud. An examination of the settled solids, as discussed later in this report, shows that the settled solids, are composed mainly of drilled solids that are significantly larger than the barite used for weight material. During the first twenty to thirty minutes of quiescence, these particles are usually large enough to settle to the bottom. In fact, the largest barite particles will also settle. However, the loss of these materials will not alter the mud weight significantly, since the large drill solids are removed at the surface, and are not included in the measured mud density. Furthermore, the largest barite particles with any potential to settle constitute less than 3% of the total barite in the mud. Therefore, the loss of these larger barite particles will not alter the mud density by more than 0.3%.

As an example consider a 10 lb/gal, mud system with the following formulation:

Component	Specific Gravity	Concentration (lbs/bbl)	Volume Percent
Bentonite	2.6	18	1.84
Barite	4.2	77	5.26
H_2O	1.0	325	92.9

A loss of 3% barite would lead to the following mud system:

Component	Specific Gravity	Concentration (lbs/bbl)	Volume Percent
Bentonite	2.6	18.1	1.84
Barite	4.2	74.1	5.08
H_2O	1.0	326	93.1

The weight of this second systems is 9.97 lb/gal, which reflects a total reduction in mud weight of 0.3% or 4 psi per 1000 feet of mud column. This number is a conservative value since less than 3% of the barite is expected to settle, the radius of the largest particles has been over estimated, and the minimum gel strength required to prevent solids from settling will be reached in less than thirty minutes.

5.0 REQUIRED DRILLING MUD WEIGHTS

Hutchison and Anderson, (1974) developed the fan chart shown in Figure 9 to illustrate the range of densities that are available for use. The maximum mud weights that may be required in oil well drilling are determined by the pressure gradients (psi/ft of depth) of the formation fluids. The pressure on the pore fluids at any given depth very seldom exceeds the pressure exerted by the weight of the earth above the depth in question, i.e., the overburden pressure. Eaton, (1969) illustrated this phenomenon by plotting the overburden stress gradient against depth for Gulf Coast formations. This plot showed the gradient at 5000 feet is approximately 0.91

FAN CHART SHOWING DENSITY RANGE OF DRILLING FLUIDS

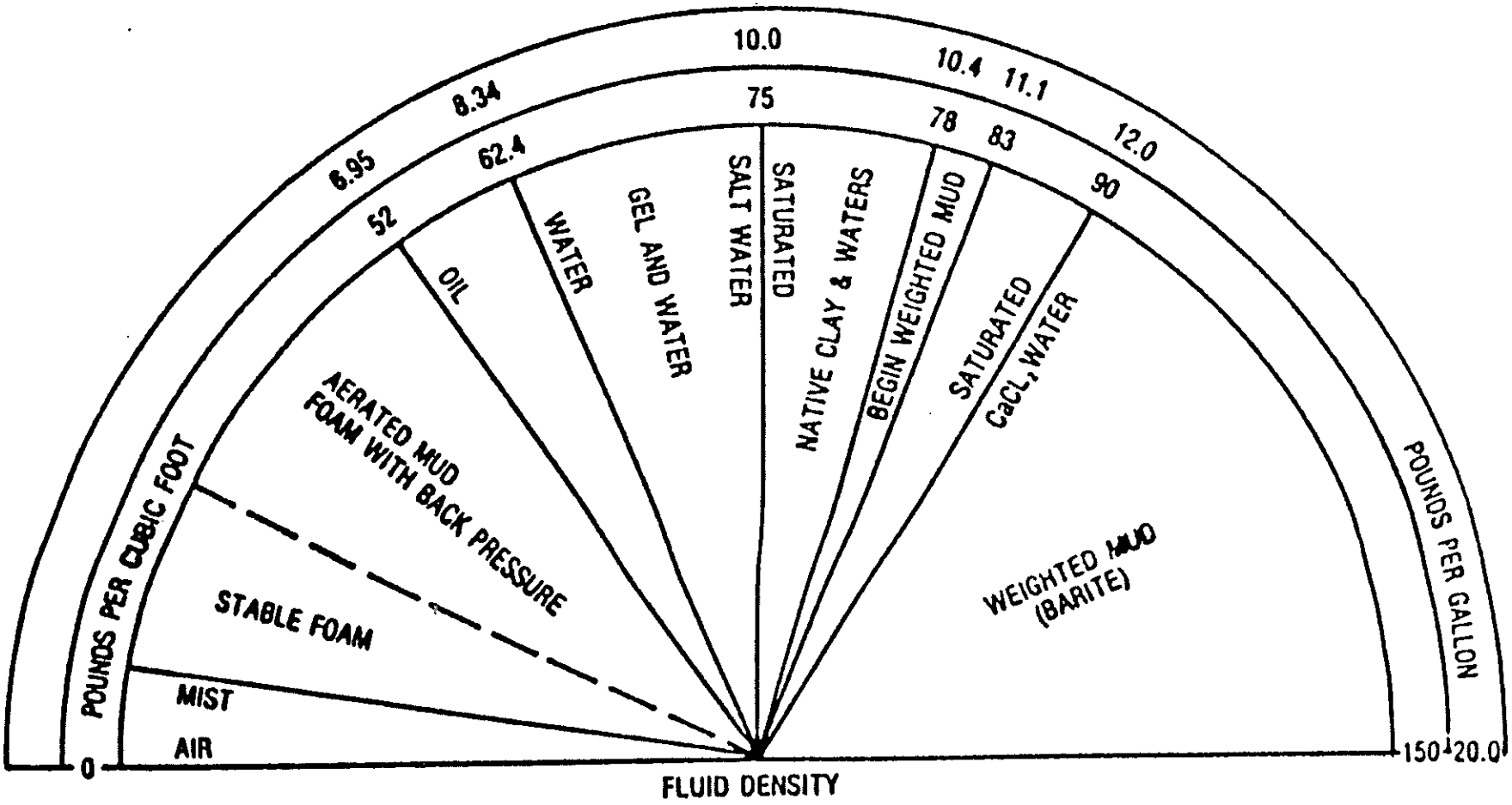

Drilling fluids can be prepared ranging in density from that of air to 2½ times that of water. (FROM HUTCHISON AND ANDERSON , 1974)

FIGURE 9

psi/ft. This gradient would be equivalent to a mud weight of 17.5 lb/gal It would therefore be expected that the highest pore fluid pressure that could be generated by the weight of the overburden at 5000 feet would be contained by 17.5 lb/gal mud. However, it is well known that the fracture gradient for formations above 10,000 feet along the Gulf Coast rarely exceed 0.80 psi/ft and that the normal pressure gradient is approximately 0.467 psi/ft. The equivalent mud density for the normal gradient would be 8.99 lb/gal. Therefore, the mud weight on wells drilled to less than 10,000 feet along the Gulf Coast rarely exceed 12.0 lb/gal.

There is some variation in the densities required for certain drilling areas. Pressures in excess or overburden are sometimes encountered. In these cases, the pore fluids are being partially contained by the strength of the rock. The highest pore pressure found in the United States thus far was reported by Parker, (1973) as 1.06 psi/ft.

6.0 RELEVANT LABORATORY DATA

Laboratory testing technique and equipment have been developed that can simulate reservoir and/or well conditions. The equipment used for these tests can accelerate the natural effects of time, temperature, and pressure. The most common of these testing techniques use the Ultrasonic Cement Analyzer (UCA) autoclave developed by Halliburton and the Fann 70 Consistometer. Cheveron's Drilling Fluid Services Laboratory has performed laboratory tests on muds using this equipment. The work was done to simulate the condition of mud left in the wellbore and/or annular space between the wellbore and casing, above the cement column.

A mud was formulated using mud additives similar to those used in actual wells located in Mississippi. This mud was subjected to filtration losses for four hours in a cell at 175° F and 500 psi pressure to simulate bottom-hole conditions. The mud slurry was then transferred to an UCA autoclave and aged for two weeks under bottom--hole temperatures and pressures. The results of this test indicated the mud developed significant compressive strength during the testing period and could only be described as a mud plug. Due to the nature of this plug it would require substantial pressure to move the plug and/or energy to restore the plug to a moveable fluid. The gel strength was too high to measure with available equipment, however, the test clearly demonstrated the mud developed some structural integrity during a relatively short test period.

Subsequently, the aforementioned tests were repeated using an NL Baroid Fann 70 Viscometer (The same type of equipment as the consistometer mentioned above.). This "state-of-the-art" instrument is capable of measuring the viscosity and gel structure of muds under downhole conditions. During these tests, a lime-treated fresh water mud, similar to the mud used in the Mississippi wells was formulated. The mud composition and gel strengths are shown on Table 3.

FANN 70 VISCOMETER GEL STRENGTH MEASUREMENTS ON A LABORATORY PREPARED LIME-QUEBRACHO MUD

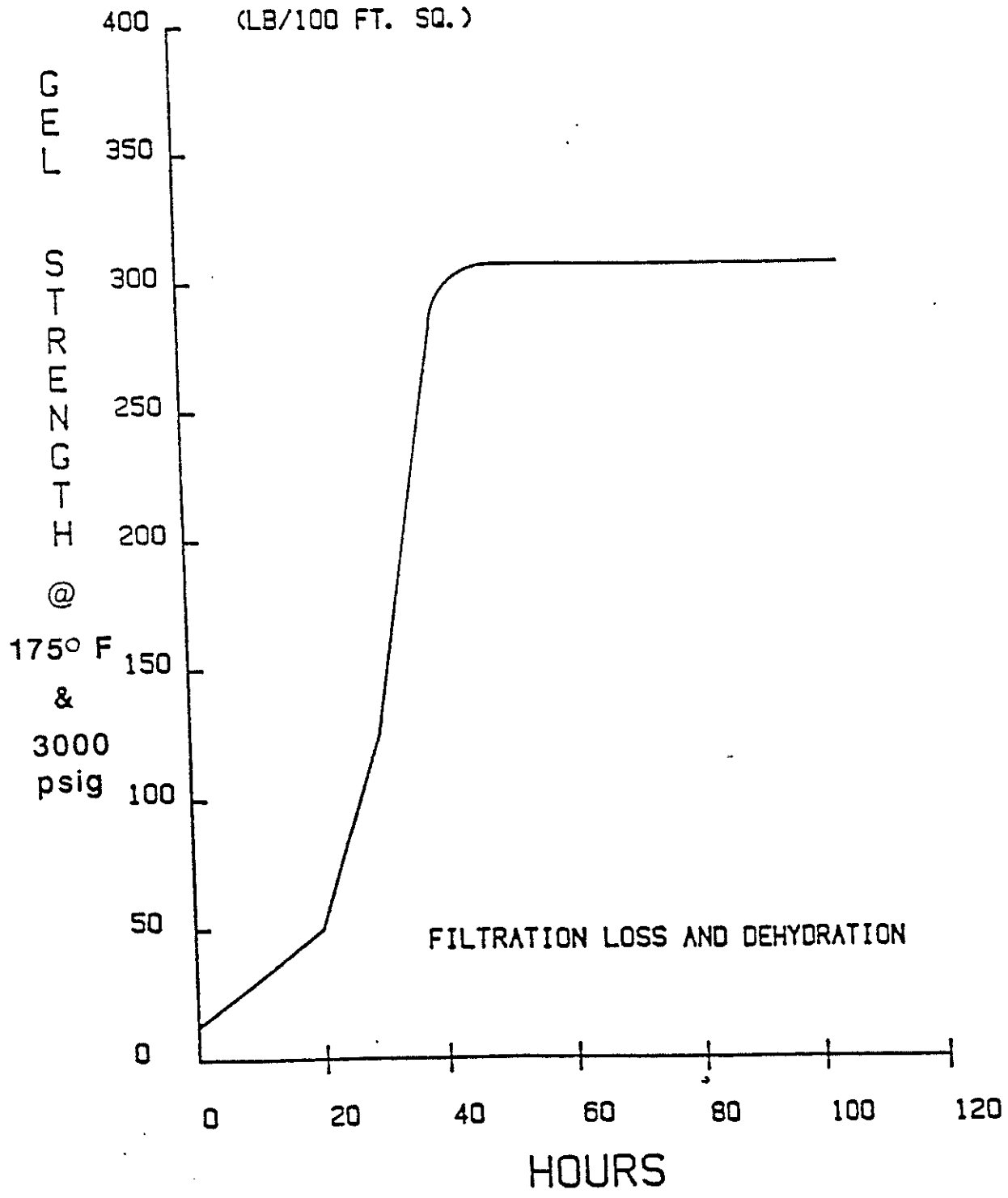

FIGURE 10

TABLE 4

PROPERTIES OF RECOVERED MUD FROM NORA SCHULZE NO. 2

0113265

SAMPLE NO.	DEPTH (ft)	MUD WEIGHT (lb/gal)	SHEAR STRENGTH (lbs/100 ft^2)	GEL STRENGTH (lbs/100 ft^2)
1	---	---	---	---
2	60	12.0	540	304
3	111	10.9	230	296
4	174	11.0	310	295
5	207	11.2	190	>320
6	240	10.9	170	284
7	273	10.7	180	237
8	306	10.9	285	254
9	339	10.5	190	288
10	372	10.9	245	272
11	405	11.1	280	220
12	438	11.1	255	222
13	471	11.1	301	292
14	504	11.1	300	230
15	537	11.0	490	292
16	570	11.0	225	217
17	603	10.9	240	236
18	636	11.3	650	>320
19	609	11.4	750	---
20	702	11.5	2100	---
21	719	10.9	4700	---
22	725	10.7	890	---
23	731	11.3	7000	---

Average mud weight using all samples - 11.1

Shear strength averaged for samples 3 through 17 - 260 lbs/100 ft^2

Average gel strength of samples 3 through 17 - 267 lbs/100 ft^2

Using the Fann 70 Viscometer, gel strengths of the mud were obtained under downhole conditions. The gel strengths were measured at intervals of 10 minutes, 30 minutes, 1, 2, 4, 8, 16, and 24 hours. During this period of time, the gel strength increased from 33 to 49 lbs/100 ft^2. A second test was performed using a mud with similar composition. The mud was first subjected to downhole conditions, such as filtration loss and temperature destabilization. Next, the gel properties of the mud were measured using the Fann 70 Viscometer at intervals up to 96 hours. In this test, the gel strengths increased to over 300 lbs/100 ft^2. Figure 10 is a graphic illustration of both these tests.

TABLE 3
RESULTS OF FANN 70 VISCOMETER TESTS
ON LABORATORY PREPARED LIME-QUEBRACHO MUD

MUD COMPOSITION

Water	.95 bbls
Aquagel	20 ppb
Rev Dust	60 ppb
Quebracho	3 ppb
Lime	2.0 ppb
Barite	36.8 ppb

Gel Strength at 175° F and 3,000 psig

Time	Pounds/100 Ft^2
10 minutes	33
30 minutes	33
1 hour	35
2 hours	43
4 hours	53
8 hours	45
16 hours	49
24 hours	50
48 hours	309
96 hours	310

Gray, Neznayko, and Gilkerson (1952) reported the thickening mechanism in lime-treated muds was the result of caustic and lime reacting with the clay minerals and silica to form hydrated alumino-silicates and silicates. These products resemble to some extent those involved in the setting of cement.

The first stage in the stiffening of limed muds is the development of a gel structure which is not significantly destroyed by mixing. Increased temperature causes a more ridged characteristic and as the cementing material concentration increases, all the liquid is retained in the solid mass. The quantity and composition of the

suspended solids affect the rate of solidification and thus the strength of the gel structure. Although the concentration of organic thinner affects gel structure development, its effect becomes negligible because the organic thinner concentration appears to decrease as the mud sets.

E.L. Cook, in his response to the Gray, Neznayko, and Gilkerson report, suggests the reduction in the organic dispersants effectiveness was related to the loss of alkalinity. A certain degree of alkalinity is necessary to render organic dispersants soluble and effective in a mud. Therefore, the loss of alkalinity through precipitation, would cause a build-up in gel strength that is additive to the gelled structure occurring as a result of the reactions of clay and silica.

Increases in gel structure development have also been experienced in other types of mud containing both organic and inorganic thinners. The mechanism is very similar and usually related to hydrolysis or precipitation of the thinner or dispersant material.

7.0 CASE HISTORY ON LONG-TERM PROPERTIES OF WATER-BASE MUD

Pearce, (1989) tested samples of a mud taken from the Nora Schulze No. 2, an abandoned well located near Corpus Christi, Texas. This well was an exploratory oil and gas well that was abandoned in November, 1959.

The samples from the reentered well were obtained by forcing 2-7/8 inch tubing into the well with a special coring device attached to the driving edge of the tubing. From a depth of 120 feet to approximately 740 feet, the tubing had to be pushed into the wellbore, because the tubing weight alone did not apply sufficient force to move the tubing through the mud. At a depth of approximately 740 feet, the tubing could no longer be pushed into the wellbore. The tubing was pulled from the well at that point, and the mud in each joint was allowed to flow into a 5 gallon plastic pail which was quickly sealed. The bottom three pup joints, each 6 feet in length, were sealed for shipment back to the laboratory because the mud in these joints did not flow easily from the tubing. From $\pm$740 feet to $\pm$1100 feet, the mud could not be cored using the above techniques, and it was therefore necessary to drill and circulate the remaining drilling fluid out of the hole to check the cement plug placed at the bottom of the surface casing.

The data obtained from these samples are presented in Table 4. It shows the average density of the mud 11.1 lb/gal over the entire 740 foot section studied. The average gel strength was 267 lb/100 ft^2 and shear strength ranged from a low of 170 lb/100 ft^2 at 240 feet to a high of 7000 lb/100 ft^2 at 731 feet.

8.0 KNOWN FORMATION FACTORS AFFECTING MUD RESISTANCE TO VERTICAL MIGRATION

An abandoned wellbore and/or uncemented annular space is subjected to numerous forces that tend to close these potential pathways to fluid migration. Along the Gulf of Mexico coastline and in areas of similar sedimentary geology the shale or clay bearing formations tend to hydrate and swell across the wellbore opening or annular space. A similar closure can also result when the hydrostatic weight of the mud column is less than the formation overburden pressure and other factors. Gnirk, (1972) made calculations that wellbore pressures in excess of 5000 psi are required to inhibit wellbore closure.

Water wetting of shale can and usually does result in borehole blockage. The instability usually results primarily from overburden pressure, pore pressure, or tectonic stress. This is true regardless of whether the clay in the shale is largely expandable or non-expandable, or whether the shale in place is brittle or plastic. Moreover, shale dispersion, hole closure or sloughing from shale swelling are all attributable to adsorption of water by shale. Davis, (1986) gave examples of normally pressured stratum drilled at depths of 5000 and 10,000 feet along the Gulf Coast using mud weights of 9.5 pound per gallon (ppg). Under these relatively common conditions the pressure differential would be 125 and 250 psi respectively. These numbers represent the pressure that filtrate from the mud is being pressed into the formation by the overbalance of hydrostatic pressure over formation pore pressure. The matrix or shale hydration force created under those conditions will be 2530 and 5060 psi respectively.

9.0 CONCLUSIONS

In review the data presented within this report indicates the following expectations for the long-term properties of mud left in wellbore and in the casing/wellbore annulus.

1. The density of clay, water-based drilling fluids should not be altered by more than 0.3% over an extended period of time, since adequate gel strength will be developed to minimize solids settling.

2. The mud density will overbalance original formation pressure by at least 100 psi or more along the length of the wellbore.

3. Gel strength will reach a minimum of 25 lbs/100 ft^2 and will most likely exceed 100 lbs/100 ft^2 over an extended period of time.

4. For cased holes, the top of the mud column in abandoned wells will be close to the surface, since the mud will remain inside the casing and hole after it is abandoned.

5. The mud left in casingless wells drilled through an unsaturated zone, may be subject to dehydration and cracking along this interval if the formations are permeable. Dehydration of the mud below this level is highly improbable, if not impossible, due to the water absorption properties of the clay.

6. Moisture tends to restore dehydrated mud and will cause the clays to swell and close off any potential cracks in the dry cake. Therefore, fluid migration pathways will close when contacted by any migrating fluid.

7. In regions such as the Gulf Coast, the stresses in the exposed formations should load the mud column and increase the hydrostatic head with time. The expected increase in hydrostatic head is caused by the effects of time, temperature, and pressure decreasing the moisture content and/or increasing the gel strength.

8. The solids in the mud cannot be forced into the formation by means other than fracturing of the weakest exposed formation.

9. Loss of water to the formation due to wellbore closure will increase both mud density and gel strength. If total compaction of the fluid in the wellbore occurs, the permeability of the compacted column could approach 10^{-9}darcies.

10. An aqueous clay-based mud provides excellent sealing characteristics and is not susceptible to the development of a micro annulus. It has good gel shear strength and is less likely to separate with time and leave water suspended above the mud column.

In all cases, for the mud systems reviewed, the long-term mud properties are expected to be more resistant to vertical migration of the fluid than the original mud. Since the original mud density typically overbalances formation pore pressure, it is realistic to expect that mud filled wellbores will not provide a conduit for fluid flow into a USDW.

REFERENCES

Annis, M.R., 1976, "High Temperature Properties of Water-Base Drilling Fluids," Journal of Petroleum Technology, August, pp. 1074-1084.

Barker, S.E., 1981, "Determining the Area of Review for Industrial Waste Disposal Wells," M.S. Thesis (Supervised by R. E. Collins), University of Texas at Austin.

Collins, R.E., and Kortum, D., 1988, "Drilling Mud as a Hydraulic Seal In Abandoned Wellbores," Proceedings of Underground Injection Practices Council, Winter Meeting, San Antonio, Texas.

Darley, H.C.H., 1969, "A Laboratory Investigation of Borehole Stability," Journal of Petroleum Technology. July, TN860/J68, pp. 883-892.

Davis, K.E. "Factors Effecting the Area of Review for Hazardous Waste Disposal Wells," Proceedings of the International Symposium Subsurface Injection of Liquid Wastes. New Orleans, Louisiana, March 3-5, 1986.

Eaton, B.E., 1969, "Fracture Gradient Prediction and Its Application in Oilfield Operations," Journal of Petroleum Technology, October, pp. 1353-1360.

Garrison, A.D., 1939, "Surface Chemistry of Shales and Clays," Petroleum Transactions. AIME, vol. 132, pp. 191-203.

Gates, G.L., and Bowie, C.P., 1942, "Correlation of Certain Properties of Oil-Well Drilling Fluids with Particle Size Distribution," U.S. Bureau of Mines Report of Investigations, No. 3645.

Gnirk, P.F., 1972, "The Mechanical Behavior of Uncased Wellbores Situated in Elastic/Plastic Media Under Hydrostatic Stress," Society Petroleum Engineers Journal, February.

Gray, G.D., Darley, H.D., and Rogers, W.F., 1980, "Composition and Properties of Oil Well Drilling Fluids," fourth edition. Gulf Publishing Company. Houston, Texas.

Gray, G.R., Neznayko, M., and Gilkerson, P.W., 1952, "Some Factors Affecting the Solidification of Lime-Treated Muds at High Temperature," API Spring Meeting, Shreveport, Louisiana.

Grim, R.E., "Clay Mineralogy," second edition. McGraw Hill Book Company, New York, 1953.

Güven, N., Carney, L.L., Malekahmadi, F., and Lee, L.J., 1984, "Factors Affecting the Behavior of Bentonite Fluids and Their In-Situ Conversion Into Cement," Sandia National Laboratories. Sand 84-7170, UC-66C.

Hiller, K.H., 1963, "Rheological Measurements on Clay Suspensions and Drilling Fluids at High Temperatures and Pressures," Journal of Petroleum Technology, July, pp. 779-789.

Hutchison, S.O., and Anderson, G.W., 1974, "What to Consider When Selecting Drilling Fluids," World Oil, October, pp. 83-94.

Magcobar Operations, Dresser Industries, Inc, 1972, Drilling Fluids Engineering Manual, Dresser Industries, Houston, Texas. Chapter 3.

Mitchell, R.F., Goodman, M.A., and Wood, E.T., 1987, "Borehole Stresses: Plasticity and Drilled Hole Effect," SPE/IADC 1987 Drilling Conference, SPE/IADC 16053, New Orleans, Louisiana, March 15-18, 1987.

NL Baroid. 1979, "Manual of Drilling Fluids Technology," NL Industries Inc. Houston, Texas. 334 pp.

Parker, C.A., 1973, "Geopressures in the Deep Smackover of Mississippi," Journal of Petroleum Technology, August, pp. 971-979.

Pearce, M.S., 1989, "Long-Term Properties of Clay, Water-Based Drilling Fluids," UIPC International Symposium on Class I & II Injection Well Technology, Dallas, Texas, May 8-11, 1989.

Rogers, W.F., 1963, "Composition and Properties of Oil Well Drilling Fluids," third edition. Gulf Publishing Company, Houston, Texas.

Stini-Vasan, S., 1957, "A Study of Temperature on Flow Properties of Non-Newtonian Drilling Fluids, 1," M.S. Thesis. University of Tulsa.

Watkins, T.E. and Nelson, M.D., 1953, "Measuring and Interpreting High-Temperature Shear Strengths of Drilling Fluids," Trans., AIME, vol. 198, pp. 213-218.

Weintritt, D.J. and Hughes, R.G., 1965, "Factors Involved in High Temperature Drilling Fluids," Journal of Petroleum Technology, June, pp. 707-716.

Plugging and Abandonment of Oil Wells: A Geomechanics Perspective

ARMA 17-451

Plugging and Abandonment of Oil and Gas Wells: A Geomechanics Perspective

Davison, J.M.
Shell Global Solutions International B.V., Aberdeen, UK
Salehabadi, M., De Gennaro, S., Wilkinson, D., Hogg, H. & Hunter, C.
Shell UK Exploration & Production, Aberdeen, UK
Schutjens, P.
Shell Global Solutions International B.V., Rijswijk, The Netherlands

This paper was prepared for presentation at the 51st US Rock Mechanics / Geomechanics Symposium held in San Francisco, California, USA, 25-28 June 2017. This paper was selected for presentation at the symposium by an ARMA Technical Program Committee based on a technical and critical review of the paper by a minimum of two technical reviewers. The material, as presented, does not necessarily reflect any position of ARMA, its officers, or members. Electronic reproduction, distribution, or storage of any part of this paper for commercial purposes without the written consent of ARMA is prohibited. Permission to reproduce in print is restricted to an abstract of not more than 200 words; illustrations may not be copied. The abstract must contain conspicuous acknowledgement of where and by whom the paper was presented.

ABSTRACT: At the end of field life, wells require permanent plugging and abandonment (P&A) as part of decommissioning activities. Some UK fields developed in the 1970's are reaching their end of field life, with UK industry estimates predicting well P&A costs over the next 30-40 years of 24 billion dollars. As well as the high financial cost, there is a significant HSSE exposure to ensure safe and reliable P&A such that no escape of hydrocarbons is possible to the near surface environment.
This paper discusses the role Geomechanics has to play in potentially reducing well P&A costs, but also ensuring integrity of the wells and formations over long time scales. Recent experience in the UK North Sea has highlighted the requirement for detailed geomechanical knowledge of the field. We will focus on three key areas for geomechanical analysis. Firstly, we discuss reservoir pressure re-charge and in-situ stress response, from simple pressure-depth plots to more complex 3-D numerical modelling of the stress changes in reservoirs and surrounding formations. An added level of complexity compared to 'conventional' geomechanical modelling is the ability to forward predict the reservoir pressure recharge over hundreds of years and the commensurate response of the in-situ stresses. Secondly, as well as the modelling of stress changes over time, Geomechanics has a key role to play in determining the opportunity of using shale creep deformation to create annular barriers in the place of cement. Lastly, in some cases the preferred P&A design for a well is not possible due to well access issues which then requires cross-flow analysis linked with the geomechanical response of permeable formations. This approach is required for containment risk assessment and application of 'as low as reasonably practicable' (ALARP) assessments for well and formation integrity. Each of these subjects will be covered with field examples from the UK North Sea which demonstrate the Geomechanical workflows employed and the impact these have had on the business.

1. INTRODUCTION

At the end of field life, wells require permanent plugging and abandonment (P&A) as part of decommissioning activities. Some UK fields developed in the 1970's are reaching their end of field life, with UK industry estimates predicting well P&A costs over the next 30-40 years of $24 billion (Decom UK, 2015). As well as the high financial cost, there is a significant HSSE exposure to ensure safe and reliable P&A such that no escape of hydrocarbons is possible to the near surface environment.

The focus of this paper is the requirement for geomechanical analysis in support of designing specific well plug and abandonment schemes. Many of Shell's UK fields are approaching end of field life and as such provide examples of specific workflows and tools used in support of the P&A planning. The Brent field, located in the UK Northern North Sea, has currently abandoned over 60% of the well stock. The experience from this activity over the last few years has thrown up many learnings about what to expect when abandoning wells more than 30 years old. As well as platform wells, there are more than 100 subsea wells to P&A. Given the large well stock and cost of offshore drilling rigs and vessels, there is an opportunity for optimising P&A activity to reduce time and hence reducing costs whilst complying with regulations and guidelines for well P&A. The sub-surface team support for Well Engineering has involved Geomechanics as part of the specialist support to help

achieve significant cost savings whilst achieving technically justified and robust P&A designs.

We will present three cases which describe the workflow and geomechanical tools used to help in the design of the P&A scheme and the integration of this understanding with other disciplines to deliver cost savings to the business. In all cases the savings are rendered whilst adhering to all current guidelines and regulations.

2. WELL P&A AND GEOMECHANICS

It is a goal of the local guidelines that the well abandonment design should achieve "restoration of the caprock" laterally across the entire wellbore; this principle is the basis for Shell UK's well P&A designs.

The most obvious input from Geomechanics to well P&A is definition of the minimum principal stress (S_3) for the field and well in question. For the UK sector of the North Sea, the minimum principal stress is the minimum horizontal stress (S_h) which is used throughout this paper.

In effect, barriers are required to be set at a depth where the formation strength is greater than the calculated maximum wellbore pressure based on the final reservoir recharge pressure and using a hydrocarbon gradient for the fluid in wellbore and/or annulus. In general terms, the higher the predicted reservoir recharge pressure, the deeper the requirement for the setting the reservoir barrier (Figure 1). This then translates into greater technical challenges in terms of executing the P&A scheme, as more wellbore equipment and tubing requires to be removed to gain access to the depth required to set the plug.

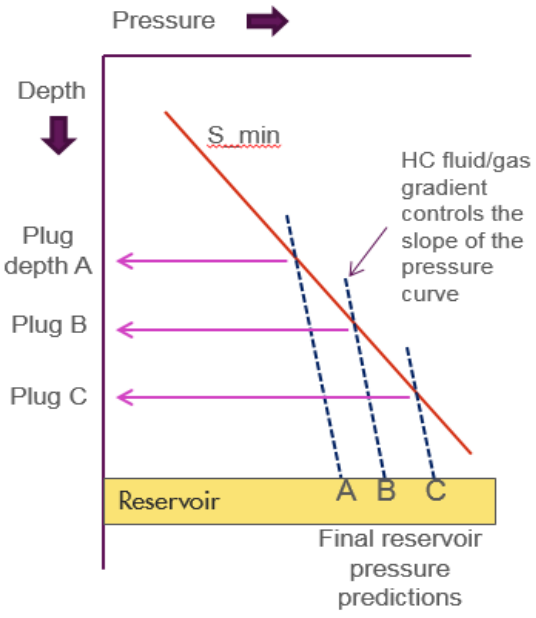

Figure 1: Pressure-depth plot illustrating the required minimum plug setting depth based on the final re-charge pressure of the reservoir unit to be isolated.

3. RESERVOIR PRODUCTION, STRESS CHANGES AND THE IMPACT ON WELL P&A

When the reservoir pressure decreases as a result of production, the effective stress increases and the porous rock compacts. Because the depleting reservoir and the non-depleting rock around the reservoir remain connected, the compaction-induced displacements at the reservoir boundaries induce deformations and stress changes in the rocks around the reservoir. These stress changes will, in turn, affect the depletion-induced effective stress change in the reservoir (coupled system, see Addis, 1997).

The isolation strategy for individual wells has to take account of the predicted final re-charge pressure. This requires forward modelling of the reservoir behaviour, including the pressure, temperature and phase changes for the full reservoir re-charge life-cycle. This is a significant technical challenge to forward model re-charge pressure taking into account connected aquifer volumes and even the impact of other producing or injecting fields which may be connected to basin-wide aquifers.

Seismic data has shown that the reservoir pressure reduction can significantly impact the stress response for significant distances in the surrounding non-depleting rock volume (Hatchell & Bourne, 2005). The depletion induced stress and strain changes result in changes to the travel times for seismic waves propagating through these rocks owing to changes in layer thicknesses. The seismic velocity is also altered by the changes in the stress and strain fields. Figure 2 shows an example of the predicted stress changes in the Shearwater field which has been validated by both 4D seismic data and measured stress reductions during drilling well intervention activity (Van Bergen et al, 2013). This example shows that stress arching above the compacting reservoir results in a reduction in the stresses above the reservoir and an increase in the stresses at the edge of the field undergoing depletion. In the example cited, the predicted reduction in minimum principal stress in the caprock of the reservoir is 1200-1500 psi, which is ~7-10% less than pre-depletion value.

If a deep-set plug is required to be set in the weakened overburden, then the plug setting depth should take into account this weakening behaviour to ensure the plug is set adjacent to a formation which has required strength given the predicted final reservoir recharge pressure. Field data has shown that an increase in reservoir pressure after initial reservoir depletion can lead to an increase in the minimum principal stress (Davison et al, 2016). How these pressure and stress changes relates to stresses and strains in the surrounding formations during long-term reservoir re-charge is still largely unknown. We are unaware of 4D seismic data which has evaluated

reservoir re-charge and stress changes over time scales of tens of years.

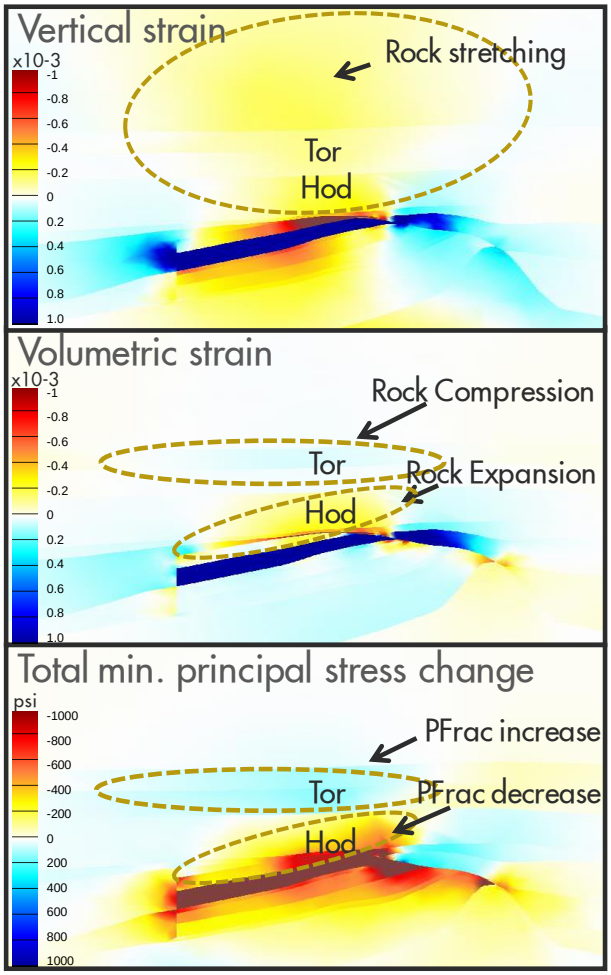

Figure 2: Predicted stress changes in Shearwater field (Van Bergen et al, 2013).

3.1. Case Study: Kingfisher Field

Kingfisher Field is located in the Central Graben of the UK North Sea region. A summary of the field can be found in Spence and Kreutz (2003). There are 2 separate reservoirs, both of Jurassic age, which have been produced independently of each other. The upper Brae reservoir has two zones separated by a thin continuous shale. The reservoir was originally overpressured to 7200 psi and currently is depleted to ~4700 psi.

The lower Heather reservoir is HPHT, with an original pore pressure of 11,900 psi which has been severely depleted to ~2300 psi. The Upper Kimmeridge Formation is the caprock to the Upper Brae reservoir and the Lower Kimmeridge Formation is the caprock to the Heather reservoir. There is approximately 1000 ft of Kimmeridge clay shale between the two reservoirs.

According to the Oil & Gas UK Guidelines (2015) it is recommended to isolate all zones with flow potential, whilst internal corporate guidelines recommend all distinct groups of permeable formations are isolated from each other and from the surface by permanent isolation, unless the risk of flow is assessed as acceptable using ALARP principles. The 2 key challenges for P&A of Kingfisher wells are:

1) How does the huge change in reservoir pressure in the Heather reservoir impact the stresses in the adjacent formations, including the Lower Kimmeridge shale, between the two reservoirs?

2) What impact do the predicted stress changes in the Kimmeridge Formation have on the ability to isolate the two reservoirs?

A mass balance recharge model for final reservoir pressure depended on the size of the aquifer model supporting the reservoir volume. The model prediction for the low case to high case covers 9900-11300 psi, with mid case ~10700 psi, which is approximately 1200 less than the original reservoir pressure.

Table 1: Summary of inputs to the Kingfisher Geomechanical Simulations

	Depletion (MPa)	Young's Modulus (GPa) Base Case (range)	Poisson's ratio	Sv (MPa)	Kh (=KH)
Upper Kimmeridge	0	10 (7-12)	0.25	86	0.8
Upper Brae reservoir	16.6	10 (10-15)	0.20	87	0.8
Lower Brae reservoir	11.7	10 (10-15)	0.20	89	0.8
Lower Kimmeridge	0	10 (7-12)	0.25	92	0.8
Heather reservoir	67.6	15 (10-25)	0.20	103	0.8

Geomechanical Model - A semi-analytical linear elastic model was used to compute the geomechanical effects of the pressure changes. It calculates displacements, strains and stresses in three orthogonal directions due to pressure changes in one or several reservoirs. The subsurface is represented as a set of horizontally layered formations each with different linear elastic properties. The tool allows screening of field-wide calculations using superposition effects of individual blocks both laterally and vertically, incorporating stiffness contrasts and pressure variations. Given some of the uncertainties in the input properties, the tool allows efficient screening of multiple scenarios to constrain the ranges of the predicted stress changes in the shale formation between the two reservoirs. A summary of the inputs to the model are given in Table 1.

Simulation Results - The results of the geomechanical simulations predict that the minimum principal stress adjacent to the heavily depleted Heather reservoir could be reduced by 6-8 MPa (870-1160 psi) (Figure 3). The range of pressures reflects the impact of different

stiffness contrasts between the Heather reservoir and the Lower Kimmeridge shale caprock. If this level of weakening occurs, and the reservoir pressure recharges to the high case aquifer volume, then it is likely that the caprock would fracture (Figure 4). In this scenario, it is likely that fracturing of the caprock would compromise the integrity of any well barrier which is attempting to isolate the Heather and Brae reservoirs.

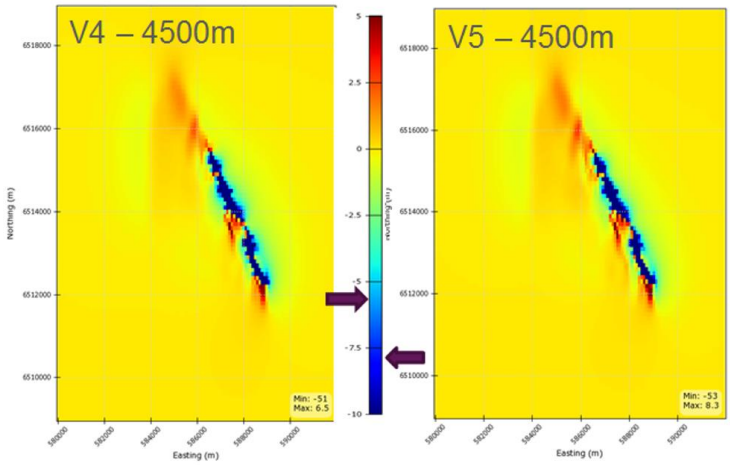

Figure 3: The figures show plan view of the change in the minimum principal stress at a depth transect of 4500 m which cuts the upper part of the Heather reservoir. The dark navy blue is the Heather reservoir itself where the S3 reduction is in the order of 50 MPa. In regions adjacent to the reservoir we can see areas of weakening in the S3 (cooler colours) and areas where S3 increases (hotter colours). V4: Young's modulus of reservoir and caprock 25 GPa, 7 GPa, respectively. V5: Young's modulus of reservoir and caprock 15 GPa, 7 GPa, respectively.

The geomechanical modelling predicts that fracturing of Lower Kimmeridge between Brae and Heather reservoirs is likely. In this scenario, there may well be natural cross-flow between the reservoirs regardless of the barriers placed in each well. We therefore considered connected volumes of the two reservoirs for re-charge pressure prediction based on comingled reservoir volumes. Figure 4 shows the final maximum re-charge pressure for the Brae and Heather reservoirs. Based on this data and information, it is proposed to isolate the two reservoirs with a single set of barriers above the Brae. The shallowest acceptable depth for the plug to isolate the combined reservoir pressure and volume is (10,330 ft TVDSS). This places the shallowest acceptable depth 2000-3000 ft above the existing production packers (12,380-13,680 ft TVDSS) in the Kingfisher wells, removing the requirement to obtain access below the production packers and removing any requirement to mill the packers to achieve access.

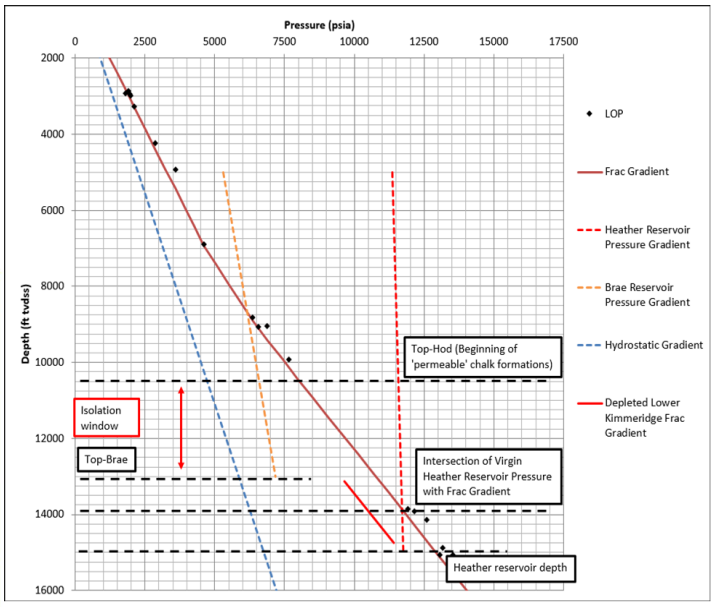

Figure 4: Pressure-depth plot showing the maximum recharge pressure for the combined Heather and Brae reservoirs. The black solid and dashed lines show the plug setting depth range available for isolation of the combined reservoir pressure and volume.

Within this 2000-3000 ft depth range of the overburden formations, the Hod Formation was chosen as the most suitable impermeable formation for the isolation plugs. By removing the requirement to place an isolation plug between the Brae and Heather reservoirs, there is no requirement during P&A operations to access the well below the production packers. This design ensures well isolation requirements are achieved and minimizes the scope of operations, saving approximately $30 million from the projected abandonment costs for the 5 wells.

4. SHALES AS ANNULAR BARRIERS

4.1. Introduction

As discussed earlier, the minimum barrier setting depth for the P&A plug is where the fracture gradient is greater than the maximum final reservoir pressure with a representative pressure gradient in the wellbore (Figure 1) and where the formation is relatively impermeable. Many wells are predicted to require milling or perforation treatments in order to meet the standards for P&A because of poor casing cement or because suitable cemented sections cannot be accessed. Experience over the last few years has shown that where the annulus is not filled with cement, sealing of the annulus may occur as a result of shale creep closing the gap between borehole wall and the casing (Williams et al, 2009). This natural sealing process eliminates the need to remediate the un-cemented annuli and as such can achieve major cost savings through the reduction in operational time. Given the remit of well abandonments is to 'restore the caprock for reservoir isolation' (Oil and

Gas UK, 2015) we could argue that shale is an obvious medium to achieve this goal.

As well as the field data and information in Williams et al (2009) for shale creep in forming annular barriers, other studies have shown the importance of clay content (Sone and Zoback, 2013) and the impact of fluid type on radial displacements (Remvik, 1995). A field test of annular closure near Orange, Texas, demonstrated that a smectite-rich shale sequence above a sandstone injection unit closed an annular gap of more than 4" in the space of 4 days (Clark et al, 2005).

4.2. Case Study: Brent Field

The isolation strategy for the Brent field includes two plugs, one to isolate the Brent and Statfjord reservoirs (plug adjacent to the Shetland Formation) and another plug to isolate the Balder Formation (set adjacent to the Horda Formation). For non-routine wells, a further plug may be placed in the Utsira shale to isolate the Skade and Frigg sands. Figure 5 shows a typical lithological column and location of cement plugs.

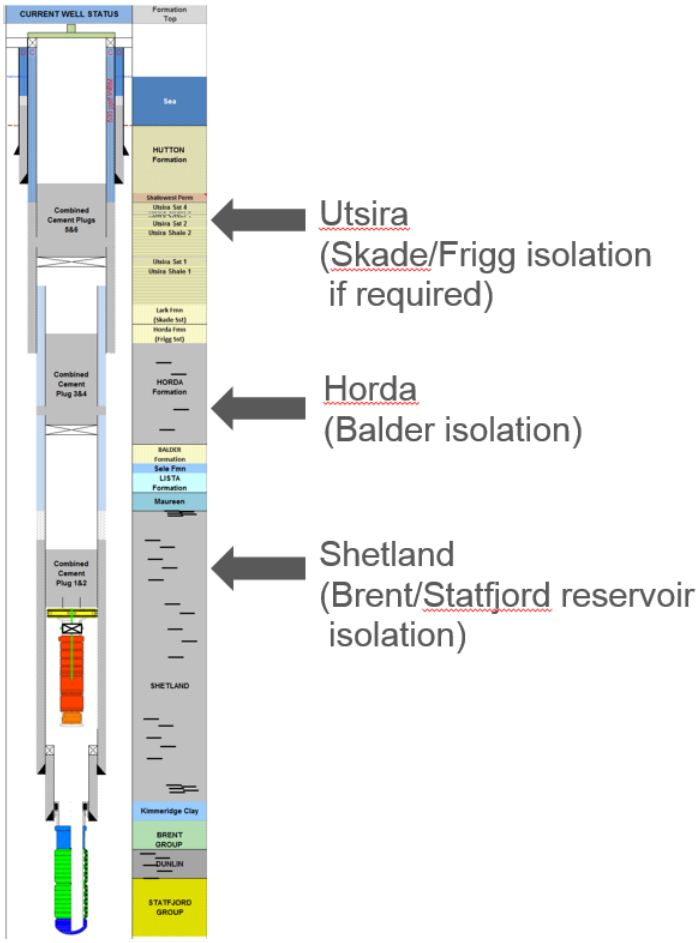

Figure 5: P&A scheme for typical Brent well.

The Horda formation is a high porosity, smectite-rich shale which often causes significant drilling problems in terms of borehole instability. For the typical Brent casing design the 13-3/8" shoe was set in top Horda Formation and the 9-5/8" shoe set in the Lower Shetland. This then requires two plugs to be set in the same section 12-1/4" hole section. The Balder and Lower Horda Formations are invariably above the theoretical top of cement which would usually require a milled plug to ensure rock-to-rock isolation for the wellbore. Since the Brent P&A activity started in 2008 numerous cement bond logs have identified the creep behaviour of the Horda formation forming a seal against the 9-5/8" casing (Figure 6). Subsequent perforating and pressure testing of these annular barriers has shown good integrity such that they can be used in well P&A. Currently on Brent this has been conservatively estimated to save over 90 day's rig-time by removing the requirement to section mill.

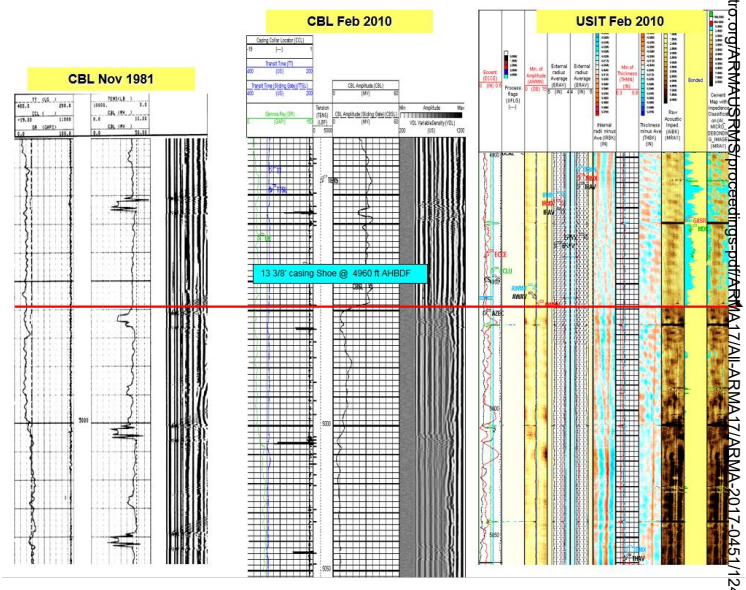

Figure 6: Cement bond log from 1981 compared to 2010. The USIT log on the right indicates once outside the 13-3/8" shoe, the Horda shale has contacted the 9-5/8" casing. This is not evident in the CBL log from 1981 (Acknowledgement: Rob Lee).

4.3. Shetland Shale Barrier

Brent well X lacked cement adjacent to the Shetland formation where the reservoir isolation barrier is required (see Figure 5). A CBL and USIT log indicated a section of mobile Shetland shale, with clear indications from the USIT log that formation behind casing (Figure 7). Based on the log data, it was decided to evaluate the sealing behaviour of the Shetland and it's use as isolation barrier in the 9-5/8" annulus. This would avoid the requirement to section mill and save approximately 3-4 day's rig time. A test was designed to evaluate the interval and provide evidence of Shetland as a viable shale for annular isolation purposes.

Figure 7 shows a schematic of the pressure test intervals. Four sets of perforations were used with each zone comprising 2ft of 6 shots per foot. A bridge plug set at the bottom of the interval of interest and the a DLT

packer was used to isolate each set of perforations whilst applying a downhole pressure to the isolated perforations. All three intervals showed no pressure fall-off or communication in the annulus to the other perforated intervals. The Shetland was therefore passed as a suitable annular isolation and only an internal cement plug was required.

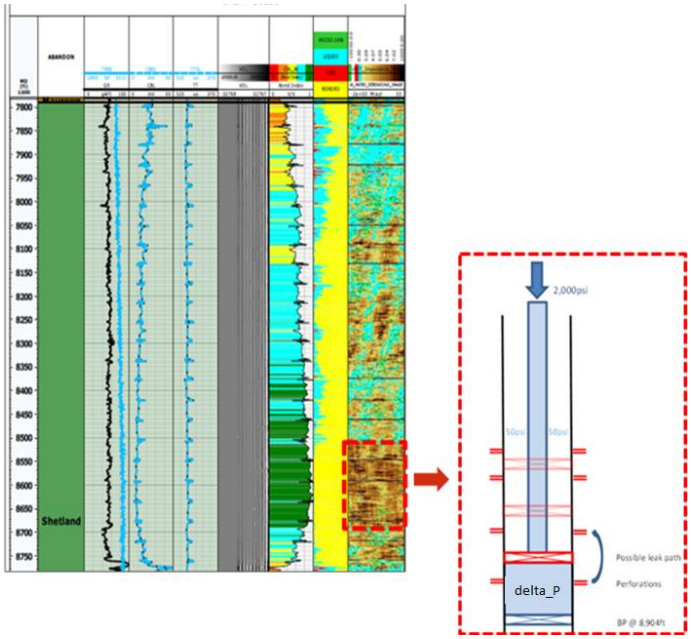

Figure 7: Pressure test of the Shetland formation where CBL/USIT logging identified shale contact with casing.

4.4. Shetland Characterisation

Why did only this section of the Shetland creep and contact the casing forming a pressure seal? The standard suite of wireline logs indicates there is nothing perhaps significantly different in this section of offset wells. Further information of the shale properties was available from di-electric constant measurement (DCM) data from shale cuttings, which were conducted to evaluate the frictional properties of shale as inputs to previous borehole stability modelling. Details of the technique and correlations with friction angle are given in Leung and Steiger (1992). The DCM value of a shale sample is heavily dependent on the type of clays present as well as the total clay content too.

Figure 8 shows the friction angle calculated from the DCM data for the Shetland Formation. There is a clear decrease in the calculated friction angle in the mid to lower Jorsalfare Formation. If we then map the squeezing shale section to the Shetland stratigraphy, the section which contacted the casing corresponds to the mid to lower Jorsalfare Formation (Appendix A). It appears subtlety in clay type and content which is not picked up in the wireline log data are the cause of this increased creep behaviour of the Shetland Formation.

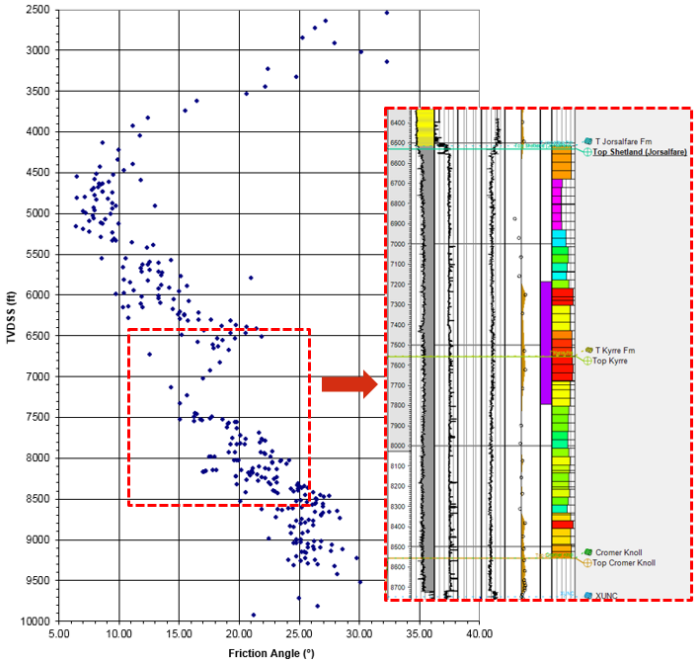

Figure 8: Brent Friction angle data calculated from DCM data. There is a clear reduction in the shale friction angle in the mid to lower Jorsalfare Formation which appears to correspond to the zone which contacted the casing.

5. X-FLOW MODELLING AND CONTAINMENT

According to the Oil and Gas UK (2015) guidelines, only those formations with a potential to flow require isolation via well barriers. If there are permeable formations which are normally pressured and have no hydrocarbon present, then they do not require to be isolated. Intrinsically, for the overburden formations, this is a relatively straightforward assessment based on the available well data and understanding of the individual formation characteristics. However, some assessment needs to be made of the potential to flow in the case of non-ideal well isolations, such as poor cement in annuli or where there are well restrictions to actually setting the cement plugs at the required depth. The purpose of the cross-flow analysis is to determine whether containment in the overburden is threatened by hydrocarbon migration though wells, faults or fractures which could ultimately lead to loss of containment and leaks to the near surface environment.

Cross-flow modelling is an invaluable tool for assessing whether an isolation strategy for a specific well is deemed ‘as low as reasonably practical’, or ALARP. This involves weighing a risk against the trouble, time and money required to control it. Flow potential and cross-flow analysis are key enablers for ALARP assessments of well P&A activity.

5.1. Case Study: Well Y

When assessing the possibility of cross-flow from reservoir to permeable formations in the overburden, there is often a distinct lack of detailed information on

the overburden sands to enable full chracterisation of them in terms of reservoir modelling. Also, given the large uncertainty in subsurface fluid flow and dynamics, we utilized a tool which allowed consideration of cross-flow upwards from the reservoir, via a well, where permeable formations, or 'thief zones', can be charged. Further upward migration of the hydrocarbons is only possible if the formation pressure exceeds the minimum principal stress overlying the sand unit.

The calculation steps and workflow are shown in Figure 9. The lower reservoir is connected to the next sand in the sequence and complete ideal gas type mixing is used to obtain an average pressure in connected volume. After mixing, a gravitational correction is made to get to a realistic gas gradient across the two connected sands. After each connected volume of sand is initiated, then we calculate the pore pressure at the top of the sand and compare this to the minimum principal stress at that depth. If the pore pressure is greater than the S_3, then seal is breached and gas can then migrate upwards to the next sand.

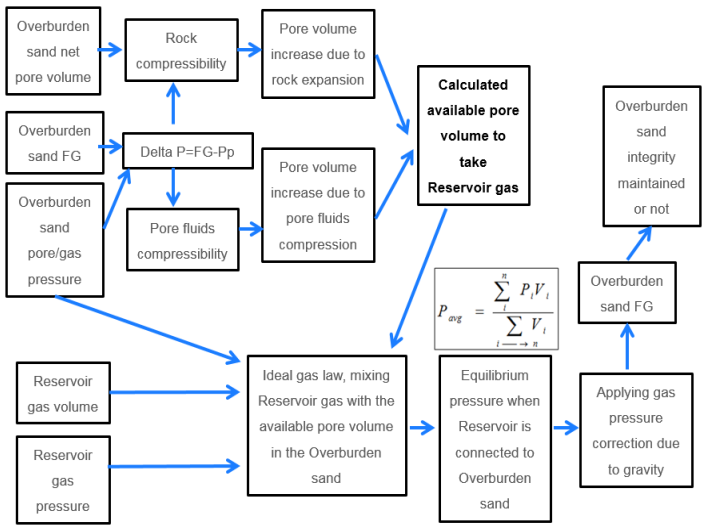

Figure 9: Workflow for cross-flow analysis using connected tank volumes with the S_3 controlling migration vertically through various sand units.

5.2. Results

This approach was used to evaluate cross-flow and containment in a well where borehole restrictions below 13-3/8" shoe meant access to deeper sections of the well were not deemed possible. A perfect connection from the reservoir to an overburden sand unit was invoked where the milled cement plug was placed above in a sealing shale (Figure 10).

The reservoir re-charge mass balance model predicted the pressure and volumes of gas, oil and water over hundreds of years. Cross-flow was simulated in time steps where the volume of gas and pressure were used to evaluate containment in the overburden sand thief zone. The same workflow is used to determine the maximum pressure and gas volume in the reservoir which is required to exceed the S_3 above the thief zone in the overburden.

Figure 11 shows the combinations of reservoir pressure (P) and gas volume (V) to exceed the S_3 of the shale above the sand unit. To simulate worst case scenario, a closed boundary condition for the overburden sand was assumed. The mass balance model for the reservoir recharge simulations were then plotted on the same pressure – volume chart. As figure 11 shows the actual high case reservoir recharge model does not have the required combination of high enough pressure and volume of gas to cause loss of containment in the overburden thief zone. This workflow and results can be used to ensure that a designed isolation strategy is ALARP given the complex well architecture.

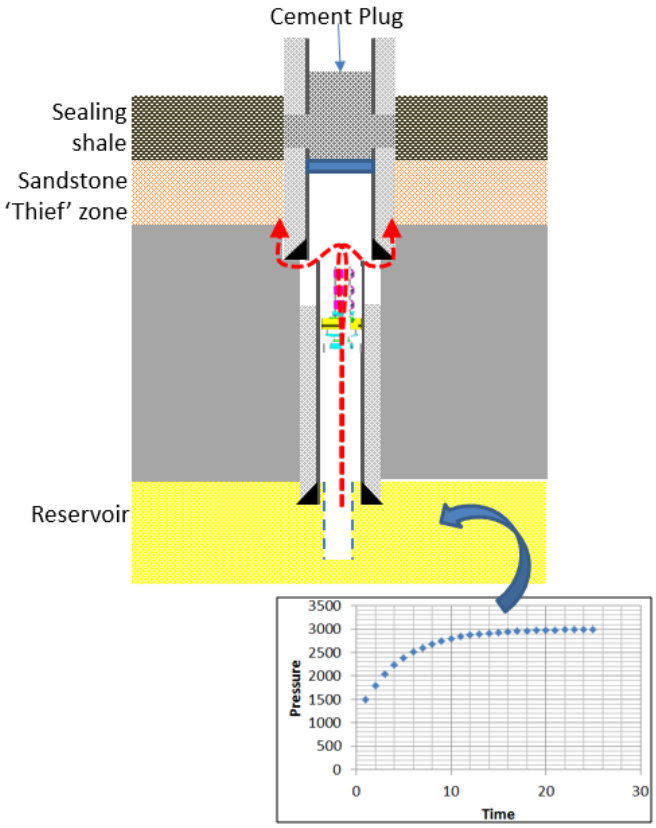

Figure 10: Schematic of Well Y where restrictions below the 13-3/8" shoe meant access to deeper sections of the well were limited.

There are limitations with this approach where the transience of the reservoir re-charge is not coupled to the gas migration in the overburden sands. Given the scope of determining flow potential for P&A assessments, this is a key area for further development of tools and workflows.

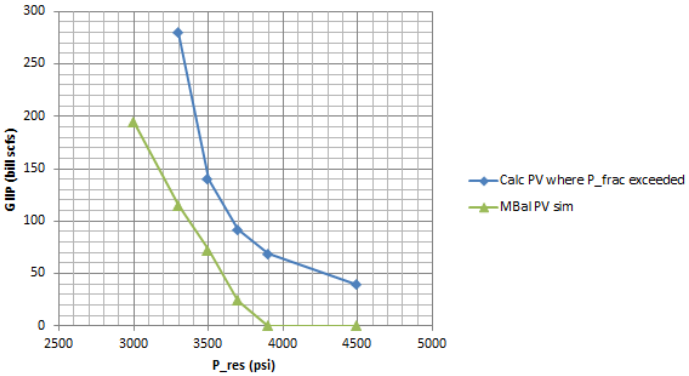

Figure 11: Cross-flow analysis and containment assessment for the connected reservoir to the thief zone. The predicted reservoir pressure and volume required to fracture the caprock is represented by the blue line whereas the high case reservoir re-charge simulation is represented by the green line. This shows the reservoir gas volume and pressure was insufficient to lead to los of containment in the thief zone.

6. CONCLUSIONS

Our recent P&A activity in the North Sea has involved multi-disciplinary Sub-Surface and Well Engineering teams to design compliant isolation strategies, whilst also reducing cost. Geomechanics has become an integral part of the sub-surface teams, providing key data and information to the isolation strategies.

This paper has demonstrated how an improved understanding of Geomechanics ensures well isolation strategies are designed to consider the long term conditions in the field and to deliver robust well abandonments with the minimum operational risk and cost. The examples provided for shale annular barriers and stress changes above an HPHT reservoir demonstrate the impact that Geomechanics workflows can bring to the field isolation designs.

Lastly, using cross-flow and containment analysis by integrating flow potential and geomechanical analysis, led to the design of the isolation strategy for a non-routine well. Geomechanical analysis of cross-flow and containment are key for the design of ALARP isolation strategies and this is a significant area for future development in tools and workflows.

7. ACKNOWLEDGEMENTS

The authors would like to thank their respective management for permission to publish this paper. The many asset staff who facilitated these studies are duly acknowledged.

8. REFERENCES

Addis, M.A. 1997. The Stress-Depletion Response of Reservoirs. Paper SPE 38720, SPE ATCE, San Antonio, Texas, 5-8 Oct 1997.

Clark, J.E., Bonura, D.K., Papadeas, P.W. & R.R. McGowen (2005). GulfCoast Borehole Closure Test Well near Orange, Texas. Underground Injection Sience and Technology, edited by Tsang, C.F. & Apps, J.A. Developments in Water Sciences, 52. Elsevier, 2005.

Davison, J. M., Foo, I., Ellis, F., & Proughten, A. (2016, June 26). The In-Situ Stress Response of Reservoirs to Pressure Reduction Followed by Pressure Increase: Depletion and Rebound Stress Paths from Two Case Studies. American Rock Mechanics Association. 2016-281, June 2016.

Decomm North Sea (2015). The Real Costs of Decommissioning. (http://decommnorthsea.com/news/The-Real-Costs-Of-Decommissioning).

Leung, P. K., & Steiger, R. P. (1992, January 1). Dielectric Constant Measurements: A New, Rapid Method to Characterize Shale at the Wellsite. Society of Petroleum Engineers. doi:10.2118/23887-MS

Oil and Gas UK (July 2015). Guidelines for the Abandonment of Wells, Issue 5, 2015.

Remvik, F. (1995, January 1). Shale-fluid Interaction And Its Effect On Creep. International Society for Rock Mechanics, 8th Congress, 1995, Paper 064.

Sone, H., & Zoback, M.D. (2013). Mechanical Properties of Shale Gas Reservoir Rocks -Part 2: Ductile creep, brittle strength and their relation to the Elastic Modulus. Geophysics, Vol. 78, No. 5 (September-October 2013); P. D393–D402, 10.1190/GEO2013-0051.1

Spence, S.& Kreutz, H. (2003). The Kingfisher Field, Block 16/8a, UK North Sea. Geological Society, London, Memoirs, v. 20:305-314.

Van Bergen, P., De Gennaro, S., Fairhurst, F., Hurry, R., Concho, M., Watson, J., Bevaart, M. (2013, September 3). Shearwater - Securing the Chalk - Effects of Depletion of a HPHT Reservoir on Chalk Overburden. Society of Petroleum Engineers. doi:10.2118/166574-MS

Williams, S. M., Carlsen, T., Constable, K. C., & Guldahl, A. C. (2009, January 1). Identification and Qualification of Shale Annular Barriers Using Wireline Logs During Plug and Abandonment Operations. Society of Petroleum Engineers. doi:10.2118/119321-MS

9. APPENDIX A

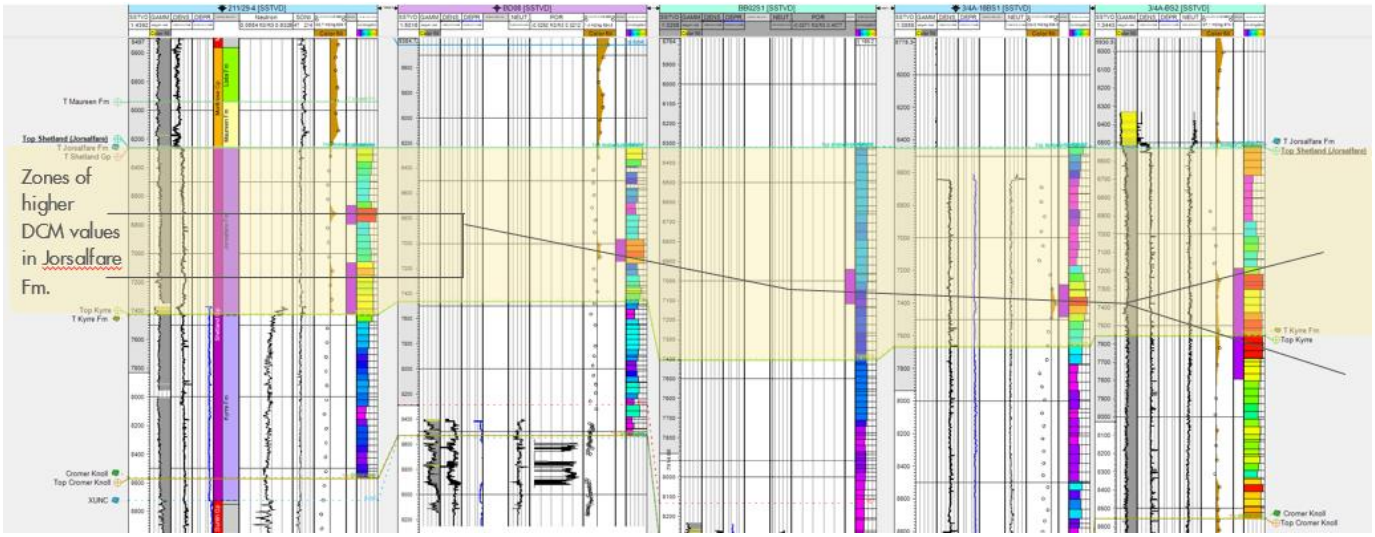

The zones of higher DCM values are referenced to the stratigraphy for wells where DCM is available. The stratigraphic section where the Shetland barrier was tested and validated coincides where the elevated DCM occurs.

Provenance and Sedimentary Context of Clay Mineralogy in an Evoling Forearc Basin, Upper Cretaceous-Paleogene and Eocene Mudstones, San Joaquin Valley, California

minerals

MDPI

Article

Provenance and Sedimentary Context of Clay Mineralogy in an Evolving Forearc Basin, Upper Cretaceous-Paleogene and Eocene Mudstones, San Joaquin Valley, California

Andrew Hurst [1,*], Michael J. Wilson [1], Antonio Grippa [1], Lyudmyla Wilson [1], Giuseppe Palladino [1], Claudia Belviso [2] and Francesco Cavalcante [2]

[1] School of Geosciences, University of Aberdeen, King's Collage, Aberdeen AB24 3UE, UK; michaelwilson191@btinternet.com (M.J.W.); antonio.grippa1@abdn.ac.uk (A.G.); lwilson@abdn.ac.uk (L.W.); giuseppe.palladino@abdn.ac.uk (G.P.)

[2] Istituto di Metodologie per l'Analisi Ambientale IMAA-CNR, 85050 Tito Scalo, Italy; claudia.belviso@imaa.cnr.it (C.B.); francesco.cavalcante@imaa.cnr.it (F.C.)

* Correspondence: ahurst@abdn.ac.uk

Abstract: Mudstone samples from the Moreno (Upper Cretaceous-Paleocene) and Kreyenhagen (Eocene) formations are analysed using X-ray diffraction (XRD) and X-ray fluorescence (XRF) to determine their mineralogy. Smectite (Reichweite R0) is the predominant phyllosilicate present, 48% to 71.7% bulk rock mineralogy (excluding carbonate cemented and highly bio siliceous samples) and 70% to 98% of the <2 µm clay fraction. Opal CT and less so cristobalite concentrations cause the main deviations from smectite dominance. Opal A is common only in the Upper Kreyenhagen. In the <2 µm fraction, the Moreno Fm is significantly more smectite-rich than the Kreyenhagen Fm. Smectite in the Moreno Fm was derived from the alteration of volcaniclastic debris from contemporaneous rhyolitic-dacitic magmatic arc volcanism. No tuff is preserved. Smectite in the Kreyenhagen Fm was derived from intense sub-tropical weathering of granitoid-dioritic terrane during the hypothermal period in the early to mid-Eocene; the derivation from local volcanism is unlikely. All samples had chemical indices of alteration (CIA) indicative of intense weathering of source terrane. Ferriferous enrichment and the occurrence of locally common kaolinite are contributory evidence for the intensity of weathering. Low concentration (max. 7.5%) of clinoptilolite in the Lower Kreyenhagen is possibly indicative of more open marine conditions than in the Upper Kreyenhagen. There is no evidence of volumetrically significant silicate diagenesis. The main diagenetic mineralisation is restricted to low-temperature silica phase transitions.

Keywords: clay minerals; mudstone; smectite; provenance; forearc basin

Citation: Hurst, A.; Wilson, M.J.; Grippa, A.; Wilson, L.; Palladino, G.; Belviso, C.; Cavalcante, F. Provenance and Sedimentary Context of Clay Mineralogy in an Evolving Forearc Basin, Upper Cretaceous-Paleogene and Eocene Mudstones, San Joaquin Valley, California. *Minerals* **2021**, *11*, 71. https://doi.org/10.3390/min11010071

Received: 4 November 2020
Accepted: 6 January 2021
Published: 13 January 2021

1. Introduction

Recently, the Moreno and Kreyenhagen Fms became a focus of global geological interest because they host the two largest and best-exposed outcrops of giant sand injection complexes, the Panoche Giant Injection Complex (PGIC) and the Tumey Giant Injection Complex (TGIC), ~400 km^2 and >200 km^2, respectively [1–4] (Figure 1). As part of understanding the background geological setting of the mudstone-dominated host strata for the PGIC and TGIC, samples were collected and analysed from formal lithostratigraphic units in the Moreno Fm and informal units (Upper and Lower) in the Kreyenhagen Fm. Given the widespread occurrence and large outcrops of the Moreno and Kreyenhagen formations (henceforth Moreno Fm and Kreyenhagen Fm) in the San Joaquin Valley and their significance to petroleum systems, the paucity of mineralogical data in the public domain is surprising. According to Jay [5], the Kreyenhagen is "virtually unmentioned in the resource shale literature" despite producing significant volumes of hydrocarbons continuously since 1956.

The smectitic dominance of the phyllosilicate fraction in the Kreyenhagen Fm is known to the southeast of our study area, where 51 mudstone samples from boreholes were investigated [6], and a single outcrop sample was investigated in later studies [7,8], approximately 220 km and 55 km from our study area, respectively. Excellent outcrop [2,3] allows continuous sampling through the stratigraphy of both formations and enables the geological evolution of the San Joaquin Basin to be evaluated from the perspective of the fine-grained sedimentary record. Specific attention is given to the origin of smectite in the context of volcanic activity and quiescence in the evolving Sierra Nevadan magmatic arc. In the present study, a broader evaluation of the lithostratigraphy and mineralogy of the San Joaquin Basin was performed. The provenance, weathering, and composition of source terrane were studied by X-ray diffraction (XRD) and X-ray fluorescence (XRF). This approach is a useful tool for the investigation of fine-grained sedimentary rock [9,10].

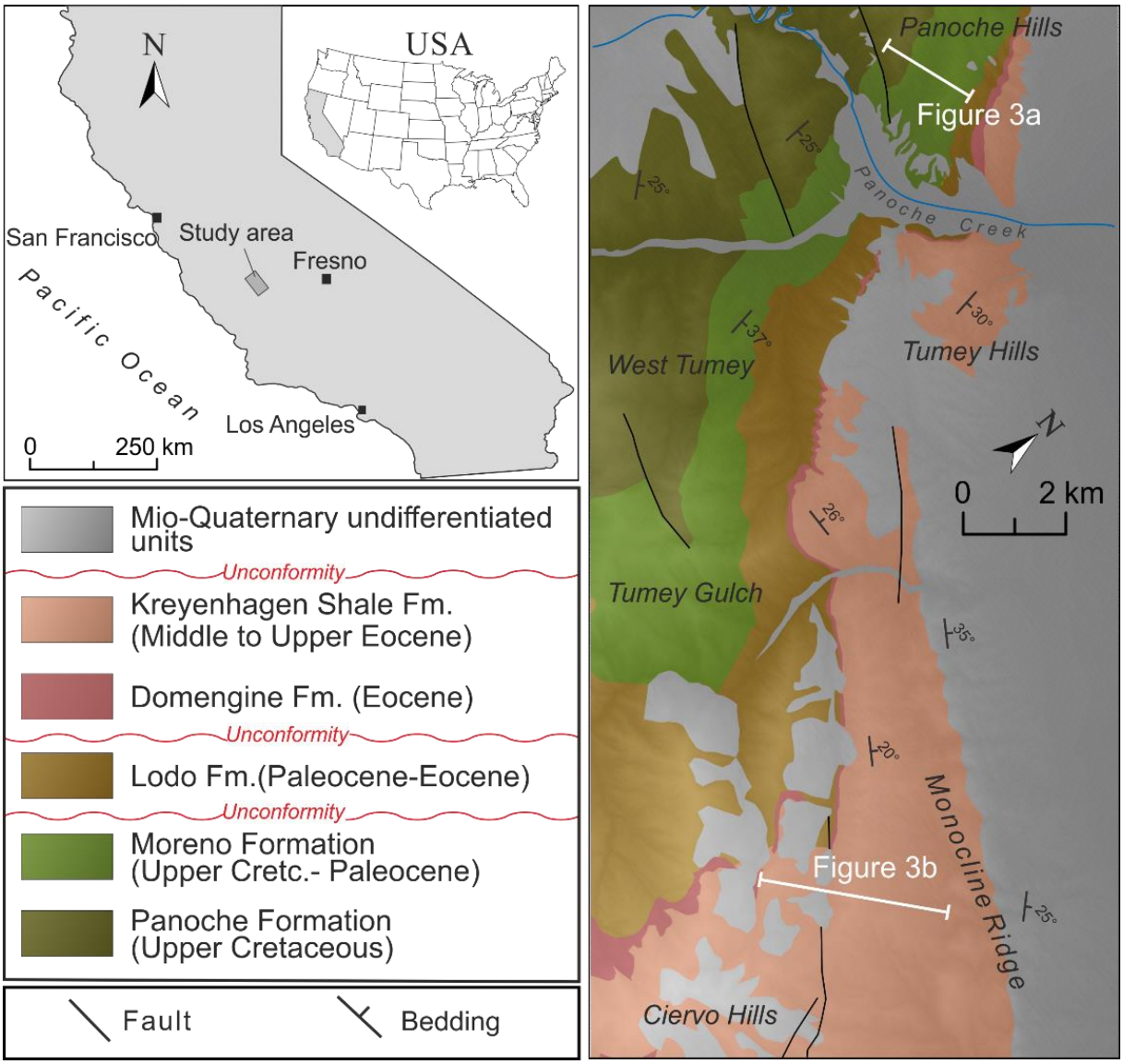

Figure 1. The location of the giant sand injection complexes in central California and a geological map. The Panoche Giant Injection Complex (PGIC) [1] occurs within Upper Cretaceous and Danian strata Panoche and Moreno formations. The white bar in the Panoche Hills is the approximate line of the section sampled and represented in Figure 3a. The Tumey Giant Injection Complex (TGIC) occurs within the Eocene Kreyenhagen Formation. The white bar along Monocline Ridge is the approximate line of the section sampled and represented in Figure 3b.

2. Geological Background

During the Upper Cretaceous, large sediment loads were deposited in the San Joaquin Basin, resulting from the rapid erosion of the Sierra Nevada arc. The basin gradually extended due to migration of magmatic activity to the east combined with the formation of the trench to the west [11]. Most of the Moreno Fm examined in this study comprises predominantly fine-grained Maastrichtian slope deposits (Figure 2), but the uppermost unit, the Dos Palos Mbr, deposited in shallower water on the upper slope. In the outcrop area, a regional unconformity truncates the top of the Moreno Fm (Figure 2). In the Eocene, rapid deformation of the basin occurred, and periods of uplift and subsidence ensued. The latter caused a regional marine transgression, associated with folding and thrusting at the basin margins. In the area of the TGIC outcrop, a regionally developed unconformity eroded deeply (in some cases >50 m) into the TGIC locally reworking shallow parts of the injection complex (Figure 2).

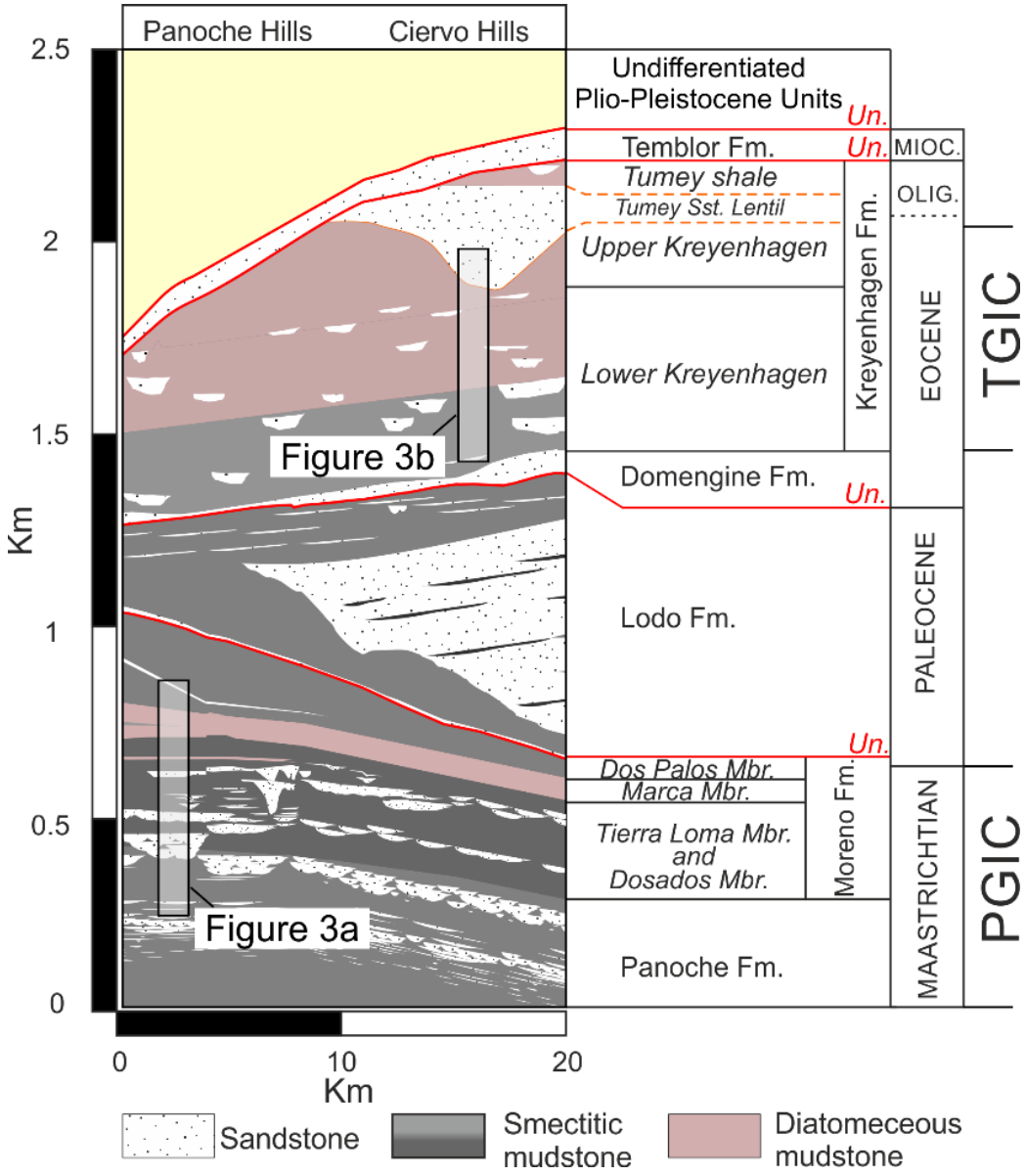

Figure 2. The geological cross-section of the upper part of the Great Valley Sequence in the area from the Panoche to Ciervo hills with locations of Figure 3a,b. The term *Un* (red) refers to regionally developed unconformities. For simplification, sandstone intrusions are omitted from this figure. Abundant turbiditic sandstone is depicted in the Maastrichtian to Paleogene.

The Eocene–Oligocene boundary is not preserved. Further tectonic movements occurred in the Oligocene, creating normal and thrust faulting and anticlinal folding at the basin peripheries [12]. In the San Joaquin Basin, the Kreyenhagen Fm records approximately 16 million years of slope and basin sedimentation from Middle Eocene to Early Oligocene, an extension of the Sierra Nevada forearc that was created during the subduction of the Pacific plate beneath the North American plate. The formation is predominantly mudstone (also known as the Kreyenhagen Shale), up to 3000 m thick, which is present at outcrop and in boreholes but includes turbiditic and transgressive shallow marine sandstone. Much of the mudstone is bio siliceous and, in some areas are important hydrocarbon source rocks [7,8]. It contains sequences where opal CT is common.

3. Materials and Methods

3.1. Materials

Mudstone samples were collected from transects through the outcrop of the Upper Cretaceous to Lower Paleocene Moreno Formation (1) and the Eocene of the Kreyenhagen Formation (3) (Figure 3). Moreno Fm samples were exclusively from the Right-Angle Canyon locality (RAC, Figure 3a), the geology of which was most recently described in Grippa et al. [13]. Regional thickness variations preserved in the Moreno Fm range from 430 m to >830 m with approximately 550 m present in RAC. Lamination in mudstone is locally preserved throughout the Moreno Fm., becoming less pervasive upward. Dense hydraulic fractures are present in parts of the Tierra Loma Mbr [2] often adjacent to large sandstone intrusions. Mudstone samples from the Kreyenhagen Fm are either dark brown (Lower Kreyenhagen) or pale pink/grey (Upper Kreyenhagen) (Figure 3b). Faint lamination is preserved in the Lower Kreyenhagen but is sparse in the Upper Kreyenhagen. Extensive areas of dense, intensive hydraulic fractures are present in the Upper Kreyenhagen. The Upper Kreyenhagen is lithified and generally of low density, from which a high content of opaline silica is inferred.

3.2. Methods

All samples were analysed using X-ray fluorescence (XRF) and X-ray diffraction (XRD) to determine chemical and mineralogical compositions of whole-rock samples (XRF and XRD) and clay fractions (XRD). Chemical analyses were carried out for major elements according to the procedure of Franzini et al. [14]. The sample preparation technique and the fusion procedure were those of Claisse [15]. A mixture containing 0.210 g of sample and 7.000 g of flux (50% Lithium tetraborate, $Li_2B_4O_7$, and 50% Lithium metaborate, $LiBO_2$), corresponding to a 1:30 sample/borate dilution, was carefully homogenized in a 95Pt/5Au crucible using Claisse Fluxer-Bis!® automatic apparatus (Malvern Panalytical, Malvern, UK). Ammonium iodide anhydrous powder was added as a non-wetting agent. The mixture was fused at 1000 °C for 20 min while continuously stirring the melt. When the sample was completely dissolved and any reaction ceased, the melt was poured into 95Pt/5Au/2Rh plate and cooled slowly. After cooling the melt formed a glass disc (ø = 32 mm), which was directly analysed by ARL 9400 XP+ sequential X-ray spectrometer (Thermo Fisher Scientific, Waltham, MA, USA) [16].

For the whole-rock XRD investigation, samples were gently crushed and then ground using a vibratory agate disc mill comminuting by friction. The particle size obtained was <5 μm. To separate the clay fraction (<2 μm), the whole sample was gently crushed (not ground) in an agate mortar, disaggregated in distilled water overnight, and then separated by settling in distilled water according to Stoke's law. Clay suspensions for quantitative analysis were saturated with Mg^{2+} cations using 1 N $MgCl_2$ solution. Oriented mounts were prepared by settling clay suspensions (concentration of 5 mg/cm^2 [17]) on glass slides. Each specimen was analysed in an air-dried state, glycolated at 60 °C for 8 h and heated at 375 °C for 1 h [18].

XRD analyses were performed on whole-rock samples and clay fractions using a Rigaku Rint Miniflex powder diffractometer (Rigaku, Tokyo, Japan) with Cu-Kα radiation,

sample spinner, and Cu anode at a voltage of 30 kV and a current of 15 mA. Mineralogical analyses of bulk samples were carried out on random mounts using side loading of bulk specimens, to guarantee a satisfactory reproducible density and random orientation [19]. Data were collected in a 2–70° range of 2θ with 0.02° step and a speed of 5 s/step. Data from the clay fraction were collected in the 2–33° range of 2θ with a step of 0.02° and a speed of 5 s/step. The content of clay minerals in <2 μm fractions was estimated by the peak areas on both glycolated and heated oriented mounts [20]. To distinguish between smectite and illite/smectite mixed-layer clay, the XRD patterns of glycolated clays were used as proposed by Moore and Reynolds [18]. The XRD patterns were processed using the WINFIT computer program [21].

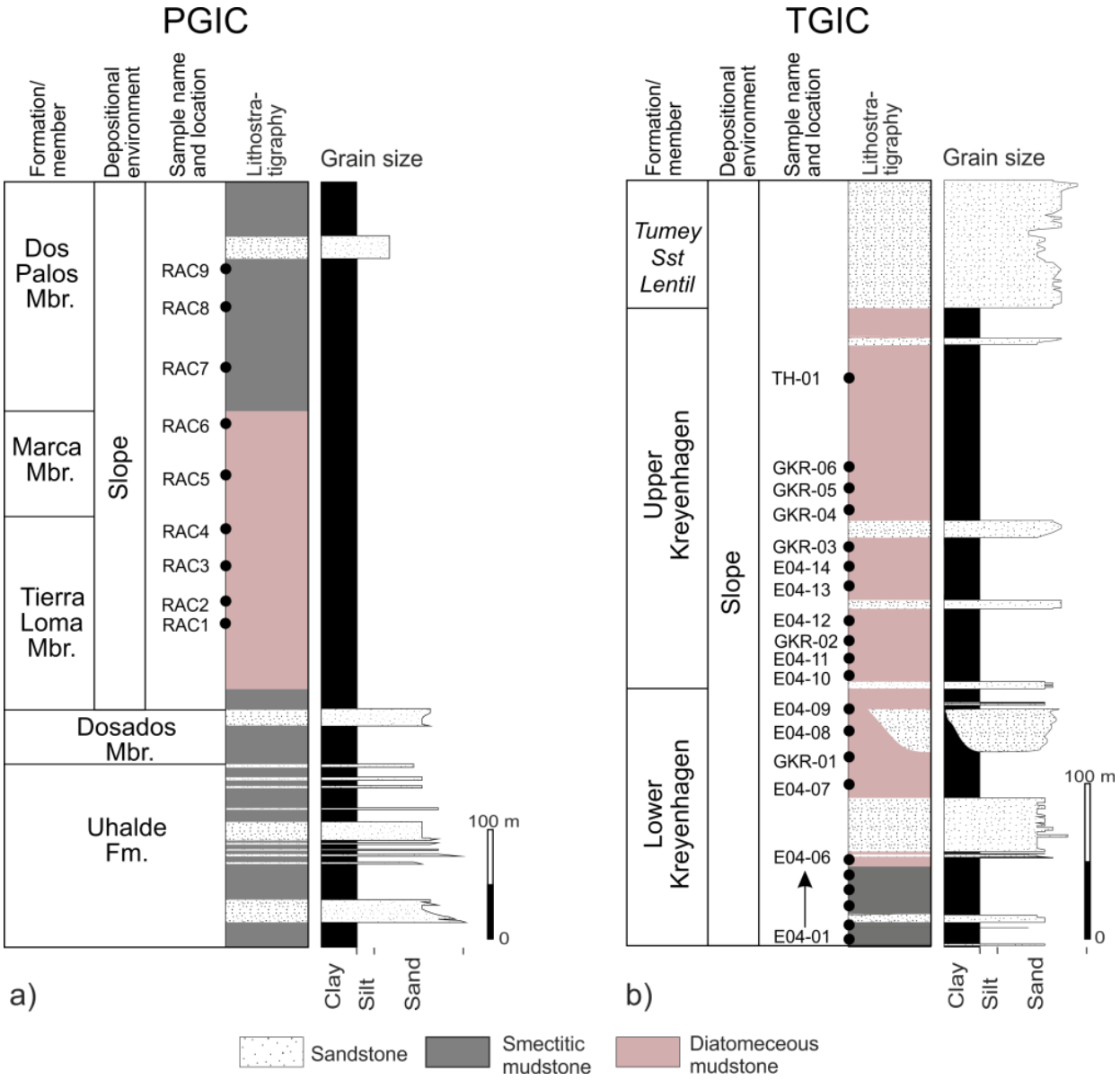

Figure 3. Simplified vertical sections through (**a**) the PGIC and (**b**) the TGIC; see Figures 1 and 2 for locations. Sample locations are marked.

The mineralogical composition was determined in two steps: (i) by XRD analysis using a Reference Intensity Ratio (RIR) method with quartz as an internal standard [20] and (ii) by combining XRD and XRF data using the vbAffina program (Microsoft Visual Basic 6.0) [22,23]. The VbAffina program requires as input data the major element composition of the bulk sample (SiO_2, Al_2O_3, Fe_2O_3, MgO, CaO, Na_2O, K_2O, and LOI) and XRDP mineralogical data. All these data were processed using a least-squares procedure that minimizes the differences between chemical compositions calculated from the XRD-determined phase percentages that are introduced into vbAffina (i.e., XRDP results) and those determined using XRF. Stoichiometric compositions of quartz, calcite, dolomite, Na-plagioclase (albite), orthoclase, clinoptilolite, gypsum, opal, cristobalite, and kaolinite were used with the vbAffina program. Illite and smectite compositions were selected from a vbAffina database that contained the compositions of these minerals.

4. Results

4.1. Bulk-Rock Mineralogy

Whole-rock analyses show that the samples are generally composed of quartz, feldspar (K-feldspar and plagioclase), cristobalite, and phyllosilicates (Table 1). Some samples show the presence of calcite, dolomite, clinoptilolite, gypsum, opal CT, and amorphous material, probably representing opal A (Figure 4). With one exception (RAC3) in which 58% of the bulk mineralogy is opal CT, samples from the Moreno Fm are dominated by phyllosilicates, and specifically, smectite. PGIC samples contain the highest amounts of quartz and cristobalite (Table 1), which accords with the chemical analyses that reveal a high proportion of SiO_2 (Table 2). Samples from the Lower Kreyenhagen are characterised by the presence of clinoptilolite (Figure 4b), which although not present throughout, comprises 7.5% of the bulk rock volume in sample EO4-08 (Table 1). In the Upper Kreyenhagen, clinoptilolite is much less common (Figure 4a) and absent in 8 of the 13 samples. Clinoptilolite is undetected in the Moreno Fm samples (Figure 4c). Opal CT is identified in several samples, and its content varies widely from a few percent up to ~70% (Table 1). It is noteworthy that opal CT is present in varied abundance in both stratigraphic successions but absent in more than half of the samples. In the Kreyenhagen Fm, amorphous material attributed to opal A is present in the upper section of the Upper Kreyenhagen and comprises 28% and 24% in the youngest, probably least deeply buried samples (GKR-6 and TH-01, Table 1). It occurs only in one other Kreyenhagen sample (EO4-12) and is absent in the Moreno Fm.

Potassium feldspar is pervasive in the Moreno Fm and more common than in the Kreyenhagen Fm, where occasionally absent (Table 1). Plagioclase is ubiquitous and always more abundant than potassium feldspar in the Moreno Fm, and generally more abundant than in the Kreyenhagen Fm (Table 1). Calcite and dolomite are absent in most samples and, where present, form diagenetic cement. Where calcite and dolomite occur, chemical data show high concentrations of CaO and MgO, respectively (Table 2). Gypsum is present in one sample only (GKR-2) as 1%, consistent with the percentage of CaO (Table 2). Phyllosilicates in bulk samples from the Moreno Fm and Kreyenhagen Fm are predominantly represented by smectite (probably montmorillonite) or mixed layers illite/smectite R0 with low illite content (<10%). Illite and kaolinite are present in small amounts. Smectite content is in the range ~50% to 70% for most samples. Exceptions with much lower smectite content (12% to 28%, Table 1) are enriched in opal CT and, in one case (EO4-04), dolomite cement. Illite is pervasive in low proportions ranging from 5% to 8% (Table 1), while kaolinite is significantly less common and absent in nine samples (Table 1).

Table 1. Whole-rock mineralogy (wt %) for Kreyenhagen and Moreno formations estimated from X-ray diffraction (XRD) analysis. Qtz = quartz; Op CT = opal CT; Opal A? = amorphous material and probably opal A; Crist = cristobalite; K-feld = K-feldspar; Pl = plagioclase; Cal = calcite; Dol = dolomite; Clin = clinoptilolite; Gy = gypsum; Sm = smectite; Ill = illite; Kao = kaolinite; Σ Phy = total phyllosilicates.

Formation	Member	Age	Sample	Non Phyllosilicates										Phyllosilicates			
				Qtz	Op CT	Opale A?	Crist	k-Feld	Pl	Cal	Dol	Clin	Gy	Sm	Ill	Kao	∑Phy
Kreyenhagen Foramtion	Upper member	Early Oligocene	TH-01	8.1	0.0	24.0	4.0	2.0	3.9	0.0	0.0	0.0	0.0	48.0	5.0	5.0	58.0
			GKR-06	8.8	0.0	28.0	3.5	1.7	4.0	0.0	0.0	0.0	0.0	48.0	3.0	3.0	54.0
			GKR-05	14.2	0.0	4.0	4.5	5.0	7.0	0.0	0.0	0.0	0.0	58.0	2.5	4.8	65.3
			GKR-04	6.0	53.4	5.0	0.0	1.5	3.5	0.0	0.0	0.0	0.0	25.6	2.5	2.5	30.6
			GKR-03	11.5	8.9	6.0	0.0	1.4	3.8	0.0	0.0	0.6	0.0	58.9	2.8	6.0	67.7
			EO4-14	11.8	5.2	0.0	2.5	1.0	2.5	0.0	0.0	0.0	0.0	69.0	2.0	6.0	77.0
			EO4-13	15.7	0.0	0.0	2.0	0.5	1.5	0.0	0.0	0.0	0.0	71.7	4.3	4.3	80.3
			EO4-12	10.0	7.3	8.0	2.0	2.1	2.8	0.0	0.0	0.0	0.0	60.0	2.6	5.2	67.8
			GKR-02	10.0	3.9	0.0	2.7	2.5	9.0	0.0	0.0	0.0	1.0	62.9	8.0	0.0	70.9
			EO4-11	13.5	2.0	0.0	2.5	1.9	5.5	0.0	0.0	0.7	0.0	61.4	3.5	9.0	73.9
			EO4-10	13.5	0.0	0.0	0.0	3.3	3.0	0.0	0.0	2.0	0.0	69.9	3.5	4.9	78.3
			Min Value	6.0	0.0	0.0	0.0	0.5	1.5	0.0	0.0	0.0	0.0	25.6	2.0	0.0	30.6
			Max Value	15.7	53.4	28.0	4.5	5.0	9.0	0.0	0.0	2.0	1.0	71.7	8.0	9.0	80.3
			Average	11.2	7.3	6.8	2.2	2.1	4.2	0.0	0.0	0.3	0.1	57.6	3.6	4.6	65.8
			St. dev	2.9	15.6	9.9	1.6	1.2	2.2	0.0	0.0	0.6	0.3	13.2	1.7	2.3	14.3
	Lower member	Middle Eocene	EO4-09	11.5	0.0	0.0	1.4	4.4	4.8	0.0	0.0	2.3	0.0	64.3	3.3	8.0	75.6
			EO4-08	6.2	43.8	0.0	0.0	3.5	12.5	0.0	0.0	7.5	0.0	23.6	2.9	0.0	26.5
			GKR-01	5.0	70.3	0.0	0.0	0.8	2.5	6.4	0.0	0.0	0.0	12.0	3.0	0.0	15.0
			EO4-07	9.0	0.0	0.0	4.4	5.9	13.1	0.0	0.0	1.2	0.0	63.3	3.1	0.0	66.4
			EO4-06	7.5	38.6	0.0	0.0	3.0	7.0	14.0	0.0	3.2	0.0	21.7	5.0	0.0	26.7
			EO4-05	11.0	0.0	0.0	1.9	0.0	8.3	0.0	0.0	0.0	0.0	68.8	5.0	5.0	78.8
			EO4-04	2.0	0.0	0.0	0.0	0.0	1.5	0.0	72.0	0.0	0.0	24.5	0.0	0.0	24.5
			EO4-03	3.3	0.0	0.0	0.0	0.0	2.8	30.5	0.0	3.2	0.0	57.1	3.2	0.0	60.3
			EO4-02	18.9	0.0	0.0	0.0	3.0	5.7	0.0	0.0	4.0	0.0	54.0	6.0	8.4	68.4
			EO4-01	8.5	0.0	0.0	0.0	2.1	7.5	12.0	0.0	4.0	0.0	55.1	8.1	2.8	66.0
			Min Value	2.0	0.0	0.0	0.0	0.0	1.5	0.0	0.0	0.0	0.0	12.0	0.0	0.0	15.0
			Max Value	18.9	70.3	0.0	4.4	5.9	13.1	30.5	72.0	7.5	0.0	68.8	8.1	8.4	78.8
			Average	8.3	15.3	0.0	0.8	2.3	6.6	6.3	7.2	2.5	0.0	44.4	4.0	2.4	50.8
			St. dev	4.8	25.9	0.0	1.5	2.1	4.0	10.1	22.8	2.4	0.0	21.4	2.2	3.5	24.5
Moreno Foramtion	Dos Palos	Lower Paleocene	RAC9	18.0	0.0	0.0	2.4	9.5	10.5	0.0	0.0	0.0	0.0	50.6	2.5	6.5	59.6
			RAC8	11.5	0.0	0.0	4.5	2.9	10.0	0.0	0.0	0.0	0.0	62.2	2.3	6.6	71.1
			RAC7	12.5	0.0	0.0	3.0	2.0	7.0	0.0	0.0	0.0	0.0	69.0	1.5	5.0	75.5
	Marca		RAC6	12.5	15.0	0.0	5.0	1.0	5.5	0.0	0.0	0.0	0.0	59.0	2.0	0.0	61.0
			RAC5	13.5	12.5	0.0	4.0	2.5	5.0	0.0	0.0	0.0	0.0	56.0	3.0	3.5	62.5
	Tierra Lama	Upper Cretaceous	RAC4	13.2	7.2	0.0	3.7	4.0	7.0	0.0	0.0	0.0	0.0	61.8	1.4	1.7	64.9
			RAC3	7.0	58.0	0.0	0.0	1.5	3.5	0.0	0.0	0.0	0.0	28.0	2.0	0.0	30.0
			RAC2	12.0	3.5	0.0	3.6	3.0	8.0	0.0	0.0	0.0	0.0	67.9	2.0	0.0	69.9
			RAC1	20.0	0.0	0.0	1.5	5.0	7.0	0.0	0.0	0.0	0.0	64.0	2.5	0.0	66.5
			Min Value	7.0	0.0	0.0	0.0	1.0	3.5	0.0	0.0	0.0	0.0	28.0	1.4	0.0	30.0
			Max Value	20.0	58.0	0.0	5.0	9.5	10.5	0.0	0.0	0.0	0.0	69.0	3.0	6.6	75.5
			Average	13.4	10.7	0.0	3.1	3.5	7.1	0.0	0.0	0.0	0.0	57.6	2.1	2.6	62.3
			St. dev	3.8	18.6	0.0	1.6	2.6	2.3	0.0	0.0	0.0	0.0	12.5	0.5	2.9	13.2

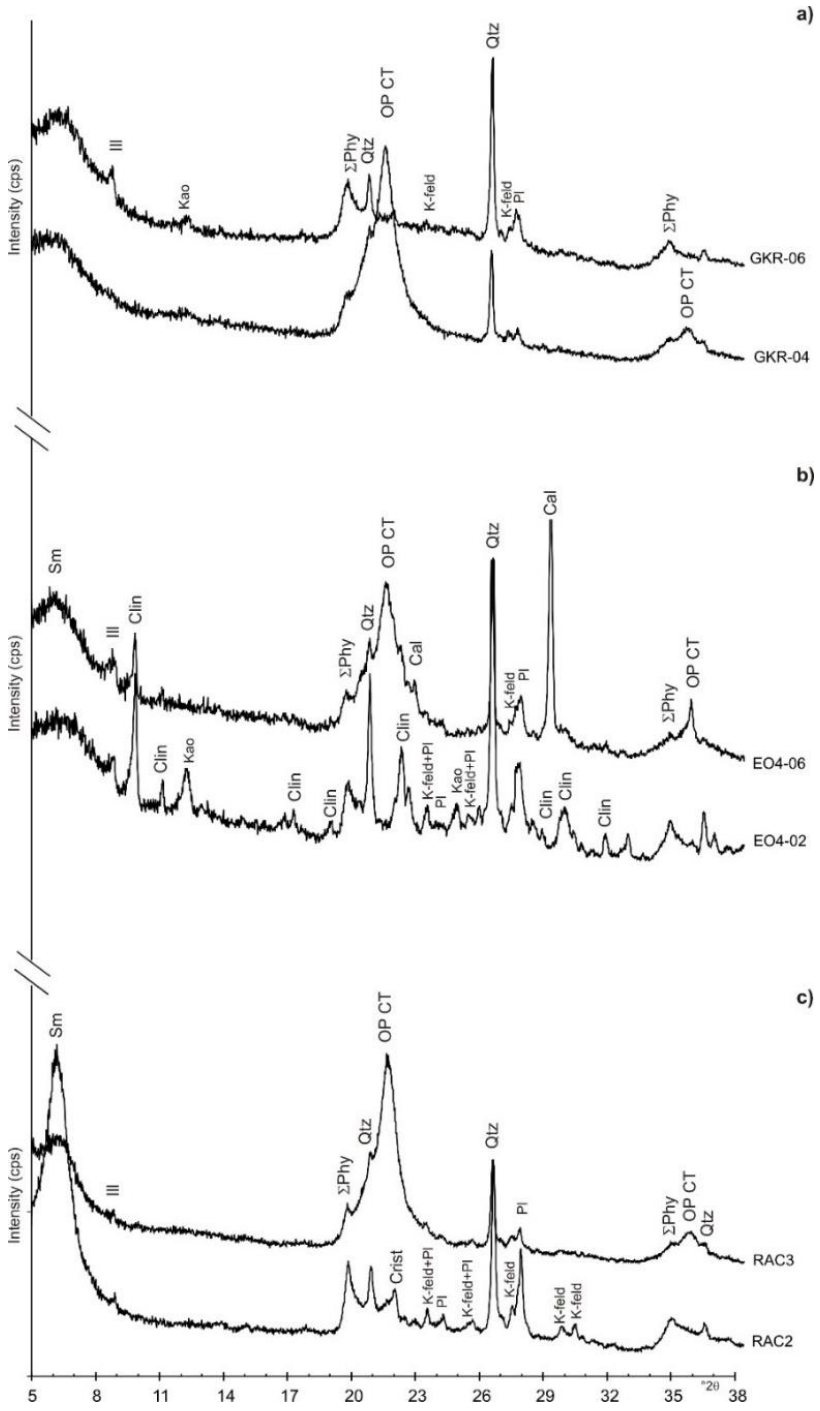

Figure 4. X-ray diffractograms for whole-rock samples: (**a**) Upper Kreyenhagen, (**b**) Lower Kreyenhagen, and (**c**) Moreno Formation. Mineral abbreviations are as in Table 1. Sample locations are shown in Figure 3.

4.2. Bulk Rock Chemistry

The chemical data have limited major element data variability (Table 2). In the Lower Kreyenhagen, some exceptional CaO and MgO concentrations are caused by the presence of calcite and dolomite. SiO_2 variability is associated with the concentration of bio siliceous opal. Na_2O and K_2O are present in low concentrations (1–2%); however, where clinoptilolite and plagioclase, and clinoptilolite and K-feldspar occur, the concentration of Na_2O and K_2O are higher, respectively. Excluding samples with carbonate minerals, Na_2O, K_2O, and CaO concentrations are lower than their average concentration in the

Upper Continental Crust [24], which is indicative of significant leaching in the source terrane. Further evidence of a leached source terrane is recorded by TiO_2 concentration that averages between 0.68% and 0.85%, slightly higher than average values from the Upper Continental Crust. Al_2O_3 content has little variability and an average content of 12% and 16% in the Lower Kreyenhagen and the Moreno formations, respectively. In accord with the mineralogical data (Table 1), the highest Al_2O_3 concentrations are where smectite and kaolinite predominate. In all samples, Al_2O_3 concentration is comparable with the average values of the Upper Continental Crust [24].

As expected from the high chemical indices of alteration (CIA) values (Table 2), sample compositions are close to the A vertex and the smectite compositional field (Figure 5). The combined presence of K-feldspar and illite shift the compositional field approximately 10% toward the A-K axis. The plots exclude all carbonate-rich samples.

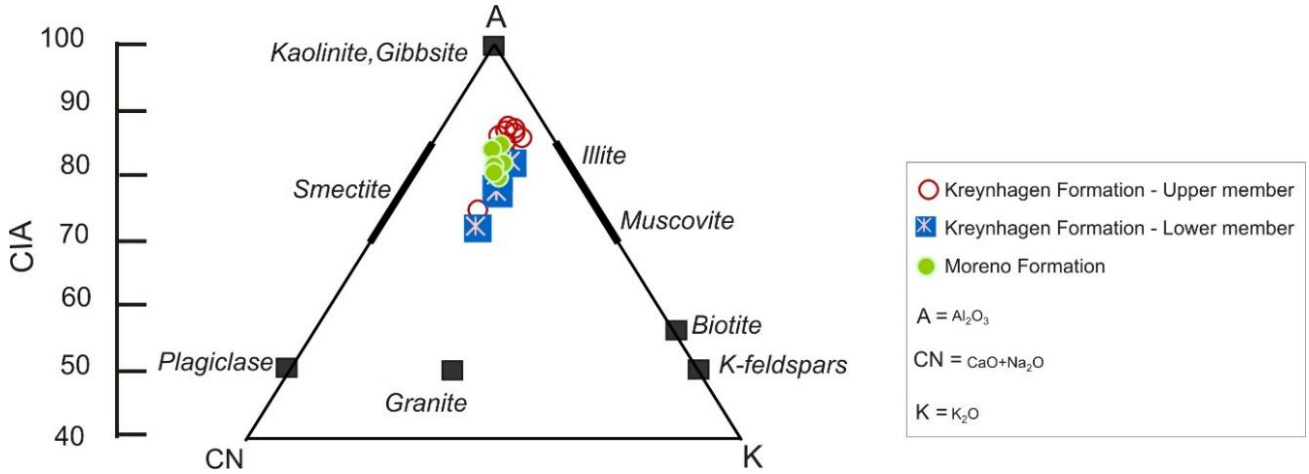

Figure 5. The A–CN–K plot of samples from Table 2 excluding those enriched in carbonate.

4.3. Mineralogy of the <2 µm Clay Fraction

The clay fraction (<2 µm) comprises mainly smectitic clay, with small amounts of illite and kaolinite (Figure 6). Smectite content ranges from 92% to 98% (mean 95.3%) in the Moreno Fm and from 70% to 95% (mean 88.9%) in the Kreyenhagen Fm (Table 3). In the Kreyenhagen Fm, the Upper and Lower Kreyenhagen have averages of 88.9% and 86.1%, respectively; illite is present in all samples ranging from 1% to 11% (Figure 6a,b). In the Moreno Fm, illite is uncommon, ranging from 1% to 8% (mean 1.9%), and slightly more common in the Kreyenhagen Fm, ranging from 1% to 11% (mean 4.5%), with 3% and 5.8% mean illite in the Upper and Lower Kreyenhagen, respectively.

In the Moreno Fm, kaolinite is 4% or less of the <2 µm fraction in samples from the Tierra Loma and Marca Mbrs (Table 3), while in the overlying Dos Palos Mbr, it constitutes 5% or more of the <2 µm fraction (compare RAC2 and RAC8, Figure 6c). Kaolinite's cumulative mean is 3% with a standard deviation of 2.65. In the Kreyenhagen Fm the kaolinite concentration varies significantly, with nine samples with 4% or less, and eight samples with 10% or more (Table 3). The mean concentration of kaolinite for the entire Kreyenhagen Fm and the Upper and Lower Kreyenhagen individually is 7.9%. The standard deviation for the Upper and Lower Kreyenhagen are significantly different, 6.63 and 9.68, respectively, and much greater than in the Moreno Fm. In the Kreyenhagen Fm (Table 3), the clusters of high kaolinite content occur in an ~40 m thick interval at the base of the sampled section (samples EO4-01 to -04), and in an ~25 m interval directly below (EO4-09) and above the transition from the Lower to the Upper Kreyenhagen (EO4-10 and -11). A less pronounced kaolinite enrichment occurs in an ~60 m interval. Samples with either low or no kaolinite content typically contain significant amounts of opal CT; for example, in EO4-06, EO-08, GKR1, GKR4, and RAC3 (Table 1).

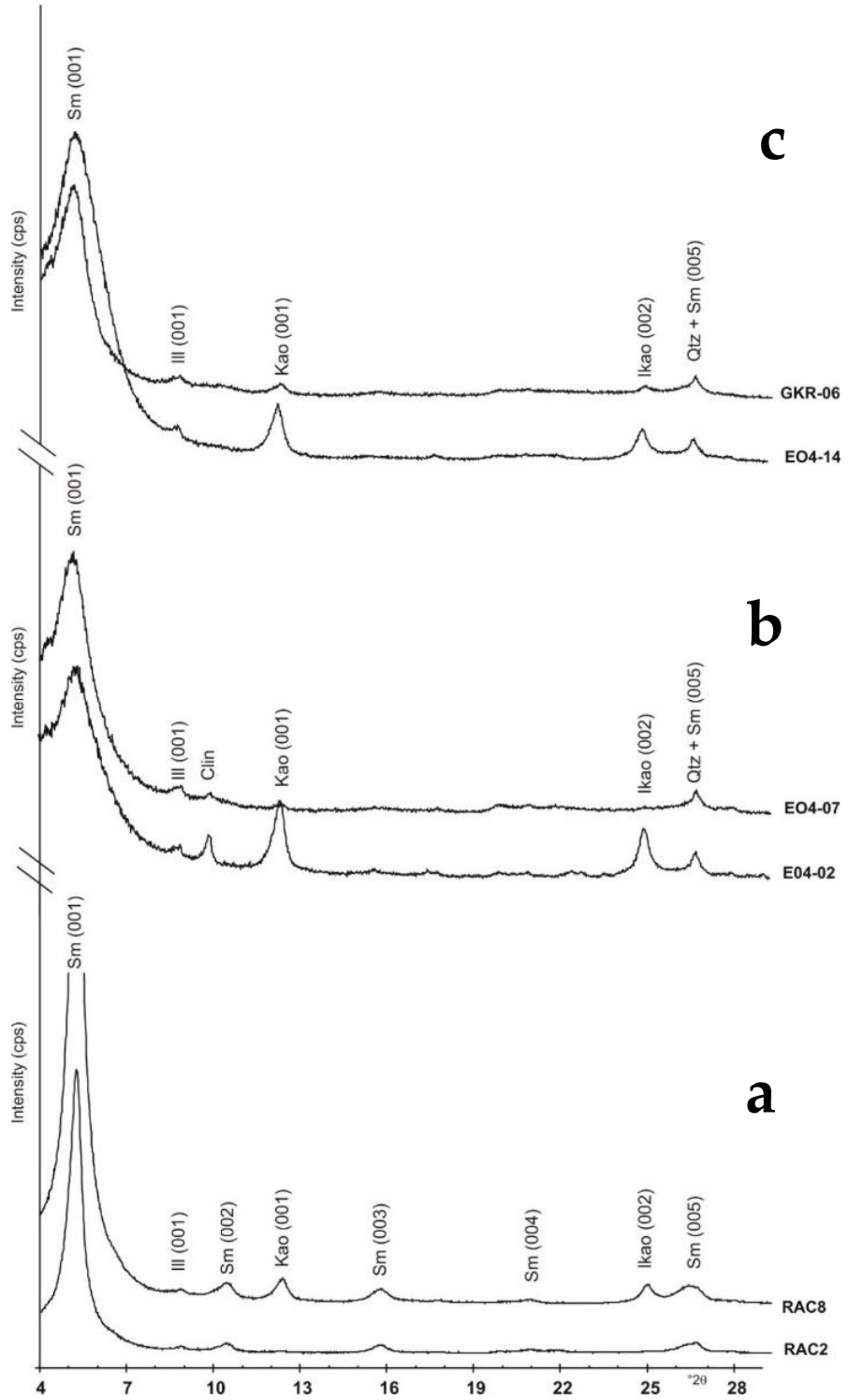

Figure 6. X-ray diffractograms of the clay mineralogy (<2 μm fraction) analysed as glycolated oriented mounts and using Cu–Kα radiation, °2θ on the horizontal axis, and counts per second (cps) on the vertical axis. (**a**) the Moreno Fm, (**b**) the Lower Kreyenhagen, and (**c**) the Upper Kreyenhagen. Mineral abbreviations are as in Table 1. Sample locations are shown in Figure 3.

Table 2. Major element chemistry for samples shown in Table 1. LOI = loss on ignition. CIA = chemical index of alteration [25].

Formation	Member	Age	Sample	Na_2O	MgO	Al_2O_3	SiO_2	P_2O_3	K_2O	CaO	TiO_2	MnO	Fe_2O_3	LOI	CIA
Kreyenhagen Foramtion	Upper member	Early Oligocene	TH-01	0.93	1.86	12.71	65.07	0.48	1.14	0.00	0.83	0.03	7.68	9.27	86.0
			GKR-06	0.97	2.63	12.08	68.99	0.30	1.57	0.00	0.73	0.03	3.75	8.95	82.6
			GKR-05	1.43	2.70	15.20	63.05	0.37	1.93	0.01	0.76	0.06	5.06	9.43	81.9
			GKR-04	0.32	0.97	7.29	77.34	0.48	0.90	0.00	0.55	0.03	4.04	8.08	85.7
			GKR-03	0.84	1.87	14.70	63.47	0.59	1.36	0.00	0.95	0.03	3.10	13.09	87.0
			EO4-14	0.85	2.23	16.71	62.29	0.30	1.53	0.00	1.00	0.03	3.64	11.22	87.5
			EO4-13	0.61	1.74	17.71	62.47	0.32	1.89	0.24	0.86	0.03	3.81	10.32	86.6
			EO4-12	0.67	1.43	15.42	64.84	0.36	1.58	0.00	0.97	0.03	2.64	12.06	87.3
			GKR-02	2.01	3.41	13.85	55.45	0.47	1.98	0.64	0.82	0.05	6.91	14.41	74.9
			EO4-11	1.17	1.85	16.51	56.25	0.53	1.74	0.00	0.81	0.03	3.71	17.40	85.0
			EO4-10	0.92	1.31	17.26	56.28	0.24	2.11	0.48	1.04	0.03	4.33	16.00	83.1
			Min Value	0.32	0.97	7.29	55.45	0.24	0.90	0.00	0.55	0.03	2.64	8.08	74.95
			Max Value	2.01	3.41	17.71	77.34	0.59	2.11	0.64	1.04	0.06	7.68	17.40	87.53
			Average	0.98	2.00	14.50	63.22	0.40	1.58	0.13	0.85	0.04	4.43	11.84	84.33
			St. dev	0.45	0.70	2.99	6.30	0.11	0.37	0.23	0.14	0.01	1.56	3.07	3.67
	Lower member	Middle Eocene	EO4-09	1.02	1.49	18.54	58.87	0.26	2.50	0.52	0.91	0.03	4.47	11.39	82.1
			EO4-08	1.86	1.64	8.41	70.94	0.45	1.35	0.00	0.60	0.03	2.52	12.20	72.4
			GKR-01	0.94	1.07	3.80	81.44	0.28	0.59	3.38	0.38	0.04	1.54	6.54	n.c.
			EO4-07	2.05	2.57	15.04	56.30	0.71	2.08	0.02	0.88	0.03	4.51	15.81	78.4
			EO4-06	1.13	1.78	7.60	64.55	0.21	1.48	7.80	0.49	0.04	3.46	11.46	n.c.
			EO4-05	1.84	3.29	16.42	55.95	0.24	2.42	0.45	0.93	0.05	7.84	10.57	77.7
			EO4-04	0.61	16.56	6.76	18.32	0.14	0.87	22.09	0.31	0.08	1.37	32.89	n.c.
			EO4-03	1.81	2.22	11.49	39.04	0.58	1.75	17.20	0.50	0.05	4.44	20.92	n.c.
			EO4-02	1.88	1.29	17.06	59.75	0.18	2.21	0.14	0.96	0.04	3.89	12.60	80.1
			EO4-01	2.06	2.08	14.93	47.98	0.31	2.26	6.85	0.80	0.04	5.63	17.06	n.c.
			Min Value	0.61	1.07	3.80	18.32	0.14	0.59	0.00	0.31	0.03	1.37	6.54	72.38
			Max Value	2.06	16.56	18.54	81.44	0.71	2.50	22.09	0.96	0.08	7.84	32.89	82.11
			Average	1.52	3.39	12.00	55.31	0.34	1.75	5.85	0.68	0.04	3.97	15.14	78.14
			St. dev	0.53	4.67	5.09	17.43	0.19	0.66	7.90	0.25	0.01	1.93	7.38	3.65
Moreno Foramtion	Dos Palos	Lower Paleocene	RAC9	2.05	1.77	19.59	62.71	0.03	2.62	0.25	0.80	0.03	2.52	7.63	79.9
			RAC8	1.94	2.07	21.18	59.46	0.03	2.10	0.14	0.79	0.05	3.86	8.38	83.5
			RAC7	1.51	1.95	19.38	63.28	0.12	1.92	0.17	0.87	0.04	2.54	8.22	84.3
	Marca		RAC6	1.04	2.89	13.15	66.55	0.32	1.35	0.00	0.76	0.03	3.41	10.50	84.6
			RAC5	1.17	1.31	15.94	69.33	0.45	1.47	0.35	0.82	0.03	2.17	6.96	84.2
	Tierra Lama	Upper Cretaceous	RAC4	1.42	1.47	15.87	68.59	0.27	2.02	0.17	0.95	0.03	2.19	7.02	81.5
			RAC3	0.59	1.12	7.24	81.12	0.78	0.92	0.10	0.43	0.04	1.99	5.67	81.8
			RAC2	1.26	1.79	17.14	66.42	0.20	2.00	0.64	0.93	0.03	1.94	7.65	81.5
			RAC1	1.53	1.97	17.97	64.07	0.14	2.20	0.58	0.80	0.03	2.43	8.28	80.7
			Min Value	0.59	1.12	7.24	59.46	0.03	0.92	0.00	0.43	0.03	1.94	5.67	79.93
			Max Value	2.05	2.89	21.18	81.12	0.78	2.62	0.64	0.95	0.05	3.86	10.50	84.62
			Average	1.39	1.82	16.38	66.84	0.26	1.84	0.27	0.79	0.03	2.56	7.81	82.44
			St. dev	0.45	0.52	4.18	6.18	0.24	0.51	0.22	0.15	0.01	0.65	1.32	1.75

Table 3. Clay minerals (wt %) for Kreyenhagen and Moreno formations estimated from XRD analyses of the <2 μm fractions. Abbreviations as in Table 1. Sample locations are in Figure 3.

Formation	Member	Age	Sample	Clay Minerals		
				Sm	Ill	Kao
Kreyenhagen Foramtion	Upper member	Early Oligocene	TH-01	91	2	8
			GKR-06	93	4	3
			GKR-05	92	4	4
			GKR-04	95	2	2
			GKR-03	93	1	6
			EO4-14	87	1	11
			EO4-13	87	2	11
			EO4-12	92	2	6
			GKR-02	92	7	0
			EO4-11	85	3	12
			EO4-10	71	5	24
			Min Value	71.4	1.3	0.4
			Max Value	95.3	7.3	23.6
			Average	89.0	3.1	8.0
			St. dev	6.6	1.9	6.5
	Lower member	Middle Eocene	EO4-09	70	8	22
			EO4-08	93	7	0
			GKR-01	95	5	0
			EO4-07	93	5	1
			EO4-06	93	7	0
			EO4-05	91	5	4
			EO4-04	78	11	10
			EO4-03	93	3	4
			EO4-02	71	2	27
			EO4-01	84	5	11
			Min Value	70.0	2.0	0.0
			Max Value	94.5	11.2	27.2
			Average	86.1	5.8	8.0
			St. dev	9.7	2.6	9.8
Moreno Foramtion	Dos Palos	Lower Paleocene	RAC9	92	1	8
			RAC8	95	1	5
			RAC7	94	1	5
	Marca		RAC6	98	1	1
			RAC5	95	1	4
	Tierra Lama	Upper Cretaceous	RAC4	96	1	2
			RAC3	92	8	0
			RAC2	98	2	1
			RAC1	98	1	1
			Min Value	91.8	0.6	0.0
			Max Value	98.4	7.7	7.6
			Average	95.4	1.8	2.9
			St. dev	2.4	2.2	2.6

4.4. Opaline Phases

The scanning electron microscopy (SEM) analysis reveals micro-textural variations that confirm the presence of opal A and differentiate it from opal CT. In the Upper Kreyenhagen, broken diatom tests exhibit pristine, box-work, shell micro-structure in a groundmass of comminuted bio siliceous debris (Figure 7). During sample preparation for XRD analysis, the opal A is assumed to disintegrate into finer-grained particles that are X-ray amorphous. By contrast, in the Moreno Fm, there is no preservation of shell tests or their micro-texture. Diatom morphology is sometimes preserved as crystalline fills of their internal geometry (Figure 8). XRD analyses of the clay fractions show an XRD pattern that is much closer to low tridymite rather than low cristobalite, with strong reflections at 4.33 Å and at 4.10 Å and weak, broad reflections at 2.49 Å and 2.31 Å.

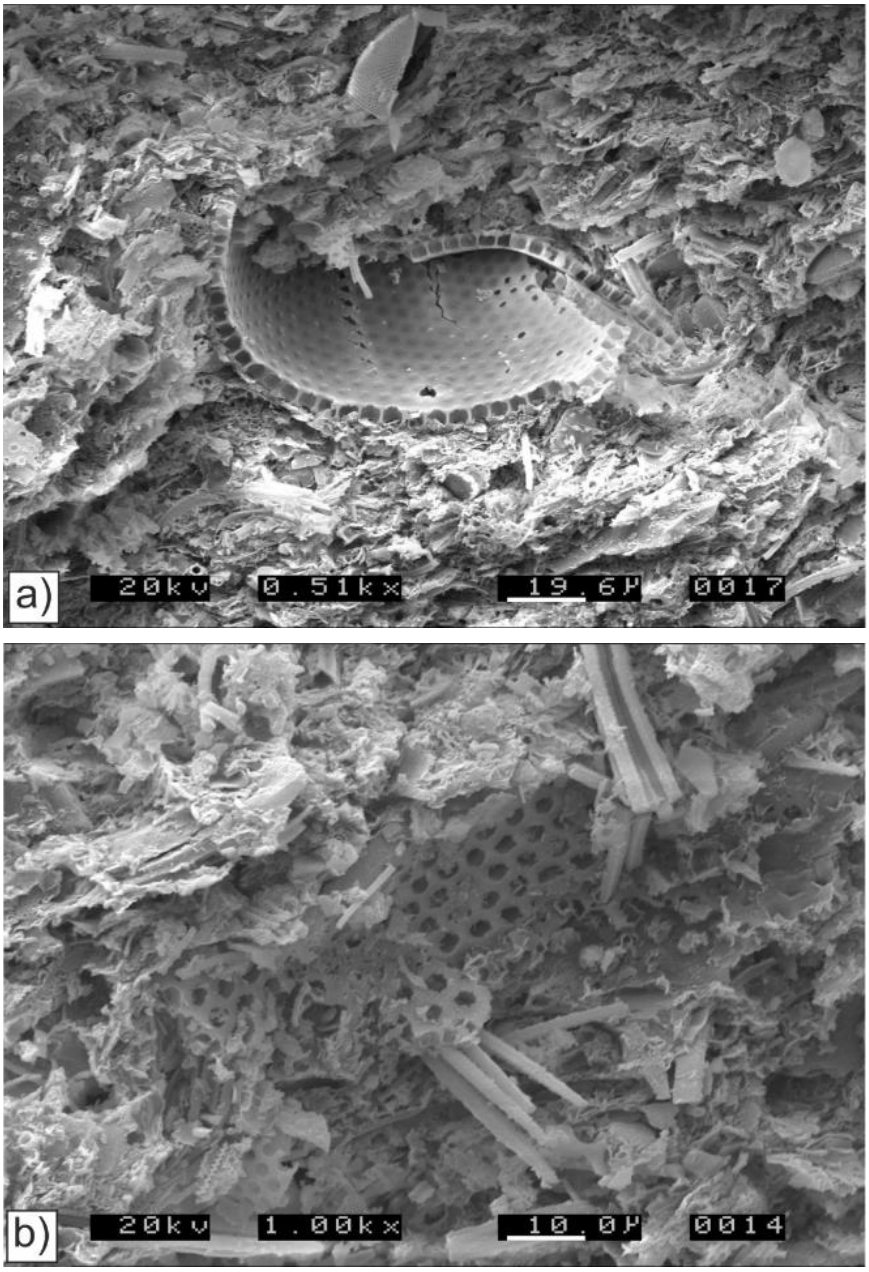

Figure 7. Scanning electron microscopy (SEM) images of the bio siliceous mudstone sample (TH-01) from the Upper Kreyenhagen, Monocline Ridge (TGIC, Figure 3b). The sample is consolidated. (**a**) Crushed parts of a large diatom test in which the pristine opal A micro-texture is preserved. The surrounding bio silicious groundmass is largely comminuted fragments from crushed diatom shells; scale bar = 19.6 µm. (**b**) Micro-porous test fragments (opal A) in a groundmass of crushed tests; scale bar = 10 µm.

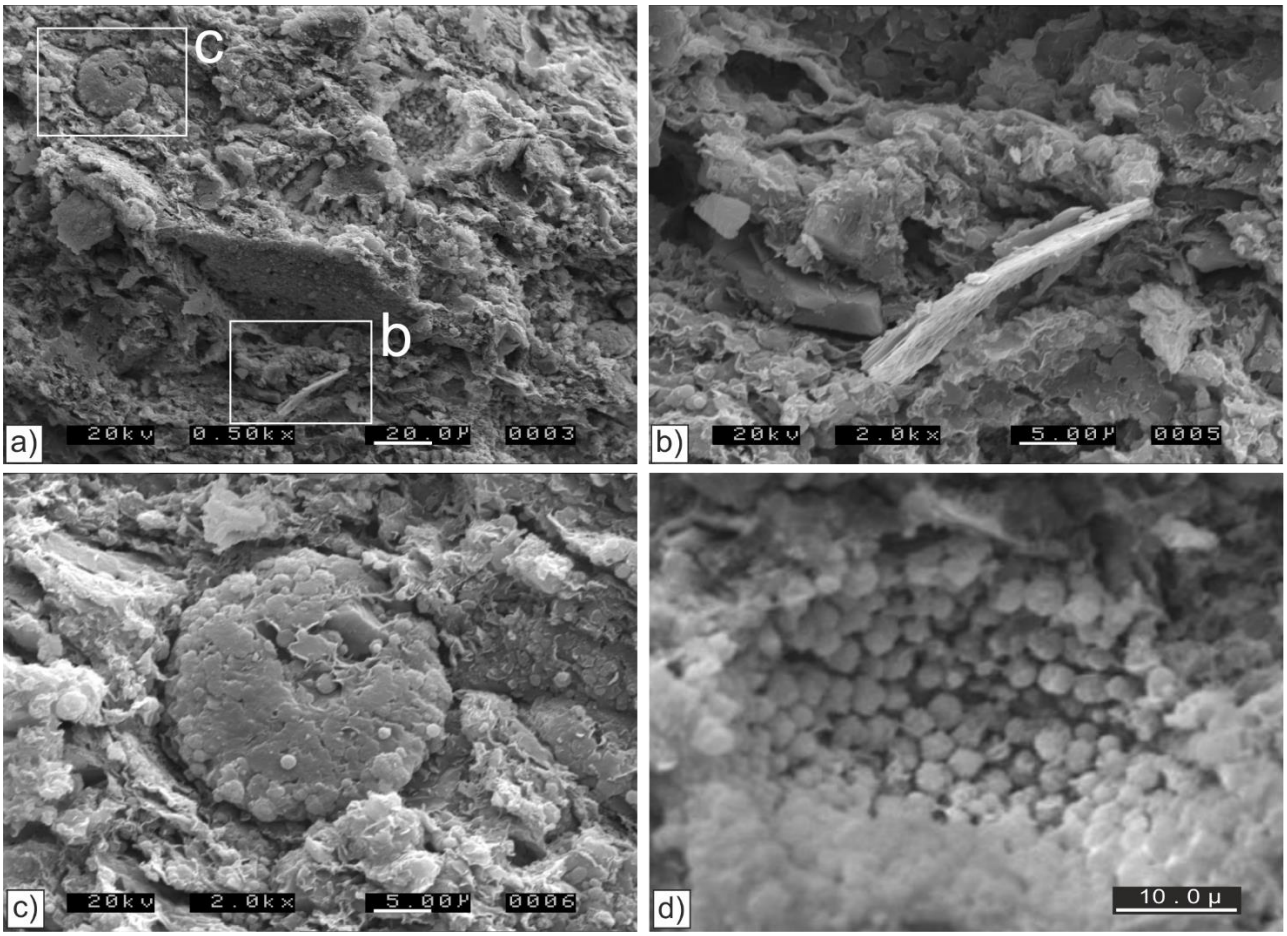

Figure 8. SEM images of the bio siliceous mudstone sample (RAC5) from the Marca Member in Right Angle Canyon (PGIC, Figure 3a). The sample is poorly consolidated and contains recrystallized test fills and more finely comminuted opaline particles, none of which preserve micro-textures associated with opal A. (**a**) Tightly packed bio silicious particles, often <5 µm across but with occasional elongate (>20 µm) gypsum (**b**) and recrystalized tests (**c**); scale bar = 20 µm. (**b**) Relic bio silicious tests (now opal CT) with gypsum as shown in (**a**); scale bar = 5 µm. (**c**) An ovoid crystalline fill of a diatom test shown in (**a**) with no evidence of micro-texture associated with opal A; scale bar = 5 µm. (**d**) Micro-textures formed by crystallization within a diatom test. Prevailing rounded, blocky equilateral and less common approximately spherical µm-scale crystals with micropores generally in the 0.1 µm to 0.2 µm range; scale bar = 10 µm.

5. Discussion

5.1. Origin of Smectite

Mudstone of the Moreno and Kreyenhagen fms are dominated by smectite. Except where opal CT or dolomite occur, it is three to more than six times as abundant as any other mineral present (Table 1). Grim and Gùven [26] concluded that the smectite in sedimentary rocks, particularly in bentonites, is most often associated with the input of volcanic material. A decade later, Moore and Reynolds [18] reaffirmed the significance of the volcanic origin for smectite, where the smectite is an alteration product of volcanic ash. It was considered that a volcanic origin could account for the occurrence of smectite in marine shales of the western interior of North America [27] and the shales and sandstones of the San Joaquin Basin in California [6]. Chamley [28] and Deconnick and Chamley [29] were particularly sceptical of the role of volcanic ash as a necessary precursor for the formation of smectite, specifically in coastal and deep-sea environments. It is now well established that smectite

forms as a weathering product and constituent of soil in many tropical and sub-tropical environments and develops on a wide range of substrate [30–32].

During the Upper Cretaceous, deposition of the Moreno Fm coincided with active volcanism in the palaeo-Sierran magmatic arc [33] and erosion of substantial volumes of clastic detritus into a forearc basin [34], the site of the present-day San Joaquin Valley (Figure 1). Alteration of volcaniclastics from rhyolitic or dacitic composition to form smectite is inferred and supported by the high average SiO_2 content (66.8%, Table 2). This accords with the occurrence of quartz, cristobalite, and opal CT (Table 1). No evidence exists for direct deposition from airborne volcaniclastics and tuff is unrecognized in our study area. Despite the prevalence of smectite (Tables 1 and 3), high (mean 84.44) CIA values [25] persist and are indicative of significant leaching of the source terrane. The widespread contemporary volcanic activity makes alteration of volcaniclastics the likely primary source of smectite; however, prior to marine deposition, we suggest that smectite was likely to be retained and formed in pedogenic settings in which it was stable [28] but where further leaching continued to modify the bulk chemistry of the detritus. The low standard deviation of CIA in the Moreno Fm is a measure of the homogeneity of the bulk chemistry (Table 2).

Contemporary volcanism was absent in the palaeo-Sierra Nevada during the deposition of the Kreyenhagen Fm (Eocene), although it did occur further east on the "Nevadaplano" [35]. As with the Moreno Fm, the absence of tuff makes direct deposition from volcaniclastics unlikely, and weathering processes and soil formation along the western margin of the Sierra Nevada are more plausible origins for most of the smectite. High CIA values prevail, averaging 84.33 and 78.14 in the Upper and Lower Kreyenhagen, respectively. These are indicative of a moderately high level of leaching of the source terrane that coincides with the Paleocene–Eocene thermal maximum followed by almost 10 Ma years of the Eocene hyperthermal [36]. Red soils/paleosols with locally abundant smectite developed along the western margin of the North American continent recording a trend of tropical to sub-tropical climate from Baja California [37] to Oregon [38]. The Kreyenhagen Fm is typically deficient in alkali and alkaline earth cations and is notably ferriferous; Upper and Lower Kreyenhagen with 4.44% and 3.97% mean Fe_2O_3, respectively, relative to 2.56% Fe_2O_3 in the Moreno Fm (Table 2). Local concentrations of kaolinite (10–24%, Table 3) record erosion of more deeply weathered contemporary terrane. Iron oxide stain along cleavage planes in feldspar in Kreyenhagen sandstone is evidence of the erosion of deeply weathered source terrane [4]. Higher concentrations of Fe_2O_3 are consistent with the generation of smectite by weathering of the granitic or dioritic-granodioritic substrate and probable soil formation rather than by alteration of volcaniclastic debris.

5.2. Opal CT

Textural differences between opal CT from the Moreno Fm (Figure 7) and opal A from the Upper Kreyenhagen (Figure 8) show how opal A dissolution occurs by the disappearance of the intricate highly micro-porous diatom fragments and growth of coarser individual crystals of opal CT that sometimes preserve diatom test morphology but none of the original micro-porous structure. In a micro-textural context, the transition of opal A to opal CT is demonstrably not a solid-state transition. Growth of opal CT is manifest as an increase in bulk density in the sedimentary rock in which it occurs and is accompanied by a visible change from a substantial proportion of sub-μm micropores in diatomaceous fragments (Figure 7b) to less but larger (~0.5 μm to 2.5 μm) pores (Figure 8d). Although we have not attempted a quantitative evaluation of this change in micro-texture, it is apparent that the pore-size distribution in opal CT is skewed to larger pore sizes than in opal A, implicitly enhancing pore connectivity. It is worth noting that XRD analyses of the clay fractions show an XRD pattern that is much closer to low tridymite rather than low cristobalite, with strong reflections at 4.33 Å and 4.10 Å and weak, broad reflections at 2.49 Å and 2.31 Å. In contrast, low cristobalite has an XRD pattern with a very strong reflection at 4.05 Å and with medium-strong reflections at 3.14 Å, 2.84 Å, and 2.48 Å [39]. Despite

these differences, most authors continue to identify opal CT as a precursor of cristobalite rather than tridymite, even though recent [40] and older work [41] presented spectroscopic evidence in support of opal CT as a precursor of tridymite rather than cristobalite.

5.3. Clinoptilolite

Global occurrence of clinoptilolite in sedimentary rocks is concentrated in strata of Upper Cretaceous to Eocene age [42]. When present in the Lower Kreyenhagen (seven of ten samples), clinoptilolite has a mean abundance of 3.63% whereas it is mainly absent from the Upper Kreyenhagen. Clinoptilolite was known in the Moreno Fm and associated with an early diagenetic alteration of smectite [43], but it is undetected in this study. The general relationship between the co-occurrence of clinoptilolite with opal CT and smectite [42,44] is not present in five of the seven clinoptilolite-bearing samples; smectite is abundant, but opal CT, opal A, and cristobalite are absent (Table 1). Clinoptilolite forms in normal salinity marine conditions in which opal A or CT are freely available and magnesium concentration is low, conditions typical of open oceans rather than where ocean circulation is restricted. In this context, it could be that the Lower Kreyenhagen deposited in more open marine conditions than the Upper Kreyenhagen. An alternative origin for clinoptilolite is from igneous rocks, often as alteration products of ignimbrites and tuffs, and as vesicular crystals [45–47]. This may be a potential contributory source for clinoptilolite in the Lower Kreyenhagen. In common with the origin of smectite, the lack of adjacent volcanic sources during the Eocene diminishes the likelihood of significant volcanic provenance.

5.4. Sedimentology and Diagenesis

Content of bio siliceous silica relative to phyllosilicates, and specifically smectite, is the main sedimentological variation present: in the Moreno Fm, the Marca Mbr is a thick, pale grey, regionally developed bio siliceous mudstone [2,13]; in the Kreyenhagen Fm, the Lower and Upper Kreyenhagen are differentiated by their clay mineral and bio siliceous content, respectively [3]. Deposition of the Dos Palos Mbr records a shallowing upward and from the medial part of the Marca Mbr into the Dos Palos Mbr kaolinite content has a significant increase, averaging 4.6% compared with 1% in the underlying mudstone (Figure 3a, Table 3). In the uppermost four samples (RAC-6, -7, -8, and -9), Fe_2O_3 is enriched along with alkali and alkali earth elements while SiO_2 is less concentrated (Table 2). In the absence of any silicate diagenesis, the increase of kaolinite and Fe_2O_3 records increased terrestrial input with other chemical variations responding to a slight gradual coarsening and increased feldspar content. Independent evaluation of diagenetic grade in the Moreno Fm estimated the thermal maximum to be <50 °C [48], and we have no evidence to contradict that in this study.

Localized diagenetic calcite and dolomite cement and opaline silica transformations are identified and gypsum is present in the Kreyenhagen Fm [4]. High silica content and deficiency in alkali and alkaline earth cations is characteristic (Table 2) and attributed to derivation of clastic material from siliceous magma. The Lower Kreyenhagen is significantly enriched in alkali and alkali earth elements and depleted in Si^{4+} relative to the Upper Kreyenhagen and the Moreno Fm. When the four samples with diagenetic carbonate cement from the Lower Kreyenhagen are excluded from the statistical analysis, Mg^{2+} and Ca^{2+} remain significantly higher than in Upper Kreyenhagen and Moreno samples, thus reinforcing the significance of the chemical difference of the Lower Kreyenhagen.

5.5. Smectite and Hydrocarbon Generation

Unsurprisingly, given the known hydrocarbon reserves in the area [5,49], most of the very few published papers on the clay mineralogy of Paleogene strata in the San Joaquin Basin are associated with hydrocarbons. Previously, smectite in the Kreyenhagen Fm was believed to promote oil expulsion efficiency and was investigated using hydrous pyrolysis to compare natural and thermal maturation of samples [50]. Using the same samples, Lewan et al. [7] concluded that oil expulsion efficiency from smectitic mudstone

was reduced by 88% compared to that of mudstone impregnated with kerogen. The reduction in expulsion efficiency was thought to be due to the kerogen in the interlayer region of the smectite structure being converted to bitumen that on heating converted to pyrobitumen through a crosslinking reaction. This actively inhibits oil generation and expulsion efficiency by changing the pore system from water-wet to bitumen-wet. Again, using the same samples, this result was confirmed by Clauer et al. [8], who monitored the changes in chemistry, mineralogy, and K–Ar isotope ratios. Mineralogical changes were monitored by XRD and consisted of recording inhibition of swelling of smectite layers and promotion of illite layers following the impregnation of the pore system and interlayer region of the smectite structure by pyrobitumen after heating to temperatures above 365 °C for 72 h.

Data from our <2 μm samples show that smectite in Kreyenhagen samples (Figure 6b,c) is dominated by randomly interstratified mixed-layer illite-smectite (I/S) where the S component exceeds ~85% in a Reichweite R0 arrangement. Samples show evidence of inhibition to swelling after treatment with ethylene glycol, a behaviour attributed to the <2 μm fraction being Mg-saturated [51]. When heated at 375 °C for 1 h it produces a very broad 10 Å reflection, which is asymmetric toward the high angle side. This XRD characteristic is caused by the difficulty of removing interlayer water associated with the interlayer Mg^{2+} cation [51]. Thus, inhibition of swelling in smectite need not be associated with the adsorption of pyrobitumen in the interlayer space although our data neither confirm nor deny the concept that formation of a pyrobitumen-smectite complex in the interlayer space [7,8] may inhibit oil generation. Further investigation is required in order to resolve this issue.

6. Conclusions

Evolution of the palaeo-Sierra Nevada provided remarkably uniform smectite-dominated fine-grained sediment input to the forearc basin during the deposition of the Upper Cretaceous and Paleogene Moreno Fm and the mid-to-late Eocene Kreyenhagen Fm. Deposition of the Moreno Fm was concurrent with volcanic activity in the magmatic arc, and the alteration of rhyolitic or dacitic volcaniclastics is the likely primary source of smectite. The absence of tuff means that there is no direct evidence of volcaniclastic deposition in the marine forearc basin. Volcaniclastics are likely to have been incorporated into terrestrial sedimentary systems, possibly pedogenic, and later reworked into marine environments.

Smectite is prevalent in the Kreyenhagen Fm but in the absence of concurrent Sierran magmatism. Weathering of granitic or dioritic-granodioritic source terrane is inferred during the extended period of sub-tropical climate in the late Paleocene and early Eocene. Local periods of kaolinite enrichment are present that record erosion of more deeply weathered terrane. Chemical data (high CIA) confirm significant leaching of source terrane.

Diatomaceous opaline silica is the main variable constituent in the fine-grained sediment budget. Opal CT is locally common in the Moreno Fm and the prevailing constituent of the Marca Member. In the Upper Kreyenhagen, opal CT is common and opal A is preserved in the youngest parts of the section.

Clinoptilolite is consistently present in small quantities in the Lower Kreyenhagen. but the common general relationship between co-occurrence of clinoptilolite, opal CT, and smectite is not unsustained; opal CT is typically absent where clinoptilolite occurs. Otherwise, the occurrence of clinoptilolite is entirely consistent with the strata of this age globally and indicative of open oceanic conditions.

Author Contributions: Conceptualization, A.G., G.P., and A.H.; methodology, M.J.W., F.C., and C.B.; validation, A.H., M.J.W., and L.W.; formal analysis, C.B., F.C., M.J.W., and L.W.; field investigation, A.G., G.P., and AH.; resources, A.H.; data curation, A.G.; writing—original draft preparation, A.H., M.J.W., and L.W.; writing—review and editing, A.H.; visualization, A.G. and A.H.; supervision, A.H.; project administration, A.H.; funding acquisition, A.H. All authors have read and agreed to the published version of the manuscript.

Funding: This research received part funding from the Sand Injection Research Group (SIRG) at the University of Aberdeen.

Institutional Review Board Statement: Not applicable.

Informed Consent Statement: Not applicable.

Data Availability Statement: The data presented in this study are available on request from the corresponding author. Some data availability is restricted by confidentially agreements with research sponsors.

Conflicts of Interest: There are no conflicts of interest.

References

1. Vigorito, M.; Hurst, A.; Cartwright, J.A.; Scott, A. Architecture of a sand injectite complex: Implications for origin and timing. *J. Geol. Soc. Lond.* **2008**, *165*, 609–612. [CrossRef]
2. Vigorito, M.; Hurst, A. Regional sand injectite architecture as a record of pore pressure evolution and sand redistribution in the shallow crust: Insights from the Panoche Giant Injection Complex, California. *J. Geol. Soc. Lond.* **2010**, *167*, 889–904. [CrossRef]
3. Zvirtes, G.; Hurst, A.; Philipp, R.P.; Palladino, G.; Grippa, A. The Tumey Giant Injection Complex, Tumey Hill, California (USA). *Geol. Soc. Lond. Spec. Publ.* **2019**, 493. [CrossRef]
4. Zvirtes, G.; Philipp, R.P.; Hurst, A.; Palladino, G.; De Ros, D.F.; Grippa, A. Petrofacies of Eocene sand injectites of the Tumey Giant Injection Complex, California (USA). *Sediment. Geol.* **2020**, *400*. [CrossRef]
5. Jay, J. Reservoir shale as oil source in California. AAPG Search and Discovery Article #90122©2011. In Proceedings of the AAPG Hedberg Conference, Austin, TX, USA, 5–10 December 2010.
6. Ramseyer, K.; Boles, J.R. Mixed-layer illite/smectite in Tertiary sandstones and shales, San Joaquin Basin, California. *Clay Clay Min.* **1986**, *34*, 115–124. [CrossRef]
7. Lewan, M.; Dolan, M.; Curtis, J.B. Effects of smectite on the oil-expulsion efficiency of the Kreyenhagen Shale, San Joaquin Basin, California, based on hydrous-pyrolysis experiments. *AAPG Bull.* **2014**, *98*, 1091–1109. [CrossRef]
8. Clauer, N.; Lewan, M.D.; Dolan, M.P.; Chaudhuri, S.; Curtis, J.B. Mineralogical, chemical and K-Ar changes in Kreyenhagen Shale whole rocks and <2 μm clay fractions during natural burial and hydrous-pyrolysis experimental maturation. *Geochim. Cosmochim. Acta* **2014**, *130*, 93–112.
9. Cavalcante, F.; Fiore, S.; Piccarreta, G.; Tateo, F. Geochemical and mineralogical approaches to assessing provenance and deposition of shales: A case study. *Clay Miner.* **2003**, *38*, 383–397. [CrossRef]
10. Perri, F.; Critelli, S.; Cavalcante, F.; Mongelli, G.; Dominici, R.; Sonnino, M.; De Rosa, R. Provenance signatures for the Miocene volcaniclastic succession of the Tufiti di Tusa Formation, southern Apennines, Italy. *Geol. Mag.* **2012**, *149*, 423–442. [CrossRef]
11. Graham, S.A.; Williams, L.A. Tectonic, depositional, and diagenetic history of Monterey Formation (Miocene), central San Joaquin Basin, California. *AAPG Bull. Am. Assoc. Petr. Geol.* **1985**, *69*, 385–411.
12. Namson, J.S.; Davis, T.L. Seismically active fold and thrust belt in the San Joaquin Valley, central California. *Geol. Soc. Am. Bull.* **1988**, *100*, 257–273. [CrossRef]
13. Grippa, A.; Hurst, A.; Palladino, G.; Iacopini, D.; Lecomte, I.; Huuse, M. Seismic imaging of complex geometry: Forward modelling of sandstone intrusions. *Earth Planet. Sci. Lett.* **2019**, *513*, 51–63. [CrossRef]
14. Franzini, M.; Leoni, L.; Saitta, M. Revision di una metodologia analitica per fluorescenza-X, basala sulla correzione complet degli efftti di matrice. Rendiconti della. *Soc. It. Min. Petr.* **1975**, *31*, 365–378.
15. Claisse, F. Accurate X-ray fluorescence analysis without internal standards. *Norelco Rep.* **1957**, *4*, 3–17.
16. Lezzerini, M.; Tamponi, M.; Bertoli, M. Calibration of XRF data on silicate rocks using chemicals ans in-house standards. *Atti Soc. Tosc. Sci. Nat. Mem.* **2014**, *121*, 65–70.
17. Lezzerini, M.; Sartori, F.; Tamponi, M. Effect of amount of material used on sedimentation slides in the control of illite "crystallinity" measurements. *Eur. J. Mineral.* **1995**, *7*, 819–823. [CrossRef]
18. Moore, D.M.; Reynolds, R.C., Jr. *X-ray Diffraction and Identification and Analysis of Clay Minerals*, 2nd ed.; Oxford University Press: Oxford, UK; New York, NY, USA, 1997; 378p.
19. Środoń, J.; Drits, V.A.; McCarty, D.K.; Hsieh, J.C.C.; Eberl, D.D. Quantitative X-ray diffraction analysis of clay-bearing rocks from random preparation. *Clay Clay Min.* **2001**, *49*, 514–528.
20. Cavalcante, F.; Fiore, S.; Lettino, A.; Piccaretta, G.; Tateo, F. Illite-smectite mixed layers in sicilide shales and piggy-back deposits of the Gorgoglione Formation (Southern Appenines): Geological inferences. *Boll. Soc Geol. It.* **2007**, *126*, 241–254.
21. Krumm, S. The Erlangen geological and mineralogical software collection. *Comput. Geosci.* **1999**, *25*, 489–499. [CrossRef]
22. Leoni, L.; Saitta, M.; Sartori, F. Analisi mineralogica quantitative di rocce e sedimenti pelitici mediante combinazione di dati diffrattometrici e dati chimici. *Rend. Soc. It. Min. Petr.* **1989**, *43*, 743–756.
23. Cesarano, M.; Bish, D.L.; Cappelletti, P.; Cavalcante, F.; Belviso, C.; Fiore, S. Quantitative mineralogy of clay-rich siliciclastic landslide terrain of the Sorrento Penisula, Italy, using a combined XRPD and XRF approach. *Clay Clay Min.* **2018**, *66*, 353–369. [CrossRef]

24. McLennan, S.M.; Taylor, S.R.; Hemming, S.R. Composition, differentiation, and evolution of continental crust: Constraints from sedimentary rocks and heat flow. In *Evolution and Differentiation of the Continental Crust*; Brown, M., Rushmer, T., Eds.; Cambridge University Press: Cambridge, UK, 2006; pp. 92–134.
25. Nesbitt, H.W.; Young, G.M. Early Proterozoic climates and plate motions inferred from major element chemistry of lutites. *Nature* **1982**, *299*, 715–717. [CrossRef]
26. Grim, R.E.; Gǜven, N. *Bentonites: Geology, Mineralogy, Properties and Uses. Developments in Sedimentology 24*; Elsevier Scientific: Amsterdam, The Netherlands, 1978; 256p.
27. Nadeau, P.H.; Reynolds, R.C., Jr. Volcanic components in pelitic sediments. *Nature* **1981**, *294*, 72–74. [CrossRef]
28. Chamley, H. *Clay Sedimentology*; Springer: Berlin, Germany, 1989; 623p.
29. Deconnick, J.F.; Chamley, H. Diversity of smectite origins in late Cretaceous sediments: Example of chalks from northern France. *Clay Min.* **1995**, *30*, 365–379. [CrossRef]
30. Deepthy, R.; Balakrishnan, S. Climatic control on clay mineral formation: Evidence from weathering profiles developed on either side of the Western Ghats. *J. Earth Syst. Sci.* **2005**, *114*, 545–556. [CrossRef]
31. Fisher, G.B.; Ryan, P.C. The smectite-to-disordered kaolinite transition in a tropical soil chronosequence, Pacific Coast, Costa Rica. *Clay Clay Min.* **2006**, *54*, 571–586. [CrossRef]
32. Guimarães, E.M. Greywacke weathering under tropical climate: Chemical and mineralogical changes (example from central Brazil). In Proceedings of the 19th World Congress of Soil Science, Soil Solutions for a Changing World, Brisbane, Australia, 1–6 August 2010; pp. 24–27.
33. Barth, A.P.; Walker, J.D.; Wooden, J.L.; Riggs, N.R.; Schweikert, R.A. Birth of the Sierra Nevada magmatic arc: Early Mesozoic plutonism and volcanism in the east-central Sierra Nevada of California. *Geosphere* **2011**, *7*, 877–897. [CrossRef]
34. Ingersoll, R.V. Initiation and evolution of the Great Valley forearc basin of northern and central California, USA. *Geol. Soc. Lond. Spec. Publ.* **1982**, *10*, 459–467. [CrossRef]
35. Cassel, E.J.; Grove, M.; Graham, S.A. Eocene drainage evolution and erosion of the Sierra Nevada batholith across northern California and Nevada. *Am. J. Sci.* **2012**, *312*, 117–144. [CrossRef]
36. McInherney, F.A.; Wing, S. A perturbation of carbon cycle, climate, and biosphere with implications for the future. *Annu. Rev. Earth Planet. Sci.* **2011**, *39*, 489–516. [CrossRef]
37. Peterson, G.L.; Abbott, P.L. Mid-Miocene climatic change, southwestern California and northwestern Baja California. *Paleogeogr. Paleoclimatol. Paleoecol.* **1979**, *26*, 73–87. [CrossRef]
38. Bestland, E.A.; Retallack, G.J.; Swisher, C.C., III. Stepwise climate change recorded in Eocene-Oligocene paleosol sequences from central Oregon. *J. Geol.* **1997**, *105*, 153–172. [CrossRef]
39. Brown, G. Associated Minerals. In *X-ray Structures of Clay Minerals and Their X-ray Identification*; Brindley, G.W., Brown, G., Eds.; Mineralogical Society of Great Britain and Ireland: London, UK, 1984; pp. 361–410.
40. Wilson, M.J. The structure of opal-CT revisited. *J. Non-Cryst. Solids* **2014**, *405*, 68–75. [CrossRef]
41. Wilson, M.J.; Russell, J.D.; Tait, J.M. A new interpretation of disordered alpha cristobalite. *Contrib. Mineral. Petrol.* **1974**, *47*, 1–6. [CrossRef]
42. Nathan, Y.; Flexer, A. Clinoptilolite, paragenesis and stratigraphy. *Sedimnetology* **1977**, *24*, 845–855. [CrossRef]
43. Curtis, C.D.; Cornell, W.C. Unusual occurrence of clinoptilolite: Fresno County, California. *Geol. Soc. Am. Bull.* **1972**, *83*, 833–838. [CrossRef]
44. Stonecipher, S.A. Origin, distribution and diagenesis of phillipsite and clinoptilolite in deepsea sediments. *Chem. Geol.* **1976**, *17*, 307–318. [CrossRef]
45. Levy, S.S.; O'Neil, J.R. Moderate-temperature zeolitic alteration in a cooling pyroclastic deposit. *Chem. Geol.* **1989**, *76*, 321–326. [CrossRef]
46. Lander, R.H.; Hay, R.L. Hydrogeologic control on zeolitic diagenesis of the White River sequence. *Geol. Soc. Am. Bull.* **1993**, *105*, 361–376. [CrossRef]
47. Merino, E.; Wang, Y.; Deloule, E. Genesis of agates in flood basalts: Twisting of chalcedony fibres and trace element geochemistry. *Am. J. Sci.* **1995**, *295*, 1156–1176. [CrossRef]
48. Hurst, A.; Morton, A.C.; Scott, A.; Vigorito, M.; Frei, D. Heavy mineral assemblages in sandstone intrusions: Panoche Giant Injection Complex, California. *J. Sediment. Res.* **2017**, *87*, 1–18. [CrossRef]
49. Scheirer, H.A.; Magoon, L.B. Petroleum Systems and Geologic Assessment of Oil and Gas in the San Joaquin Basin Province, California. In *USGS Professional Papers*; US Geological Survey: Reston, VA, USA, 2007; p. 1713.
50. Dolan, M.P. The Role of Smectite in Petroleum Formation: Comparing Natural and Experimental Thermal Maturation. Master's Thesis, Colorado School of Mines, Golden, CO, USA, 1998; 217p.
51. Farmer, V.C. Water on particle surfaces. In *The Chemistry of Soil Constitutents*; Greenland, D.J., Hayes, M.H.B., Eds.; John Wiley and Sons: Chichester, UK, 1978; pp. 405–448.

Appendix 4-15

Test Results for the Nora Schultz Well No. 2 (Pearce, 1989)

KEN E. DAVIS ASSOCIATES

January 6, 1989

Mr. James E. Clark
E. I. DuPont de Nemours & Company
ESD
P. O. Box 3269
Beaumont, Texas 77704

Re: Test Results for the Nora Schulze Well No. 2
KEDA Job No. 10-1182

Dear Mr. Clark:

This letter report summarizes the test results that KEDA, Inc. (KEDA) has collected for mud samples obtained from the upper 730+ feet of the Nora Schulze Well No. 2 located in Nueces County, Texas (Figure 1).

The Nora Schulze No. 2 well was drilled and completed between November 13, 1959 and November 25, 1959. On November 25, 1959 this well was plugged and abandoned. According to Dresser-Magcobar records, Attachment 1, the well was drilled to total depth with a mud weight that ranged between 10.6 and 11 ppg for depths below 7300 feet. This mud was used to fill uncemented portions of the cased hole during the final plugging operations.

On August 26, 1988, KEDA commenced operations to reenter this well for the purposes of cementing the top portion of the well from 1035 feet to the surface.

However, before initiating the plugging operations requested by the Texas Water Commission (TWC), KEDA, in consultation with the TWC, elected to core the mud in the hole using a special coring bit and tubing string which could be pushed into the mud.

The tubing, which initially contacted the mud 12 feet below the surface, was pushed into the cased hole to a total depth of 734 feet. At this depth, the shear strength of the mud exceeded the weight that could be applied on the tubing, and no further progress could be made. Therefore, the tubing was pulled out of the hole and the recovered mud was allowed to flow into 5 gallon buckets. The bottom 18 feet of sample did not flow from the tubing and was, therefore, retained in the three 6-foot pipe joints that were initially installed on the tubing for this purpose.

3121 SAN JACINTO HOUSTON, TX 77004
SUITE 102 (713) 522-5784

O BOX 80558 BATON ROUGE, LA 70898
1805 SUN BELT COURT BATON ROUGE, LA 70809
(504) 293-2561

300 N MICHIGAN SOUTH BEND, IN 46601
SUITE 409 (219) 287-2282

A total of 22 mud samples were obtained from the well. Each 5 gallon bucket contains the mud that was captured in each 33-foot tubing joint below 111 feet. The depths reported for each mud represents the midpoint for the sample that was collected from each tube. The first two samples represent the mud from two joints of tubing.

Table I presents the data that was collected on the mud samples which were recovered from the Nora Schulze No. 2 well. The average mud weight in the column was determined to be 11.1 lbs/gal and the average shear strength for Samples 3 through 17 was 260 lbs/100 ft^2. The average gel strength was 267 lbs/100 ft^2.

If you have any questions, or require more details, please contact me at your earliest convenience.

Sincerely,

KEN E. DAVIS ASSOCIATES

Mark S. Pearce

Mark S. Pearce
Regional Manager

MSP/js
Attachments

WELL : NORA SCHULZE No. 2

LOCATION : CORPUS CHRISTI AREA

MUD TYPE : LIGNOSULFATE ?

MUD DENSITY : 11.0 POUNDS/GALLON

GEL STRENGTH : 0/3 POUNDS FORCE/100 FEET^2

DRILLING COMMENCED : NOVEMBER 13, 1959

WELL P&A : NOVEMBER 25, 1959

DATE OF MUD SAMPLE : AUGUST 26, 1988

DEPTH OF MUD SAMPLES : 12' TO 754' BGL

WELL DIAGRAM

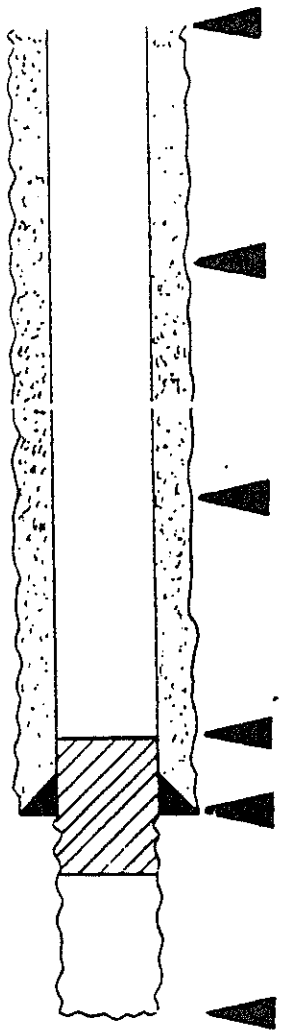

ALL DEPTHS RELATIVE TO GROUND LEVEL

STARTED PUSHING 4" PIPE AT 120'

STARTED DRILLING AT 734'

CEMENT PLUG 1035'-1172'

9-5/8" CASING
SET AT 1122'

TOTAL DEPTH AT 8512'

KEN E. DAVIS ASSOCIATES

HOUSTON, TX BATON ROUGE, LA SOUTH BEND, IN

NORA SCHULZE No. 2
FISHER AND DAVIDSON
ROBSTOWN, TEXAS

DATE	CHECKED BY	JOB NO
DRAWN BY	APPROVED BY	DWG NO

WELL DATA SHEET

DRESSER

HAG-380 A

OPERATOR: FISHER & DAVIDSON
WELL: Schultz #2
CONTRACTOR: Gilmour Drilling Company
ENGINEER: Kenneth Stewart

SURVEY: SEC. 84 20 T A-52 R
FIELD: E. Minnie
COUNTY: Nueces
STATE: Texas

CASING SIZE: DEPTH:
SURFACE:
INTERMEDIATE:
PRODUCTION:

DATE	DEPTH	WT.	VIS.	AV	PV	YP	GELS		PH	W/L	PM	CL PPM.	CA PPM.	SOL %	OIL %	M.B.T.	REMARKS
	4500	9.6	36				0	5		14.4		1300					Drills real good to 6500 f
	6500	10.0	47				0	3		8.6		1800			10		Below this depth drills w Oil usually added at 6500
	7000	10.2	62				5	15		5.6		2200			12½		The 10.2 pound per gallon go to 7500 feet.
	7300	10.6	47				0	3		5.6		2000			12		Had a 10.8 pound per gallon 7600 feet.
	7500	10.7	45				0	3		5.2		2100			12		Had a 11.01 pound per gall 8000 to 8500 feet.
	7600	10.6	48				0	5		5.6		2100			11½		
	7900	10.6	50				0	5		5.2		2100			10		Very bentonetic. Takes lot water.
	8470	11.0	47				0	3		5.0		2100			9		Natural weight is about 10. pounds per gallon.

TOTAL MUD COST: $2,987.00

DATE SPUDDED: DATE T.D.: B.H.T. COMPLETION FLUID TYPE: COST:

PACKER MUD TYPE: COST:

TABLE I

RECOVERED MUD PROPERTIES FOR NORA SCHULZE NO. 2 WELL

SAMPLE NO.	DEPTH (ft)	MUD WEIGHT (lb/gal)	SHEAR STRENGTH (lbs/100 ft^2)	GEL STRENGTH (lbs/100 ft^2)
1	---	---	---	---
2	60	12.0	540	304
3	111	10.9	230	296
4	174	11.0	310	295
5	207	11.2	190	<320
6	240	10.9	170	284
7	273	10.7	180	237
8	306	10.9	285	254
9	339	10.5	190	288
10	372	10.9	245	272
11	405	11.1	280	220
12	438	11.1	255	222
13	471	11.1	301	292
14	504	11.1	300	230
15	537	11.0	490	292
16	570	11.0	225	217
17	603	10.9	240	236
18	636	11.3	650	>320
19	609	11.4	750	---
20	702	11.5	2100	---
21	719	10.9	4700	---
22	725	10.7	890	---
23	731	11.3	7000	---

Average mud weight using all samples - 11.1

Shear strength averaged for samples 3 through 7 - 260 lbs/100 ft^2

Average gel strength of samples 3 through 7 - 267 lbs/100 ft^2

Plug and Abandonment of Offshore Wells: Ensuring Long-Term Well Integrity and Cost-Efficiency

Journal of Petroleum Science and Engineering 173 (2019) 478–491

Contents lists available at ScienceDirect

Journal of Petroleum Science and Engineering

journal homepage: www.elsevier.com/locate/petrol

Plug & abandonment of offshore wells: Ensuring long-term well integrity and cost-efficiency

Torbjørn Vrålstad[a,*], Arild Saasen[b], Erling Fjær[a], Thomas Øia[a], Jan David Ytrehus[a], Mahmoud Khalifeh[b]

[a] SINTEF Industry, Trondheim, Norway
[b] University of Stavanger, Stavanger, Norway

ARTICLE INFO

Keywords:
Plug and abandonment
Well integrity
Cost-efficiency
Barriers
Subsea

ABSTRACT

There is an upcoming "P&A wave" of wells that need to be permanently plugged and abandoned, especially in mature, offshore areas such as the North Sea and Gulf of Mexico. It is important to ensure that plugged wells do not leak after abandonment, as there could be several potential leak paths such as microannuli in plugged wells. To ensure well integrity after abandonment, permanent well barriers must extend across the full cross section of the well. That includes establishing barriers in all annuli, which could however be quite time-consuming and thus costly.

This paper is a review of challenges and technologies for P&A of offshore wells, with an emphasis on cost-effective solutions while establishing permanent well barriers. An overview of cement and other plugging materials is given, as well as a discussion of different types of potential leak paths and failure mechanisms in permanently plugged and abandoned wells. Moreover, recent technology developments such as utilizing shale as barrier for P&A are described. A discussion on the special considerations related to P&A of subsea wells is also included.

1. Introduction

When a well reaches the end of its lifetime, it must be permanently plugged and abandoned. Such plug and abandonment (P&A) operations usually consist of placing several cement plugs in the wellbore to isolate the reservoir and other fluid-bearing formations. Permanent P&A of wells has been an important topic for several years (Calvert and Smith, 1994; Jordan and Head, 1995; Barclay et al., 2001), but there has been an increased focus in recent years which is probably due to the large number of old offshore wells in mature areas such as the North Sea and Gulf of Mexico (Liversidge et al., 2006; Saasen et al., 2013; Rassenfoss, 2014; Davison et al., 2017). Operators are now informally talking about an upcoming “P&A wave” of wells that need to be permanently plugged.

Depending on well conditions, P&A operations can however be quite time-consuming and thus very costly. Moreover, offshore wells are considerably costlier to abandon than onshore wells (Oil & Gas UK, 2015a). In the North Sea for example, approximately two thousand wells are planned to be permanently plugged and abandoned in the upcoming decade. Up to £3 billion each year is forecasted to be spent on decommissioning activities in the North Sea during the upcoming years, where about 50% of these costs are on well P&A operations alone (Oil & Gas UK, 2016).

Furthermore, an essential aspect of P&A is to ensure well integrity after abandonment (King and Valencia, 2014). In earlier years, not too much emphasis was put on ensuring that wells were properly plugged since regulations covering P&A operations were vague and inadequate (NPC, 2011). Several old, plugged and abandoned wells are therefore leaking (Watson and Bachu, 2009; Vielstädte et al., 2015, Kaiser, 2017). Catalyzed by the 2010 Macondo accident and subsequent serious oil spill, changes in technology and regulatory regimes have caused the industry to make some significant shifts in their attitude towards P&A in recent years (Smith and Shu, 2013). The focus of P&A operations is now on environmental issues such as preventing leakages, in addition to cost-efficiency.

1.1. Plug and abandonment operations

Fig. 1 shows a simplified illustration of a typical production well before and after P&A.

The details of an operational P&A procedure may differ significantly from well to well, depending on the type of well and the actual well

* Corresponding author.
E-mail address: torbjorn.vralstad@sintef.no (T. Vrålstad).

https://doi.org/10.1016/j.petrol.2018.10.049
Received 21 September 2018; Accepted 16 October 2018
Available online 17 October 2018

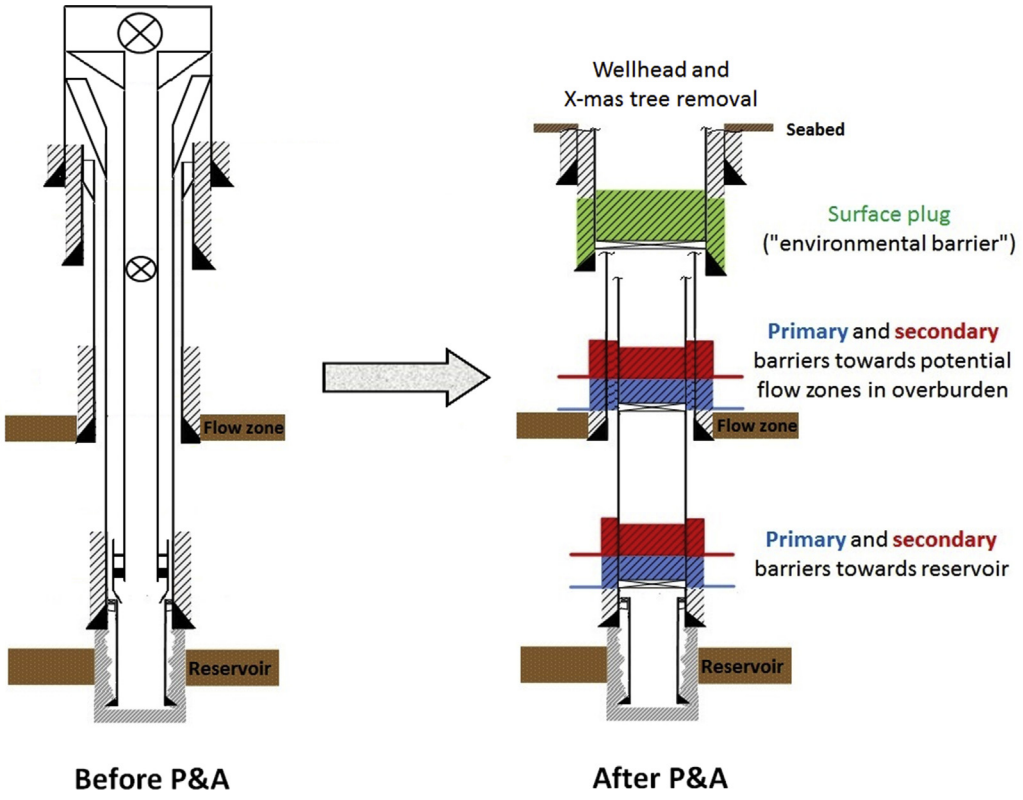

Fig. 1. Simplified illustration of a typical offshore production well before and after P&A. The colour coding of primary barriers (blue), secondary barriers (red) and surface plug (green) are based on current Norwegian well barrier definitions (NORSOK D-010, 2013). (For interpretation of the references to colour in this figure legend, the reader is referred to the Web version of this article.)

conditions. There are however several common steps, and a typical P&A operation can be briefly summarized as follows:

First, the well is prepared for P&A by circulating high density drilling fluid and installing deep set mechanical plug, before the barriers towards the reservoir are installed. A well-regulated area such as the North Sea requires two independent barriers towards the reservoir (NORSOK D-010, 2013; Oil & Gas UK, 2015b), where the primary and secondary barriers shall not have common well barrier elements. Secondly, any fluid-bearing formations in the overburden, such as high-pressure zones and hydrocarbon-containing formations, are also isolated with two independent barriers. Furthermore, an openhole-to-surface plug (also called the “environmental barrier”) is installed below the seabed, which prevents any residual fluid contamination to the environment. Finally, the conductor and wellhead are removed.

Oil & Gas UK (2015a) have divided the operational sequence of P&A operations into three distinct phases: Phase 1 is defined as “Reservoir abandonment” and includes installing primary and secondary barriers towards the reservoir. Phase 2 is defined as “Intermediate abandonment” and includes installing potential barriers towards flow zones in the overburden and the surface plug. Phase 3 is defined as “Wellhead and conductor removal” and includes cutting and retrieval of casing strings and conductor, as well as wellhead removal. In addition to these three phases, Moeinikia et al. (2014) have suggested to include a fourth phase as well, entitled Phase 0 ″Preparatory work”, which includes pre-P&A work such as killing the well and installing deep set mechanical plugs. Table 1 lists these different phases of the P&A operation and summarizes their respective contents.

An important benefit of dividing the full operational P&A sequence into different phases is that this approach highlights the opportunities for performing simpler parts of the P&A operation by rigless methods, instead of more traditional and costly rig-based methods. For example, for P&A of subsea wells, considerable costs can be saved by performing Phases 0 and 3 by a riserless well intervention (RLWI) vessel instead of a drilling rig (Sørheim et al., 2011; Moeinikia et al., 2015a; Varne et al., 2017a; Canny, 2017).

1.2. Potential leak paths in plugged and abandoned wells

Placing a cement plug in a cased wellbore is in most cases not sufficient to prevent leakages from the well after abandonment, as leakages may also occur in the annulus outside the casing. Especially for old wells where the annulus cement is likely to be damaged, since cracks and microannuli (i.e. debonding) may form in the cement sheath due to forces occurring in normal well operations such as pressure testing, injection, stimulation and production (Boukhelifa et al., 2005; Bois et al., 2011; Therond et al., 2017). For example, for a well after 30 years of CO_2 injection, prominent leak paths at both the cement-casing and cement-formation interfaces were found after coring (Carey et al.,

Table 1
Different phases of P&A operations for typical well with vertical Xmas tree.

Operational phase	Contents
Phase 0: Preparatory work	Retrieve tubing hanger plugs, kill well, install deep set mechanical plug, punch/perforate tubing, circulate well clean
Phase 1: Reservoir abandonment	Rig up BOP, pull tubing hanger and tubing, install primary barrier with its base at top of influx zone (i.e. reservoir), install secondary barrier where the base of barrier can withstand future anticipated pressures
Phase 2: Intermediate abandonment	Remove casing strings (if necessary), install primary and secondary barriers towards potential flow zones in overburden, install surface plug ("environmental barrier")
Phase 3: Wellhead and conductor removal	Cut conductor and casing strings below seabed to avoid interference with marine activity, retrieve casing strings, conductor and wellhead

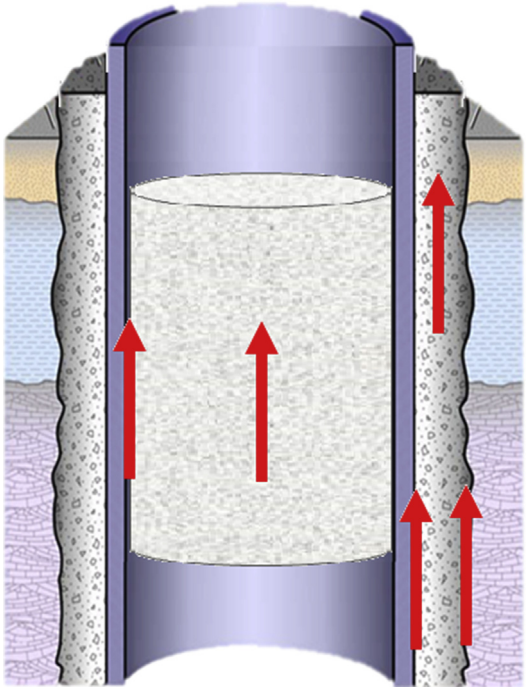

Fig. 2. Illustration of potential leak paths in a plugged and abandoned well: Through the cement or around the cement.

2007).

As illustrated in Fig. 2, there are several potential leak paths in a plugged and abandoned well (Gasda et al., 2004; Carrol et al., 2016; Kiran et al., 2017). For the cement plug, leakages may go through the plug itself, depending on cement matrix permeability or presence of internal cracks, or around the plug at the cement-casing interface, due to microannuli formation during cement shrinkage or poor mud removal. Similarly, for the annulus cement, leakages may go through the cement sheath, or around the cement sheath at the cement-casing interface or at the cement-formation interface. It is assumed that the casing itself does not represent a potential leak path, since it is covered and protected by cement at all sides, although this assumption may be incorrect in the extreme long-term.

Norwegian well barrier requirements therefore state that *"permanent well barriers shall extend across the full cross section of the well"* (NORSOK D-010, 2013), which means that the barrier starts and ends at the formation surrounding the wellbore and includes all annuli as well as the cement plug. For example, the primary well barrier envelope towards the reservoir shown in Fig. 1, consists of the in-situ formation, annulus cement, casing and cement plug. In other words, all these well barrier elements must seal sufficiently for the well to be properly abandoned, and if one of them fails the whole well barrier envelope is breached and the well may start leaking. The wellbore must therefore be sealed off from rock to rock, and this point has been elegantly expressed by Oil & Gas UK (2015b), when describing that the aim of P&A operations is *"restoring the cap rock"*.

2. Plugging materials

Although Portland cement is by far the most commonly used plugging material, there are other types of alternative and emerging plugging materials (Oil & Gas UK, 2015c; Khalifeh et al., 2013). A description of some of these materials is given in the following, with an emphasis on Portland cement. Table 2 provides an overview of these different plugging materials.

2.1. Portland cement

Throughout history, setting materials have played an important role and were used widely in the ancient world (Blezard, 2007). For example, the Romans found out that a setting material could be made which sets under water and it was used for the construction of marine structures such as harbours. In 1824, Joseph Aspdin patented a setting material he produced by calcining a mixture of limestone and clay at 1450 °C. The cured produced material looked like Portland stone, a widely-used building stone in England and a building stone preferred by London's famous architect and church builder Christopher Wren, a century before Aspdin's invention. Because of the similarity with Portland stone, Aspdin called his invention “Portland cement".

The major components of Portland cement clinker, being the material leaving the cement kiln, are CaO, SiO_2, Al_2O_3, and Fe_2O_3. The clinker mainly contains four major mineral phases: 50–70% tricalcium silicate ($3CaO{\cdot}SiO_2$ or “C_3S”), 15–30% dicalcium silicate ($2CaO{\cdot}SiO_2$ or “C_2S”), 5–15% tricalcium aluminate ($3CaO{\cdot}Al_2O_3$ or “C_3A”) and 5–10% tetracalcium aluminoferrite ($4CaO{\cdot}Al_2O_3Fe_2O_3$ or “C_4AF”). The calcium silicates are amorphous unstable material that will re-crystallise or develop stable amorphous forms after blending with water. First, there is a reactive period where water reacts with the mineral surfaces and creates a gel like layer that prevents further reaction. This creates a dormant period, i.e. an induction period, where it is possible to pump the cement. When the calcium concentration in the mix water is sufficiently over-saturated, further curing reactions occur and the calcium silicates and the mentioned gel starts to form and build strength, i.e. the cement sets to become a solid material. For the aluminates there are no dormant period. To control setting of these minerals, calcium sulphate minerals (gypsum, anhydrite, hemi-hydrite, etc) are added. As long as there is gypsum left, metastable crystals (ettringite) will be formed onto the aluminate, and an artificial dormant period is created. The ferrite phase reacts similarly as the aluminate but very much slower. For a more thorough description of cement curing, the reader is referred to *Lea's Chemistry of Cement and* Concrete (Hewlett, 1998) and Taylor (1992).

Use of Portland cement in well cementing is described by Nelson and Guillot (2006), and there are now several different types of Portland cement. In the early days of well construction, cement was a material available from the construction industry. Thus, in absence of other zonal isolation or plug back material, this cement was accepted without any of the present qualification programmes. Originally, plain construction cement types were used. Hence, these became API classes A, B and C cements, dependent on their reactivity and sensibility for other present materials. As the wells became deeper, and the temperature increased, there was a need for materials that did not solidify equally rapid. The simple solution was to grind coarser material. This would delay the cement thickening time, and the results were API classes D, E and F cement. As cement production technology developed, these types, D, E and F, are seldom used because specialised oil well cements for general application were developed; the API cement types classes G and H. The essential difference between these two types is again, fineness. Class G cement is somewhat finer than class H. These two cements dominate as material for current offshore cementing operations.

Portland cement is rarely used as neat cement without any additives, so a description of cement is incomplete without also mentioning necessary additives. These include:

- Barite, ilmenite, hematite or manganese tetra oxide to increase slurry density
- Bentonite (pre-hydrated or dry), hollow glass spheres or pozzolans to reduce density or increase cement yield (cemented volume per volume of cement)
- Microsilica or latex to make the cement slurry gas tight
- Silica flour to make the cement tolerant for temperatures above

Table 2
Overview of different plugging materials; both currently used and alternative/emerging.

Plugging material	Description
Portland cement	Most commonly used plugging material worldwide. Consists mainly of calcium hydroxide ("portlandite") and various calcium silicate phases. Addition of selected additives enables a wide range of different specialised cement systems such as expandable cements and flexible cements.
Blast Furnace Slag (BFS)	This waste product from steel manufacturing process has been used in well cementing applications, by itself and as additive to Portland cement. Not widely used as plugging material.
Bentonite	Bentonite has been applied as plugging material due to its ability to swell and its low permeability.
Low melting point metal alloys	Bismuth containing low melting point metal alloys has been suggested as a potential plugging material. An advantage would be a good metal-to-metal bond to casings.
Thermosetting polymers (resins)	Resins are particle-free fluids which solidify into an impermeable material upon curing. The curing process is temperature-activated and occurs at a predefined temperature. Have been used as plugging material.
Unconsolidated sand slurries	Sand slurries as plugging material fills the well with a deformable, low porosity, non-permeable and non-shrinkable material, that is easy to remove. Well-suited for temporary abandonment, and has also been used for permanent abandonment.
Geopolymers	Geopolymers are a type of inorganic, rock-like, materials that can be described as "artificial stone". Were originally developed as construction material for the civil engineering sector but several laboratory studies have shown their potential in oil well applications as well, including as an alternative plugging material.
Thermite	Potential step-change technology where burning thermite is used to melt the casing, cement and rock to form an impermeable plug. A potential concern is whether any leak paths are formed around the plug after cooling.

110 °C
- Flexible particles to reduce stiffness and improve flexibility
- Expandable agents such as magnesium oxide and calcium oxide

These additives will affect both the short- and long-term properties of the placed cement volume as well as interfere with the placement itself. A brief review of cement additives has been given by Nelson et al. (2006).

2.2. Alternative and emerging plugging materials

2.2.1. Blast Furnace Slag (BFS)

Blast Furnace Slag (BFS) is a by-product of steel manufacture during operation of a blast furnace. The BFS is accumulated on top of the molten iron in the furnace, and consists of lime, silica, alumina, magnesia and iron oxides. Depending upon the cooling process, this waste product can be used as hydraulic binder material (i.e. cement), both by itself and as additive to Portland cement, and has been used in well cementing applications (Saasen et al., 1994).

In the late 1980s and the following years, a technique was developed for converting drilling fluid to cement. Cowan et al. (1992) developed the Mud-to-Cement system based on adding BFS to certain water-based drilling fluids, where BFS was used partly as weight material and partly as fluid loss control material. When cementing was to be performed, the BFS concentration was increased while alkali activators were added. The BFS formulated mud-to-cement was used in several onshore fields in Texas, US (Daulton et al., 1995). The initial response was that the cementing operations were reasonably successful, and the following offshore experience was similarly promising (Nahm et al., 1995).

Later, the drilling industry abandoned use of BFS in well cementing. According to Bensted (2007), this was because the cured slag cement was vulnerable for crack development. Furthermore, the logistics around the application was complex. The use of BFS as sole plug material may thus be limited. Also, the wide application of oil-based drilling fluid may restrict the use of BFS for cementing operations.

2.2.2. Bentonite

Concentrated bentonite has been applied as material for P&A of oil and gas wells due to its ability to swell and its low permeability (Englehardt et al., 2001; Clark and Salsbury, 2003). The material has been tested and used successfully for P&A operations in several wells in the US and Australia in recent years. According to Towler et al. (2016) laboratory tests have shown that the concentrated bentonite would reheal itself if cracks occurred.

2.2.3. Low melting point metal alloys

Low melting point eutectic metals have been tested for removing sustained casing pressures both in presence of oil-based and water-based drilling fluids (Carpenter et al., 2004). Also, in the formulation of the low melting point eutectic metal plug, bismuth was one of the ingredients. This is beneficial for proper bonding to the well and pipe surfaces, since this metal expands significantly on solidification, thereby creating a good metal-to-metal bond. Recently, bismuth alloys have been suggested as plugging material for permanent P&A (Carragher and Fulks, 2018).

2.2.4. Thermosetting polymers (resins)

Thermosetting polymer (resins) are particle-free fluids which solidify into an impermeable material upon curing. The curing process is temperature-activated and occurs at a predefined temperature. In addition, viscosity and density can be tailored for various applications by addition of particles. Resins have been used as plugging material both in the North Sea and Gulf of Mexico (Beharie et al., 2015; Davis, 2017). With respect to durability, laboratory tests have shown a loss of strength in downhole environments such as crude oil and H_2S (Beharie et al., 2015). Other uses of resins are in squeeze operations in the annulus between two casings to regain zonal isolation (Al-Ansari et al., 2015), and repair of casing leaks (Sanabria et al., 2016).

2.2.5. Unconsolidated sand slurries

Unconsolidated sand slurries have been used for permanent plug and abandonment (Saasen et al., 2011), and the permeability should theoretically be less than 0.01 mDarcy. The purpose of sand slurries as plugging material is to fill the well with a deformable, low porosity, non-permeable and non-shrinkable material. If a system with solely monodisperse particles was used, the maximum sand concentration would be just a bit larger than 50%, leaving the rest to a permeable pore volume. However, if particle sizes are selected carefully, it is possible to fill the pore volume with successively smaller particles, to create a high solids fraction slurry. These high solid fraction slurries will be easily mobile but will behave like a fluid with reasonably high yield stress.

Such a sand slurry was developed and originally qualified for temporary abandonment (Saasen et al., 2004), and it is well-suited for such an application due to its non-setting and thus easily removable nature. In this example, the sand concentration was around 80%. Care must be taken to hinder access to additional water, since addition of water can trig an internal segregation process that will make the sand slurry paste-like and thus not pumpable. Change of fluid properties must be conducted by addition of solids (Godøy et al., 2004).

2.2.6. Geopolymers

Geopolymers are a type of inorganic, rock-like materials that can be

described as “artificial stone”. They are alkali-activated aluminosilicate materials with low calcium content (Davidovits, 2011). Geopolymers are based upon different raw materials (i.e. precursor materials) such as fly ash, kaolinite and various types of rocks. By varying the type of raw material, different types of geopolymers with selected properties can be obtained.

Three main mechanisms are distinguished, which result in solidification of aluminosilicate material: dissolution or depolymerization, transportation or orientation and geopolymerization or polycondensation (Provis and van Deventer, 2009). In dissolution process, alkaline activator (known also as hardener) attacks precursor materials and depolymerizes the silicates. As a result, small species of inorganic polymer units, oligomers, are formed. These oligomers have the opportunity to be transported through the liquid phase and rearrange themselves. In the geopolymerization stage, these oligomers make covalent bonding together and form long chains of molecules, known as geopolymers. The geopolymerization process is a fast reaction and difficult to control.

Geopolymers were developed and are used as construction materials in the civil engineering sector (Davidovits, 2011), and has not yet been used in plug cement operations or other well applications. However, several studies have shown their potential as well cement material (Khalifeh et al., 2014, 2018; Salehi et al., 2017). Properties such as low shrinkage, low permeability, strength development, stability at elevated temperatures, and tolerance to contamination with oil-based mud (OBM), suggest geopolymers to be an alternative to Portland cement for many oil well cementing applications including P&A (Khalifeh et al., 2016, 2017; Salehi et al., 2016). There are currently some unanswered questions regarding their usability, such as controlling pumpability while optimizing waiting on setting. Others have observed self-healing properties of geopolymer solutions (Liu et al., 2017), which may be beneficial in a long-term perspective.

2.2.7. Thermite

A recent, emerging development from Norway is the potential use of thermite to permanently plug wells. To our knowledge, no publications exist yet that describes this procedure, although it was mentioned by Stein (2018). The concept is to initiate slow burning of a thermite plug at selected depth, which is an exothermic reaction that reaches thousands of degrees Centigrade. The reactants melt through the wellbore, including casing, cement and formation, and bond with the surrounding rock formation. After cooling, the result will be a solid and impermeable barrier that extends across the full cross section of the well.

This concept could be a major game changing P&A technology if it works as intended. At present, the technology is still under development and is being tested and validated. A potential drawback and current concern is whether the rock around the formed plug is damaged; i.e. if any leak paths are created around the plug after cooling.

3. Ensuring plug integrity

To fulfil the objective of “restoring the cap rock”, the plug itself must seal the wellbore and retain its integrity for the future. NORSOK D-010 (2013) lists the following characteristics of permanent well barrier materials, and a similar list is also given by Oil & Gas UK (2015b):

- Provide long term integrity (eternal perspective)
- Impermeable
- Non-shrinking
- Able to withstand mechanical loads/impact
- Resistant to chemicals/substances (H_2S, CO_2 and hydrocarbons)
- Ensure bonding to steel
- Not harmful to the steel tubulars integrity

For simplicity, it is assumed in this section that cement is used as plugging material, since cement is used in most plugging operations. However, most of the discussion is relevant for other plugging materials as well.

As shown in Fig. 2, potential leakages related to the wellbore plug can occur *through* the plug or *around* the plug. Leakages through the plug is mostly determined by the permeability of the plugging material. Chemical or thermal degradation of the plugging material due to downhole conditions may influence the integrity of the plug, and thus potentially increase the leak rate through the plug. Whereas leakages around the plug occurs between the plug and casing (or formation), i.e. in so-called “microannuli”, and could be caused by debonding due to shrinkage during cement curing or by poor mud removal during plug placement.

3.1. Plug placement

There are several methods available for placement of cement plugs inside wellbores and an overview of plug placement methods has been given by Daccord et al. (2006). Most commonly used is the balanced plug method, where cement is pumped through the work string and placed at the designated depth. However, placement of good cement plugs can be an operational challenge.

A critical issue during cement plug placement is to prevent flow of cement further down into the well, due to instabilities of the lower interface towards the fluid below caused by differences in density or viscosity (Calvert et al., 1995; Crawshaw and Frigaard, 1999; Malekmohammadi et al., 2010). This phenomenon is known as Rayleigh-Taylor instability. It is therefore important to have a good base or foundation for the cement plug to ensure good placement. Gel plugs or viscous pills have been used as foundation for cement plugs, but Harestad et al. (1997) has shown that the use of viscous pills underneath a denser cement will be insufficient to hinder downwards cement flow. Mechanical bridge plugs are often used as foundation and these devices ensure a good base for the cement. In fact, in some countries like Norway, the required cement plug length is halved when a mechanical plug is used as foundation (NORSOK D-010, 2013), since it is believed that the cement plug integrity will improve due to its good base. A disadvantage with this approach is that the bridge plug will resist the testing pressure after cement placement, and there is thus no method to directly verify the cement quality. A soft packer on the other hand, like the umbrella tool developed by Harestad et al. (1997), only prevents motion of the fluid across the packer, and therefore allows for pressure testing of the cement plug.

3.2. Durability of cement at downhole conditions

For wellbore plugs to retain their sealing ability over time, the plugging material should be unaffected by the ambient downhole conditions. In other words, the plugging material should not degrade thermally or chemically. Typical potentially detrimental downhole chemicals include CO_2, H_2S and hydrocarbons, but water (i.e. brine) should perhaps also be included to this list since it is usually always present downhole. The durability of plugging materials such as cement can be determined by performing controlled ageing tests in the laboratory, but as Zhang and Bachu (2011) have pointed out, the specific test conditions used in ageing tests can have a major impact on the obtained results. Care should therefore be taken when designing a test procedure for ageing tests, and Oil & Gas UK (2015c) has suggested a guideline on how to perform durability tests of plugging materials.

Durability of well cement in CO_2-rich environments has been studied rather extensively in recent years as part of research on Carbon Capture and Storage (CCS), and the degradation mechanisms of Portland cement due to CO_2 are relatively well-known (Kutchko et al., 2007; Zhang and Bachu, 2010; Carrol et al., 2016). It is beyond the scope of this paper to give a comprehensive overview of this work, but a brief description of the degradation mechanisms can be summarized as

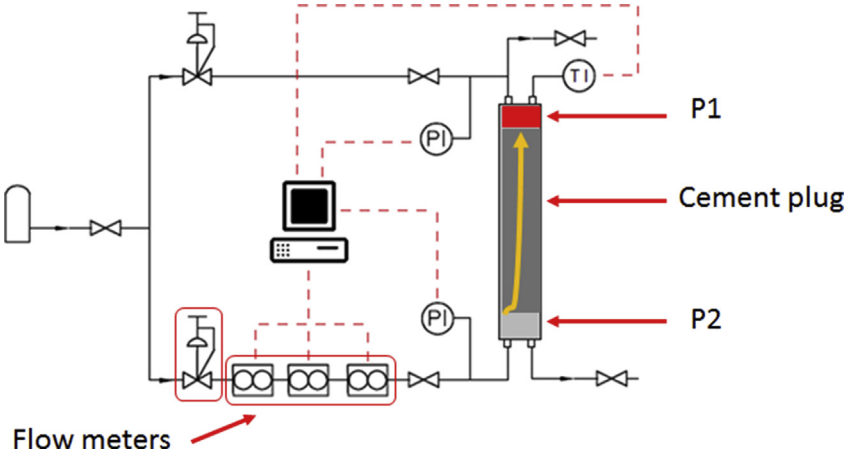

Fig. 3. Illustration of a typical laboratory set-up for determination of cement plug sealing ability: a cement plug is placed inside a steel casing with a pressure difference across the plug (P1 < P2) and the resulting flow rate is measured by flow meters (After Opedal et al., 2018).

follows: Degradation of Portland cement by CO_2 occurs in two main steps, where the first step is reaction of calcium hydroxide (portlandite) with CO_2 where calcium carbonate is formed. This step is called "carbonation" of cement, and leads to a decrease in cement porosity and permeability, but not necessarily a decrease in mechanical properties. The next step is called "bi-carbonation" of cement, where calcium carbonate is dissolved in CO_2-rich (i.e. low-pH) water. The resulting silica-rich, degraded material is highly porous, which may be unsuitable as barrier material due to its high permeability. It should however be noted that since CO_2 degradation of Portland cement is a diffusion-driven chemical reaction, the actual degradation kinetics is very slow and can thus be a self-decelerating process. For example, the decrease in permeability caused by the carbonation step significantly slows down the reaction rate of the second step, and local equilibria of Ca^{2+} ions inside pores also prevent the second degradation step (Zhang and Bachu, 2010). A full degradation of a cement plug of tens of meters by CO_2 will therefore be extremely slow, i.e. occur over thousands or hundreds of thousands of years. Furthermore, the service industry has developed cement systems that are more CO_2-resistant than neat Portland cement (Barlet-Gouédard et al., 2009; Brandl et al., 2011; Garnier et al., 2012), by including selected additives such as different pozzolans and by decreasing the permeability of the cement matrix to decrease CO_2 diffusion further.

There exist some durability studies of cement in other relevant downhole environments such as H_2S and crude oil as well (Noik and Rivereau, 1999; Lecolier et al., 2006, 2007; Garnier et al., 2012), but these studies are rather few. Recently, Vrålstad et al. (2016) performed durability tests of well cement in crude oil, brine and H_2S, respectively, at downhole temperatures and pressures. For crude oil, they found no significant effect on cement properties, which was consistent with the findings of Lecolier et al. (2007). For brine, they found an increase in volume (i.e. swelling), possibly due to further cement hydration, which indicates an improvement in sealing ability. For H_2S, they found a detrimental effect of the exposure; the cement decreased in weight and lost most of its mechanical strength. This is consistent with the findings of Garnier et al. (2012) and Lecolier et al. (2006) and is due to a process called "calcium leaching", where the calcium hydroxide (portlandite) is dissolved by acid. However, Vrålstad et al. (2016) also found that the H_2S resistance of Portland cement was considerably improved when silica flour was included as additive, which was possibly due to the pozzolanic nature of silica. Cement additives may therefore improve the H_2S resistance of well cement. Furthermore, as for CO_2 degradation, H_2S degradation of cement is also a diffusion-controlled process and actual degradation of a plug in the field will be quite slow.

Regarding ageing tests of cement and other plugging materials, it should be noted that most quantitative results obtained from chemical degradation tests cannot be directly transferred to field conditions. This is because the chemical degradation reactions occur several orders of magnitude faster in laboratory ageing tests than in a well. In laboratory tests, the material samples are submerged directly into the reactive fluids, which creates a large reaction surface area and an unrestricted supply of reactive compounds. Whereas in the field, all reactive compounds (such as CO_2 or H_2S) have to diffuse through a porous material such as sandstone to be able to reach the reaction surface at the cement. Degradation reactions in the field are therefore diffusion-limited and occurs quite slowly. The quantitative results obtained from ageing tests can thus vary quite significantly, depending on how realistically the tests are performed. For example, Zhang and Bachu (2011) reviewed ageing tests of cement exposed to CO_2 and found that the predicted carbonation depth after 30 years exposure varied between 1 mm to over 2500 mm. There is a need for more data on realistically performed ageing tests of cement, also over longer time periods than one year, to better understand the actual long-term durability of well cement. Recently, Ichim and Teodoriu (2017) reported the development and establishment of a cement repository that stores cement samples under downhole conditions for minimum 5 years, to improve the understanding of long-term behavior of cement.

3.3. Microannuli: leakages around plugs

Leakages around cement plugs occur through microannuli, where the cement has fully or partially debonded. Experimental determination of the sealing ability of cement plugs is in principle relatively straightforward, as illustrated in Fig. 3: a cement plug is placed inside a steel casing with a pressure difference across the plug, and the corresponding fluid flow rate is measured.

Among the first to perform a systematic study on cement plug sealing ability were Nagelhout et al. (2010), who performed laboratory tests in both small-scale and large-scale on two different cement systems. They found that the measured leak rate depended on the radial scale of the cement plugs and that the leak rate increased with increasing pressure difference across the plug. Furthermore, for a non-expanding cement system, they found an "equivalent permeability" in the milli-Darcy range, which is considerably higher than the permeability of good cement and thus indicates that the measured leakage occurs through microannuli around the cement and not through the cement itself. However, they found a significantly improved sealing ability for an expanding cement system. Recently, van Eijden et al. (2017) further developed and improved the methodology described by Nagelhout et al. (2010), and they also provide more details on the laboratory set-up and experimental procedure. They describe both a small-scale set-up and a large-scale set-up, where plug size is 2 in.

diameter and 38 cm length in small-scale and 6 or 8 in. diameter and 114 cm in large-scale, and they also found that an effect of radial size on sealing ability; where small plugs seal better than large plugs (van Eijden et al., 2017). During sample preparation, the cement is placed inside a casing and left to cure for several days under N_2 pressure. At the start of the test, the pressure is decreased at one side of the plug, to obtain a pressure difference across the plug and to avoid potential ballooning of casing. The gas flow across the plug is subsequently measured by flow meters.

By using such a laboratory set-up and experimental procedure, it is possible to determine both the breakthrough pressure, i.e. the lowest required pressure difference needed for detecting a flow rate, and the "equivalent permeability", i.e. the measured flow rate for different pressure differences. The sealing ability of a specific cement system can thus be determined in a systematic manner and different cement systems can be compared. Oil & Gas UK (2015c) has therefore included the small-scale and large-scale set-ups described by van Eijden et al. (2017) as examples on how to perform functions tests on zonal isolation for different plugging materials. Furthermore, Opedal et al. (2018) has also built a small-scale set-up based on the one developed by van Eijden et al. (2017) with the objective of performing systematic studies on cement plug integrity. Their initial findings show that the sealing ability of neat Portland cement plugs improve significantly when the cement has access to external water during curing (Opedal et al., 2018).

In addition to laboratory tests, cement plug integrity can also be estimated by modelling tools. For example, Bois et al. (2018) present a model that predicts the hydraulic integrity of cement plugs, where microannuli formation is predicted based upon cement shrinkage during hydration and the initial state of stress in cement. They show a sensitivity analysis that demonstrate that the hydraulic plug integrity is dependent upon different cement properties such as Young's modulus, and they validate their model with field data from pressure testing of cement plugs (Bois et al., 2018).

However, a challenge during modelling of microannuli leakages, is which geometry and thickness to use as input data. Is the microannulus uniformly present around the entire circumference of the plug, or not? It is often assumed that microannuli are homogeneous with a uniform thickness, and although incorrect, this assumption about microannulus uniformity is also used for simplicity in experimental studies when estimating corresponding "microannuli thicknesses" from leak rate studies (Boukhelifa et al., 2005; Nagelhout et al., 2010; Aas et al., 2016). Recently, x-ray computed tomography (CT) has been used to visualize and quantify cement integrity (Vrålstad et al., 2015; De Andrade et al., 2016; Skorpa and Vrålstad, 2018). It is found that microannuli and cracks in cement start from initial, random defects and that microannuli are not homogeneous nor uniform. Fig. 4 shows two such examples of CT visualizations of experimentally obtained cement microannuli and it is seen that the microannuli are non-uniform and somewhat random. Furthermore, Skorpa and Vrålstad (2018) performed CFD simulations of fluid flow through such experimentally obtained leak path geometries, and they found a non-linear (i.e. non-Darcian) relationship between pressure difference and flow rate for fluid flow through connected cracks and partial microannuli. However, there was a linear relationship when the microannulus was uniform (Skorpa and Vrålstad, 2018). Uniform microannuli therefore provide more easily predictable leak rates.

3.4. Risk-based approach to P&A?

An important issue regarding plug integrity is the plug length. Currently, requirements for plug length varies between different countries and regulatory regimes (Barclay et al., 2001; van der Kuip et al., 2011). In the North Sea for example, at the Norwegian side of the border the required plug length is 100 m (50 m if a mechanical plug is used as foundation), whereas the required plug length is 30 m (100 feet) at the UK side of the border.

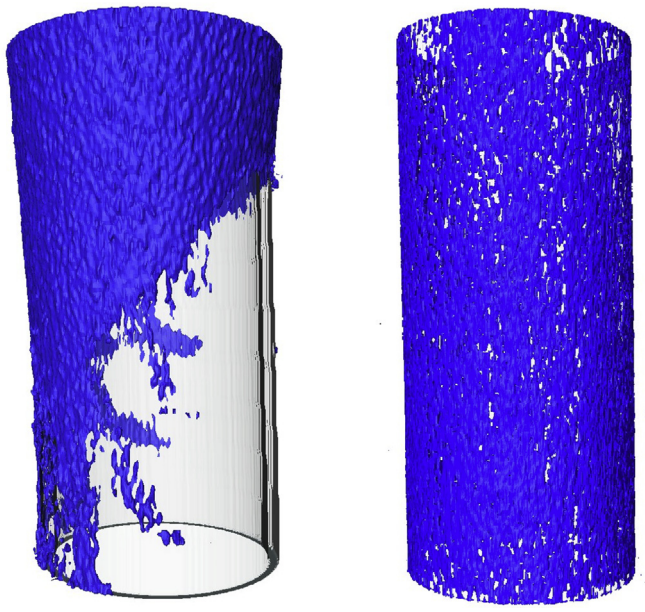

Fig. 4. Two different examples of x-ray computed tomography (CT) visualizations of experimentally obtained, non-uniform microannuli. The blue colour shows debonded cement. (For interpretation of the references to colour in this figure legend, the reader is referred to the Web version of this article.)

As an alternative to this "one-size-fits-all", prescriptive approach to plug length (and the number of plugs), a risk-based approach to P&A has been suggested (Buchmiller et al., 2016; Fanailoo et al., 2017; Arild et al., 2017). This approach accounts for the fact that all wells are different with respect to for example flow potential and pressure difference, and provides a "fit-for-purpose" alternative. In such a risk-based approach, different P&A solutions are evaluated in terms of the probability that the permanent barrier system will fail within a given time-frame (Arild et al., 2017). The methodology for risk-based assessments consists of five steps: establishing the risk context, identifying well barrier failure modes, performing a risk analysis, performing a risk evaluation, and conducting qualification for well abandonment design (Buchmiller et al., 2016; Fanailoo et al., 2017). The P&A procedure can therefore be tailor-made to fit each unique well, and an advantage of such a risk-based approach is the potential for considerable cost savings, as less stringent requirements may be sufficient for "simple" wells. Furthermore, as an extension of this approach, the resulting leakage rates for different P&A scenarios may also be estimated (Arild et al., 2017; Ford et al., 2017; Ford et al., 2018). However, there is currently a lack of sufficient amounts of good quality experimental results that can be used as reliable input data to such models. For such an approach to be reliable, more experimental studies on plug sealing ability are needed.

4. Establishing annulus barriers

To obtain a full cross-sectional barrier from rock to rock, zonal isolation must also be ensured in the annulus. Fig. 2 shows that although the cement plug maintain its integrity, there are still several potential leakage pathways in the well, i.e. in the annulus. Such leakage paths in the annulus cement sheath are caused by formation of microannuli and radial cracks, which can form due to pressure testing and injection (Goodwin and Crook, 1992; Jackson and Murphey, 1993; Shadravan et al., 2015) and/or due to temperature variations during production and injection (Bois et al., 2011; Vrålstad et al., 2015; Therond et al., 2017). Such cement sheath failure is one of the reasons why many wells experience well integrity problems such as sustained casing pressure as they age (Bourgoyne et al., 1999; Vignes and

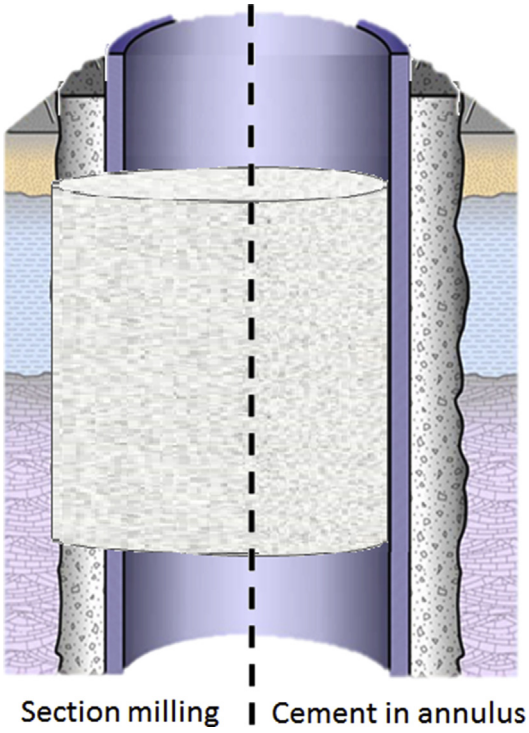

Fig. 5. Illustration of good annulus cement (right) and establishing annulus barrier by section milling (left).

Aadnoy, 2010).

If the annulus cement is of insufficient quality to be qualified as a barrier element for P&A, then this cement must be removed, or the barrier quality otherwise restored. Several methods and technologies exist for establishing annulus barriers, depending on whether the annulus is cemented and on the quality of the annulus cement, if present. The right part of Fig. 5 shows a cemented annulus of good quality, where the cement provides zonal isolation and there is no need for further action. However, if the cement is of poor quality, then the cement and casing must be removed by section milling before a cement plug is placed in the milled wellbore, as shown in the left part of Fig. 5. If the annulus is uncemented or poorly cemented, then the annulus can be cemented by the perforate-wash-cement method, which results in a cemented annulus as shown in the right part of Fig. 5. A special option exists for openhole, uncemented annuli, where creeping shale formation potentially can be used as annulus barrier. These methods will be discussed in more detail below.

4.1. Section milling

Section milling is a method to create a cross-sectional barrier directly towards formation where the annulus material disqualifies as an annular barrier (Fig. 5 left). Special milling blades and cutters are used to mill out, i.e. remove, designated well sections in situations where the casing string is fully or partly cemented. Section milling is a time-consuming and thus costly operation, especially in regulatory regimes with substantial required plug lengths. The milling operation creates small metal cuttings called “swarf” that cause several operational problems. Swarf can accumulate as so-called “bird nests” in the well and if the bird nest occurs inside the BOP, it can damage the well control equipment and cause potential well integrity problems if the BOP malfunctions. Furthermore, the section milling tool can get stuck when pulling out of hole, and it should be noted that retrieved swarf at surface can create HSE problems.

Section milling is used in many P&A operations throughout the world and there is considerable focus on technology development to increase milling efficiency and operational safety. Some examples include improvement of cutter and milling blade technologies (Scanlon et al., 2011; Stowe and Ponder, 2011), development of dual string section milling tools (Deshpande et al., 2016; McTiffen et al., 2017), saving rig time by single trips instead of dual trips (Hogg et al., 2014), and development of plasma-based tools (Gajdos et al., 2015). A recent development is the upwards milling tool (Joppe et al., 2017a; Nelson et al., 2018), which leaves the swarf in the well below the milled section and thereby probably avoiding swarf-related problems.

4.2. Perforate-wash-cement

Perforate-wash-cement is a method that can be used to establish annulus barriers when the annulus is uncemented or partly filled with poor cement. The method consists of perforating the casing to obtain access to the annulus, washing the annulus with fluids to clean out mud, debris, settled barite or poor cement, and then subsequently pumping new cement into the annulus. There is thus no need to section mill or cut-and-pull the casing to place cement in the annulus, so the method can be very time efficient and cost effective (Ferg et al., 2011). In Fig. 1 for example, the perforate-wash-cement technique has been used to establish annulus barrier elements as part of the primary and secondary barrier envelopes towards the flow zone in the overburden.

The perforate-wash-cement technique is routinely used by several operators during P&A operations in the North Sea (Ferg et al., 2011; Stokkeland et al., 2017; Joneja et al., 2018) and has also been used to establish annulus barriers in wells in the Middle East (Ansari et al., 2016a, 2016b; 2017). Furthermore, Norwegian operators have developed barrier acceptance criteria for the perforate-wash-cement process, which is suggested for implementation in NORSOK guidelines (Delabroy et al., 2017).

4.3. Shale as annulus barrier

In well sections running through shale formations, it is occasionally found that the annulus is closed even though it was left open during the completion process (Williams et al., 2009; Fjær and Larsen, 2018). This is revealed by sonic or ultrasonic logs that can distinguish between solid and fluid behind the casing (Allouche et al., 2006; Wang et al., 2016; Fjær and Larsen, 2018), and the sealing efficiency of these naturally occurring barriers can be verified by pressure tests. Such “shale barriers” may extend over hundreds of meters along the well and eliminates the need for additional sealing of the annulus. This simplifies the plugging operations and implies significant cost reductions during P&A operations. For example, operators in Norway are currently routinely using shale as annulus barrier (Williams et al., 2009; Kristiansen et al., 2018), thereby considerably reducing their costs during well abandonment.

A shale barrier is formed as the rock surrounding the borehole is pushed towards the casing by the compressive in situ stresses. In other words, the shale “creeps” into the casing and thus fills up the annulus. This process has been reproduced in downscaled laboratory tests (Fjær et al., 2018) where it has been found that the ability of different shales to form a sealing barrier depends upon the properties of the respective shale such as mineral composition and mechanical properties. Furthermore, post-test micro-CT scans show that the rock in the vicinity of the hole has suffered a permanent, plastic deformation (Fig. 6). The micro-CT scans also reveal that the permanently deformed region extends several borehole radii into the formation. The porosity of this deformed region is higher than that of the intact shale, hence the permeability of the shale barrier tends to be higher as well. The sealing efficiency of a shale barrier is therefore less than it would have been if the space around the casing were filled with intact shale. However, the relevant comparison is rather with the realistic alternative, that the annulus is filled with cement with permeability that is typically 3-4 orders of magnitude higher than the intact shale (Fjær et al., 2018).

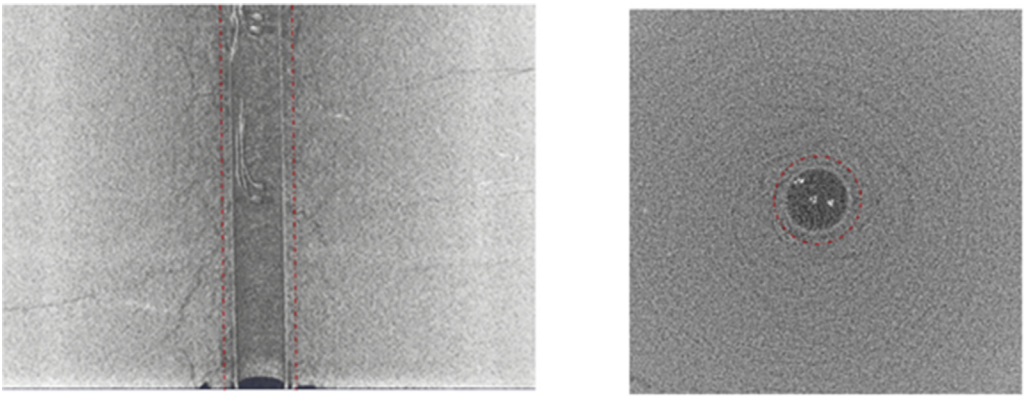

Fig. 6. micro-CT images of a shale barrier, formed in a laboratory test on a field shale core. Side view (left) and top view (right). The red dash-dot lines indicate the hole size prior to the test. (For interpretation of the references to colour in this figure legend, the reader is referred to the Web version of this article.)

Annulus closure due to formation creep is a well-known process in salt formations (Willson et al., 2003). However, salt behaves essentially like a highly viscous fluid and will in the end always close the annulus given reduced annulus pressure and sufficient time. Shale on the other hand has a finite shear strength and is able to maintain a stable arch around the hole if the in situ stresses are not too high. Even if the arch is broken, the shale may not be able to establish a sealing barrier, as the rock may break up into separated pieces rather than deforming uniformly maintaining a low permeability. However, self-sealing may to some extent occur in fractured shale due to creep and various other mechanisms (Blümling et al., 2007; Bock et al., 2017). Over time, the sealing efficiency of a shale barrier is therefore likely to improve rather than deteriorate.

5. Casing cut and pull

Occasionally, during P&A and slot recovery operations, there is a need to remove a casing string fully or partly. Section milling can be used for this operation, but an alternative and sometimes preferred method is to cut and pull the casing (Abshire et al., 2013; Obodozie et al., 2016). However, a major problem that can occur during casing cut and pull operations is that the casing can get "stuck" due to settled barite in the annulus outside the casing (Joppe et al., 2017). For example, a North Sea operator recently needed nearly 40 cuts and over 70 days to cut and pull 3000 m of a single production casing from one well (Abshire et al., 2013).

Settled barite is a sediment phase that is formed during gravity separation when the drilling fluid is left static in the annulus for several years. The number and properties of different sediment phases that are formed during gravity separation depend the type of drilling fluid (Vrålstad et al., 2018). It is likely that friction and/or bonding between the sediments and casing create a significant portion of the problems when trying to pull the casing. However, it is also quite possible that the casing collars could be the most important cause of the stuck casing. For example, recent laboratory tests on casing pulling have shown that casings without collars are significantly easier to pull than casings with collars (Taghipour et al., 2018). This point is illustrated in Fig. 7: If the annulus sediments do not "flow" around the collars when the casing is pulled upwards, the casing is stuck. The consistency and rheological properties of the sediments can therefore determine how easily the casing is removed (Vrålstad et al., 2018).

Due to such problems with stuck casing, the service industry develops technologies such as downhole hydraulic pulling tools and other improvements (Abshire et al., 2013; Hartman et al., 2017; Melder et al., 2017). Recently, Joppe et al. (2017b) presented case studies with different methods of casing removal. The considered methods were use of jack-up rigs, rig-less intervention systems and jacking units. They concluded that the optimal solution must be selected based the availability

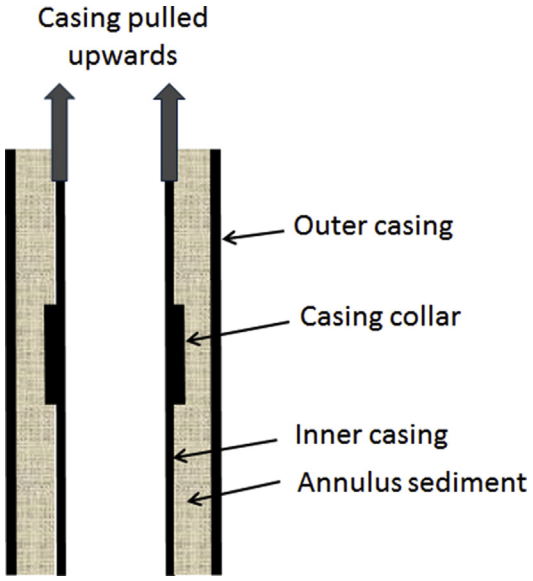

Fig. 7. Schematic illustration of possible cause of stuck casing during casing pulling operations: if the annulus sediment (settled barite) does not flow around the casing collars during pulling, the casing is stuck (After Vrålstad et al., 2018).

of tools, actual scope and the capabilities of the surface equipment. Pre-planning on a detailed level was emphasized as crucial, since cost escalation due to unforeseen events can be a challenge that prevents cost-effective solutions.

6. P&A of subsea wells

Subsea wells are different from platform wells in several ways that affect P&A operations. For example, due to the wellhead arrangements on subsea wells, it is only possible to monitor the annulus pressure between the production tubing and production casing, i.e. the A-annulus, and not possible to monitor the pressures in the outer annuli, i.e. in B- and C-annuli. The well integrity status of subsea wells is therefore partly unknown prior to P&A, which may significantly affect encountered problems during P&A operations and thus resulting durations. Technologies for wireless monitoring of B-annulus pressure is therefore currently under development (Rodriguez et al., 2017).

However, the main difference between platform wells and subsea wells is the "wetness" of the x-mas trees, i.e. subsea wells have the x-mas tree and all their production equipment at the seabed. Subsea wells therefore require mobile offshore units (MOU) such as semi-submersible drilling rigs to perform P&A operations. Due to the high spread rates of such units, subsea P&A operations can be much costlier than

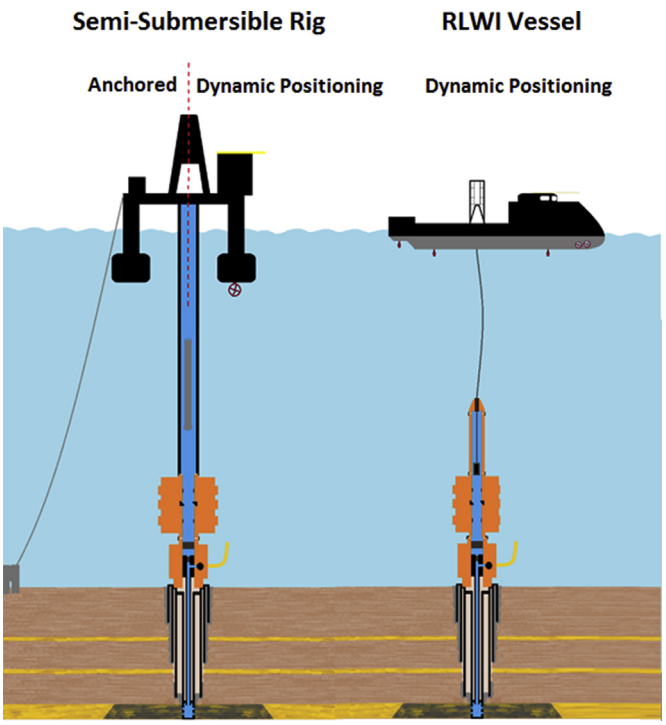

Fig. 8. Illustration of subsea P&A with semi-submersible rig and RLWI vessel, with respective available positioning alternatives (After Øia et al., 2018).

platform P&A operations (Oil & Gas UK, 2015a).

6.1. Use of rigs vs vessels for subsea P&A

Several field examples have shown that considerable cost savings can be obtained by performing part of subsea P&A operations with lighter vessels such as riserless light well intervention (RLWI) vessels instead of drilling rigs (Sørheim et al., 2011; Varne et al., 2017a; Canny, 2017). The technologies used for subsea P&A by RLWI vessels, such as well control package, lubricator and RLWI stack, are essentially the same as those used during conventional subsea riserless well interventions (Munkerud and Inderberg, 2007; Jøssang et al., 2008; Fjærtoft and Sønstabø, 2011; Varne et al., 2017b).

Regardless of type of MOU, the unit must adjust and hold its position to ensure that it is in-line with the subsea wellhead before and during a P&A operation. This is achieved either by anchoring or with an integrated dynamic positioning (DP) system. Fig. 8 shows a simplified illustration of use of rig and vessel for subsea P&A, where these two positioning approaches are included. A semi-sub rig can hold its position by either being anchored (depending on water depth) or by a DP system, whereas a RLWI vessel only relies on DP system. A significant difference between a semi-sub rig and a RLWI is the well control equipment and how they securely connect to a subsea well to allow fluid transport and intervention, as briefly illustrated in Fig. 8. The semi-sub uses a subsea BOP together with a workover riser (for high pressure) or a marine riser (for low pressure) to act as a conduit and ensure safe operations, whereas the RLWI vessel uses a riserless system.

As described in Table 1, the Oil & Gas UK (2015a) has divided the operational sequence of P&A operations into three different phases; Phase 1 ″Reservoir abandonment”, Phase 2 ″Intermediate abandonment” and Phase 3 ″Wellhead and conductor removal”. In addition, a fourth phase, Phase 0 ″Preparatory work”, has been suggested as well (Moeinikia et al., 2014). Furthermore, it can also be convenient to divide Phase 2 into two parts as well, where Phase 2a consists of placing primary and secondary barriers towards flow zones in the overburden (i.e. “overburden abandonment”), and Phase 2b consists of placing the openhole-to-surface plug. Such an approach of dividing the full P&A operation into different phases and sub-phases is especially fruitful for subsea wells, since it elucidates the possibility for cost reductions by moving parts of the P&A operation to lighter vessels. Table 3 lists all these phases together with which type of MOU that can be used for the respective P&A work (based upon present technology). A semi-sub rig can be used for all phases of P&A operations, whereas a RLWI vessel can normally be used for all phases except Phases 1 and 2a, since these usually require drill string and heavy lifting capacity to perform operations such as section milling and pipe pulling. A simple operation such as wellhead and conductor removal, that does not require well control equipment, can be performed by a light construction vessels (LCV). It should be noted that the operability is higher for semi-sub rigs than light intervention vessels, allowing semi-subs to operate through the winter season with less waiting on weather (WOW).

Table 3
Current applicability of semi-submersible rig, riserless well intervention vessel (RLWI) and light construction vessel (LCV) for different phases of subsea P&A operations.

P&A operational phase	Semi-sub rig	RLWI	LCV
Phase 0: Preparatory work	OK	OK	Not ok
Phase 1: Reservoir abandonment	OK	Not ok	Not ok
Phase 2a: Overburden abandonment	OK	Not ok	Not ok
Phase 2b: Openhole-to-surface plug	OK	OK	Not ok
Phase 3: Wellhead and conductor removal	OK	OK	OK

6.2. Planning and coordination of multi-well P&A campaigns

Since subsea wells are located at different locations around the seabed, and not located at a single point, i.e. a platform, then the MOU must physically move from wellhead to wellhead (or template to template) to perform the necessary operations. This continuous MOU relocation is time-consuming and significant time and thus costs can be saved by abandoning several adjacent subsea wells together in multi-well campaigns. For example, Clyne and Jackson (2014) present a field case where 19 subsea wells were abandoned together in two consecutive multi-well campaigns. As lessons learned, they emphasize the need for thorough preparations and planning, the importance of knowing the well integrity status of the wells prior to P&A, and to use light vessels with ROV for pre-P&A work and for removing the wellhead (Clyne and Jackson, 2014).

This final point on using light vessels for parts of the P&A operation highlights a logistical advantage when performing multi-well P&A campaigns: it is not necessary to perform full P&A on one well before moving to perform full P&A on the next well, it can be more efficient to separate the operations into the different phases listed in Table 1, where each respective phase for all wells is performed before moving on to the subsequent phases. Such an approach enables use of different types of MOUs for the different P&A operational phases as described in Table 3. For example, a multi-well campaign could start with a RLWI vessel performing Phase 0 for all the wells, a semi-sub rig performs Phases 2 and 3 for all the wells (perhaps several months later, depending on rig availability), and then finally an LCV or RLWI vessel performs Phase 3 for all wells at a suitable time, depending on vessel availability and weather conditions. Sørheim et al. (2011) emphasized such an approach when they used a dedicated light vessel to cut and retrieve the wellhead from a subsea well, i.e. Phase 3. They estimated that it was not cost efficient to use a dedicated vessel to remove the wellhead from only one well, but if two or more wellheads were removed together in a multi-well campaign then the use of such a dedicated vessel was cost beneficial (Sørheim et al., 2011). Moreover, Varne et al. (2017a) exemplify this approach when they performed pre-P&A work (Phase 0) on several subsea wells for a Norwegian operator before a semi-sub rig performed the remaining P&A operations.

However, accurate time and cost estimations for the operational sequence are crucial during planning of multi-well P&A campaigns. Moeinikia et al. (2014; 2015a; 2015c) developed a probabilistic Monte-Carlo simulation tool that estimated time and cost-savings of rig-less P&A technologies for subsea wells. They used this approach to demonstrate the cost efficiency of performing Phases 0 and 3 by RLWI vessels instead of rigs. Furthermore, Aarlott (2016) and Bakker et al. (2017) introduced methods from operations research by using an optimization model for P&A planning of a simple subsea field. The optimization approach allows planners to evaluate how different strategies for vessel allocation, changed rental rates and effects of improved technology affect decisions and the impact on total cost. Due to the large number of possible scenarios when considering use of both semi-sub rigs and light vessels for a multi-well campaign, an optimization model can analyze the different possible scenarios and suggest optimal solutions for MOU allocation and routing for the entire campaign (Bakker et al., 2017).

6.3. Full P&A of subsea wells by RLWI vessels?

Further costs could perhaps be saved if all phases of the P&A operation were performed by a light vessel instead of a rig. As seen from Table 3, it is currently not feasible to perform the full P&A operation with a RLWI vessel. It could however be possible in the near future, and Valdal (2013) described potential scenarios for such an approach. Recently, Øia et al. (2018) presented several constructed cases on how existing technologies could be used for full P&A of subsea wells by RLWI vessels. They found that for wells of low to medium complexities, it could be possible to perform full P&A by using RLWI vessels, but for complex wells where for example section milling and heavy lifting is required, a semi-sub rig is still needed. They also found that although considerable costs could be saved by performing the operation by RLWI vessel instead of semi-sub rig, the semi-sub would in most cases be the least risky option, due to the large uncertainties in time estimations for RLWI vessel P&A operations (caused by the lack of experience for these operations).

A prerequisite for full P&A by RLWI vessel will in many cases be that the production tubing is left in the well, due to the limited lifting capacity on most vessels. If achievable in practice, then considerable costs can be saved by not removing the tubing (Moeinikia et al., 2015b). If the tubing string is left in the well, then the control lines will constitute a potential leak path (Dahmani and Hynes, 2017). The control lines must therefore be cut or retrieved, or the barrier placed at a depth with no control lines. Furthermore, a potential challenge with leaving tubing in the well, will be to place cement in the annulus between the tubing and casing, since the tubing is not centralized. However, Aas et al. (2016) have shown by large-scale experimental tests that it is possible to obtain good cement placement in this annulus when the tubing is left in hole.

7. Conclusions

To fulfil the objective of "*restoring the cap rock*", permanent barriers in plugged and abandoned wells must extend across the full cross section of the well. This includes establishing proper annulus barriers and preventing leak paths such as microannuli around plugs, which may cause P&A operations to be time-consuming. However, recent technology developments such as the perforate-wash-cement technique and utilizing shale as annulus barrier have significantly reduced the time spent on P&A operations. Furthermore, risk-based approaches to determining plug length and the number of plugs may further reduce time-consumption while maintaining well integrity.

There is still need for further technology developments however. Operators, service companies, vendors, research institutes and universities are all working on reducing risk of leakages, developing new technologies and improving P&A operations further. For example, while cement has been used as plugging material for a century and new and improved cement systems are still being developed, completely new plugging materials and approaches such as bismuth-alloys and burning termite may perhaps change the industry. And in a few years' time, it may be possible to perform full P&A of subsea wells without using a drilling rig.

Acknowledgements

This paper was prepared as a part of the project "Economic Analysis of Coordinated Plug and Abandonment Operations" (ECOPA), financed by the Research Council of Norway through the PETROSAM2 and PETROMAKS2 programs (p-nr: 247589). Also, the authors acknowledge the Research Council of Norway, Aker BP, ConocoPhillips, Equinor and Wintershall for funding part of the work through the research centre SFI DrillWell.

Abbreviations

API	American Petroleum Institute
BFS	Blast Furnace Slag
BOP	Blowout Preventer; CFD Computational Flow Dynamics
CT	x-ray Computed Tomography
DP	Dynamic Positioning
HSE	Health, Safety and Environment
LCV	Light Construction Vessel
MOU	Mobile Offshore Unit
P&A	Plug and Abandonment
RLWI	Riserless Light Well Intervention
ROV	Remotely Operated Vehicle
WOW	Waiting on Weather

References

Aarlott, M.M., 2016. Cost Analysis of Plug and Abandonment Operations on the Norwegian Continental Shelf. MSc thesis. Norwegian University of Science and Technology, Trondheim, Norway.

Aas, B., Sørbø, J., Stokka, S., Saasen, A., Godøy, R., Lunde, Ø., Vrålstad, T., 2016. Cement placement with tubing left in hole during plug and abandonment operations. In: Paper Presented at the IADC/SPE Drilling Conference and Exhibition, Fort Worth, TX, USA, 1-3 March, IADC/SPE-178840-MS.

Abshire, L., Hekelaar, S., Desai, P., 2013. Offshore plug & abandonment: challenges and technical solutions. In: Paper Presented at the Offshore Technology Conference, Houston, TX, USA, 6-9 May, OTC-23906.

Al-Ansari, A.A., Al-Refai, M., Al-Beshri, M.H., Pino, R.M., Leon, G.A., Knudsen, K., Sanabria, A.E., 2015. Thermal activated resin to avoid pressure build-up in casing-casing annulus (CCA). In: Paper Presented at the SPE Offshore Europe Conference and Exhibition, Aberdeen, UK, 8-11 September, SPE-175425-MS.

Allouche, M., Guillot, D., Hayman, A.J., Butsch, R.J., Morris, C.W., 2006. Cement job evaluation. In: second ed. In: Nelson, E.B., Guillot, D. (Eds.), Well Cementing, vol. 2006 Schlumberger, Sugar Land, Texas, USA.

Ansari, A., Ringrose, D., Libdi, Z., Larsen, A.G., 2016a. Extending life for offshore wells by fixing the integrity high annulus-B pressure and creating zonal isolation using a novel remediation technique. In: Paper Presented at the IADC/SPE Asia Drilling Technology Conference, Singapore, 22-24 August, IADC/SPE-180555-MS.

Ansari, A., Libdi, Z., Larsen, A.G., 2016b. Innovative planning and remediation techniques for restoring the well integrity by curing high annulus-B pressure and zonal communication. In: Paper Presented at the International Petroleum Technology Conference, Bangkok, Thailand, 14-16 November, IPTC-18894-MS.

Ansari, A., Al-Azizi, B., Larsen, A.G., 2017. Innovative remediation techniques for restoring well integrity by curing high annulus-B pressure and zonal communication. In: Presented at the SPE Bergen One Day Seminar, Bergen, Norway, 5 April, SPE-185911-MS.

Arild, Ø., Lohne, H.P., Majourmerd, M.M., Ford, E.P., Moeinikia, F., 2017. Establishment of a quantitative risk-based approach for evaluation of containment performance in the context of permanently plugged and abandoned Petroleum wells. In: Paper Presented at the Offshore Technology Conference, Houston, Texas, USA, 1-4 May, OTC-27711.

Bakker, S.J., Aarlott, M.M., Tomasgard, A., Midthun, K., 2017. Planning of an offshore well plugging campaign – a Vehicle routing approach. In: Presented at the 8th International Conference on Computational Logistics, Southampton, United Kingdom, 18-20 October, . https://doi.org/10.1007/978-3-319-68496-3_11.

Barclay, I., Pellenbarg, J., Tettero, F., Pfeiffer, J., Slater, H., Staal, T., Stiles, D., Tilling, G., Whitney, C., 2001. The beginning of the end: a review of abandonment and decommissioning practices. Oilfield Rev. 28–41 Winter 2001/2002.

Barlet-Gouédard, V., Rimmelé, V.G., Porcherie, O., Quisel, N., Desroches, J., 2009. A

solution against well cement degradation under CO2 geological storage environment. International journal of greenhouse gas control 3, 206–216.
Beharie, C., Francis, S., Øvestad, K.H., 2015. Resin: an alternative barrier solution. In: Paper Presented at the SPE Bergen One Day Seminar, Bergen, Norway, 22 April, SPE-173852-MS.
Bensted, J., 2007. Special cements. In: Hewlett, P.C. (Ed.), Lea's Chemistry of Cement and Concrete, fourth ed. Elsevier, Oxford, UK.
Blezard, R.G., 2007. The history of calcareous cements. In: Hewlett, P.C. (Ed.), Lea's Chemistry of Cement and Concrete, fourth ed. Elsevier, Oxford, UK.
Blümling, P., Bernier, F., Lebon, P., Martin, C.D., 2007. The excavation damaged zone in clay formations time-dependent behaviour and influence on performance assessment. Phys. Chem. Earth 32, 588–599.
Bock, H., Dehandschutter, B., Martin, C.D., Mazurek, M., de Haller, A., Skoczylas, F., Davy, C., 2017. Self-sealing of Fractures in Argillaceous Formations in the Context of Geological Disposal of Radioactive Waste. 978-92-64-99095-1 NEA Report 6184.
Bois, A.-P., Garnier, A., Rodot, F., Sain-Marc, J., Aimard, N., 2011. How to prevent loss of zonal isolation through a comprehensive analysis of microannulus formation. SPE Drill. Complet. 26 (01) Paper SPE-124719-PA.
Bois, A.-P., Vu, M.-H., Noël, K., Badalamenti, Delabroy, L., Thérond, E., Hansen, K., 2018. Cement plug hydraulic integrity – the ultimate objective of cement plug integrity. In: Paper Presented at the SPE Bergen One Day Seminar, Bergen, Norway, 18 April, SPE-191335-MS.
Boukhelifa, L., Moroni, N., James, S.G., Le Roy-Delage, S., Thiercelin, M.J., Lemaire, G., 2005. Evaluation of cement systems for oil and gas well zonal isolation in a full-scale Annular geometry. SPE Drill. Complet. 20 (01) Paper SPE-87195-PA.
Bourgoyne, A.T., Scott, S.L., Regg, J.B., 1999. Sustained casing pressure in offshore producing wells. In: Paper Presented at the Offshore Technology Conference Held in Houston, Texas, USA, 3-6 May, OTC-11029.
Brandl, A., Cutler, J., Seholm, A., Sansli, M., Braun, G., 2011. Cementing solutions for corrosive well environments. SPE Drill. Complet. 26 (02) Paper SPE-132228-PA.
Buchmiller, D., Jahre-Nilsen, P., Sætre, S., Allen, E., 2016. Introducing a new recommended practice for fit for purpose well Abandonment. In: Paper Presented at the Offshore Technology Conference, Houston, Texas, USA, 2-5 May, OTC-27084.
Calvert, D.G., Smith, D.K., 1994. Issues and techniques of plugging and abandonment of oil and gas wells. In: Paper Presented at the 1994 SPE Annual Technical Conference and Exhibition, New Orleans, Sept. 25-28, SPE-28349-MS.
Calvert, D.G., Heathman, J.F., Griffith, J.E., 1995. Plug cementing: horizontal to vertical conditions. In: Paper Presented at the 1995 SPE Annual Technical Conference and Exhibition, Dallas, Texas, 22-25 October, SPE-30514-MS.
Canny, S.A., 2017. Campaigns of opportunity – rigless subsea phase III well Abandonment operations in the UK continental shelf. In: Paper Presented at the Abu Dhabi International Petroleum Exhibition & Conference, Abu Dhabi, UEA, 13-16 November, SPE-188339-MS.
Carey, J.W., Wigand, M., Chipera, S.J., WoldeGabriel, G., Pawar, R., Lichtner, P.C., Wehner, S.C., Raines, M.A., Guthrie Jr., G.D., 2007. Analysis and performance of oil well cement with 30 years of CO_2 exposure from the SACROC Unit, West Texas, USA. International Journal of Greenhouse Gas Control 1, 75–85.
Carpenter, R.B., Gonzalez, M.E., Granberry, V., Becker, T.E., 2004. Remediating sustained casing pressure by forming a downhole annular seal with low-melt-point eutectic metal. In: Paper Presented at the IADC/SPE Drilling Conference, Dallas, Texas, USA, 2-4 March, SPE-87198-MS.
Carragher, P.J., Fulks, J., 2018. Well Abandonment solutions utilizing bismuth and thermite. In: Paper Presented at the Offshore Technology Conference, Houston, Texas, USA, 30 April – 3 May, OTC-28897.
Carrol, S., Carey, J.W., Dzombak, D., Huerta, N.J., Li, L., Richard, T., Um, W., Walsh, S.D.C., Zhang, L., 2016. Review: role of chemistry, mechanics, and transport on well integrity in CO2 storage environments. International Journal of Greenhouse Gas Control 49, 149–160.
Clark, J., Salsbury, B., 2003. Well Abandonment using highly compressed sodium bentonite – an Australian case study. In: Paper Presented at the SPE/EPA/DOE Exploration and Production Environmental Conference, 10-12 March, San Antonio, Texas, USA, SPE-80592-MS.
Clyne, I., Jackson, N., 2014. Abandonment of 19 subsea wells in the jabiru/challis fields. In: Presented at the IADC/SPE Asia Pacific Drilling Technology Conference, Bangkok, Thailand, 25-27 August, SPE-14860-MS.
Cowan, K.M., Hale, A.H., Nahm, J.J., 1992. Conversion of drilling fluids to cements with blast furnace slag: performance properties and applications for well cementing. In: Paper Presented at the 67th Annual Technical Conference and Exhibition, Washington, DC, 4-7 October, SPE 24575-MS.
Crawshaw, J.P., Frigaard, I., 1999. Cement plugs: stability and failure by buoyancy-driven mechanism. In: Paper Presented at 1999 Offshore Europe Conference, Aberdeen, Scotland, 7-9 September, SPE-56959-MS.
Daccord, G., Guillot, D., James, S., 2006. Remedial cementing. In: Nelson, E., Guillot, D. (Eds.), Well Cementing, second ed. Schlumberger, Sugar Land, Texas, USA.
Dahmani, L., Hynes, L., 2017. Enhancing well construction for more efficient well Abandonment. In: Paper Presented at the SPE/IATMI Asia Pacific Oil & Gas Conference and Exhibition, Jakarta, Indonesia, 17-19 October 2017, SPE-186392-MS.
Daulton, D.J., Bosworth, S.J., Pumphrey, B., McCathy, S., Cantu, R., Clendennen, J., 1995. Field experience with application of blast furnace slag to the drilling and cementing program in the stratton field, south Texas. In: Paper Presented at the Production Operation Symposium, Oklahoma City, USA, 2-4 April, SPE 29472-MS.
Davidovits, J., 2011. Geopolymer Chemistry & Applications, third ed. Institut Geopolymere, Saint-Quentin. France.
Davis, J.E., September 2017. Using a resin-only solution to complete a permanent abandonment operation in the Gulf of Mexico. In: Paper presented at the SPE Offshore Europe Conference & Exhibition, Aberdeen, Scotland UK, pp. 5–8 SPE-186113-MS.
Davison, J.M., Salehabadi, M., De Gennaro, S., Wilkinson, D., Hogg, H., Hunter, C., Schutjens, P., 2017. Plugging and abandonment of oil and gas wells: a geomechanics perspective. In: Paper ARMA 17-451 Presented at the 51st US Rock Mechanics/Geomechanics Symposium Held in San Francisco, California, USA, 25-28 June 2017.
De Andrade, J., Sangesland, S., Skorpa, R., Todorovic, J., Vrålstad, T., 2016. Experimental laboratory setup for visualization and quantification of cement-sheath integrity. SPE Drill. Complet. 31 (04) Paper SPE-173871-PA.
Delabroy, L., Rodrigues, D., Norum, E., Straume, M., 2017. Perforate, wash and cement PWC verification process and an industry standard for barrier acceptance criteria. In: Presented at SPE Bergen One Day Seminar, Bergen, Norway, 5 April, SPE-185938-MS.
Deshpande, K.M., Haq, M.A., Teale, D., 2016. Dual string section milling tool design optimisation using advanced numerical simulations. In: Paper Presented at the SPE Asia Pacific Oil & Gas Conference and Exhibition, Perth, Australia, 25-27 October, SPE-182288-MS.
Englehardt, J., Wilson, M.J., Woody, F., 2001. New abandonment technology new materials and placement techniques. In: Paper Presented at SPE/EPA/DOE Exploration and Production Environmental Conference, 26-28 February, San Antonio, Texas, USA, SPE-66496-MS.
Fanailoo, P., Buchmiller, D., Ouyang, S., Allen, E., Buchmiller, D., 2017. Risk based approach to well plugging & abandonment – reducing costs while verifying risk. In: Paper Presented at the Offshore Technology Conference, Houston, Texas, USA, 1-4 May, OTC-27921.
Ferg, T.E., Lund, H., Mueller, D., Myhre, M., Larsen, A., Andersen, P., Lende, G., Hudson, C., Prestegaard, C., Field, D., 2011. Novel approach to more effective plug and abandonment cementing techniques. In: Paper Presented at the SPE Arctic Extreme Environments Conference & Exhibition, Moscow, Russia, 18-20 October, SPE-148640-MS.
Fjær, E., Larsen, I., 2018. Shale as a sealing barrier around deep wells. In: Paper OMAE2018-78749 Presented at the ASME 37th International Conference on Ocean, Offshore & Artic Engineering, June 17-22, Madrid, Spain.
Fjær, E., Stenebråten, J.F., Bakheim, S., 2018. Laboratory test for studies on shale barrier formation. In: Paper ARMA 18-1146 Presented at the 52nd US Rock Mechanics/Geomechanics Symposium Held in Seattle, Washington, USA, 17-20 June 2018.
Fjærtoft, L., Sønstabø, G., 2011. Success from subsea riserless well interventions. In: Paper Presented at the SPE/ICoTA Coiled Tubing & Well Intervention Conference and Exhibition, the Woodlands, Texas, USA, 5-6 April 2011, SPE-143296-MS.
Ford, E.P., Moeinikia, F., Lohne, H.P., Arild, Ø., Majourmerd, M.M., Fjelde, K.K., 2017a. Leakage calculator for plugged and abandoned wells. In: Paper Presented at the SPE Bergen One Day Seminar, Bergen, Norway, 5 April, SPE-185890-MS.
Ford, E.P., Moeinikia, F., Majourmerd, M.M., Lohne, H.P., Arild, Ø., 2018. Consequence quantification of barrier system failures in permanently plugged and abandoned wells. In: Paper Presented at the SPE Norway One Day Seminar, Bergen, Norway, 18 April, SPE-191298-MS.
Gajdos, M., Kristofic, T., Jankovic, S., Horvath, G., Kocis, I., 2015. Use of plasma-based tool for plug and abandonment. In: Paper Presented at the SPE Offshore Europe Conference and Exhibition, Aberdeen, Scotland, UK, 8-11 September, SPE-175431-MS.
Garnier, A., Laudet, J.B., Patil, S., Patil, R., Ravi, K., Ferreira, L., 2012. Effect of acid gas on cement sheath integrity: experimental findings. In: Paper Presented at the SPE Saudi Arabia Section Technical Symposium and Exhibition, Al-Khobar, Saudi-Arabia, 8-11 April, SPE-160890-MS.
Gasda, S.E., Bachu, S., Celia, M.A., 2004. Spatial characterization of the location of potentially leaky wells penetrating a deep saline aquifer in a mature sedimentary basin. Environ. Geol. 46, 707–720.
Godøy, R., Svindland, A., Saasen, A., Wallevik, O., 2004. Experimental analysis of yield stress in high solids concentration sand slurries used in temporary well Abandonment operations. Ann. Trans. Nordic Rheology Soc. 12, 81–84.
Goodwin, K.J., Crook, R.J., 1992. Cement sheath stress failure. SPE Drill. Eng. 7 (4), 291–296 SPE-20453-PA.
Harestad, K., Herigstad, T.P., Torsvoll, A., Nødland, N., Saasen, A., 1997. Optimization of balanced-plug cementing. SPE Drill. Complet. 12, 168–173 SPE-35084-PA.
Hartman, C.J., Cullum, J.L., Melder, J.E., 2017. Efficient and safe casing removal with downhole hydraulic pulling assembly. In: Paper Presented at the Offshore Technology Conference, Houston, TX, USA, 1-4 May, OTC-27610.
Hewlett, P.C. (Ed.), 1998. Lea's Chemistry of Cement and Concrete, fourth ed. Elsevier, Oxford, UK.
Hogg, H., Lees, G., Fearn, M., Khan, Z., Adetona, G., Strachan, R., 2014. Solving dual trip zonal isolation issue: single trip plug & abandonment system saves operator six days rig time, UK North Sea. In: Paper Presented at SPE Annual Technical Conference and Exhibition, Amsterdam, The Netherlands, 27-29 October, SPE-170876-MS.
Ichim, A., Teodoriu, C., 2017. Development of a cement repository to improve the understanding of well integrity with time. In: Paper Presented at the SPE Oklahoma City Oil and Gas Symposium, Oklahoma City, Oklahoma, USA, 27-31 March, SPE-185089-MS.
Jackson, P.B., Murphey, C.E., 1993. Effect of casing pressure on gas flow through a sheath of set cement. In: Paper Presented at the SPE Drilling Conference, Amsterdam, February 23-25, SPE-25698-MS.
Joneja, G., Nafikova, S., Reid, J., Rublevskyi, A., Salazar, J., 2018. Perf-and-Wash cement placement technique as a cost-effective solution for permanent abandonment of a well with multiple permeable zones: a case study from North Sea, UK. In: Paper Presented at the IADC/SPE Drilling Conference and Exhibition, Fort Worth, Texas, USA, 6-8 March, IADC/SPE-189580-MS.
Joppe, L.C., Ponder, A., Hart, D., Bruun, B.T., Grindhaug, G., 2017a. Create a rock-to-rock

well Abandonment barrier without swarf at surface. In: Paper Presented at the Abu Dhabi International Petroleum Exhibition & Conference, Abu Dhabi, UAE, 13-16 November, SPE-188332-MS.
Joppe, L.C., Nelson, J.F., Kelman, G.L., 2017b. We're stuck: efficient casing removal for well Abandonment applications. In: Paper Presented at the Offshore Technology Conference, Houston, TX, USA, 1-4 May, OTC-27807.
Jordan, R., Head, P., 1995. Cost effective well Abandonment. In: Paper Presented at Offshore Europe Meeting. Aberdeen, United Kingdom, 5–8 September, SPE-30349-MS.
Jøssang, S.N., Friedberg, R., Buset, P., Gramstad, B., 2008. Present and future well intervention on subsea wells. In: Paper Presented at the IADC/SPE Drilling Conference and Exhibition, Fort Worth, TX, USA, 4-6 March, IADC/SPE-112661-MS.
Kaiser, M.J., 2017. Rigless well abandonment remediation in the shallow water U.S. Gulf of Mexico. J. Petrol. Sci. Eng. 151, 94–115.
Khalifeh, M., Saasen, A., Hodne, H., Vrålstad, T., 2013. Techniques and materials for North Sea plug and abandonment operation. In: Paper Presented at the Offshore Technology Conference, Houston, Texas, USA, 6–9 May, OTC-23915.
Khalifeh, M., Saasen, A., Vrålstad, T., Hodne, H., 2014. Potential utilization of class C fly ash-based geopolymer in oil well cementing operations. Cement Concr. Compos. 53, 10–17. https://doi.org/10.1016/cemconcomp.2014.06.014.
Khalifeh, M., Saasen, A., Vrålstad, T., Bøvik Larsen, H., Hodne, H., 2016. Experimental study on the synthesis and characterization of aplite rock-based geopolymers. Journal of Sustainable Cement-Based Materials 5 (4), 233–246. https://doi.org/10.1080/21650373.2015.1044049.
Khalifeh, M., Todorovic, J., Vrålstad, T., Saasen, A., Hodne, H., 2017. Long-term durability of rock-based geopolymers aged at downhole conditions for oil well cementing operations. Journal of Sustainable Cement-Based Materials 6 (4), 217–230. https://doi.org/10.1080/21650373.2016.1196466.
Khalifeh, M., Hodne, H., Saasen, A., Vrålstad, T., Godøy, R., 2018. Geopolymers as an alternative for oilwell cementing applications. A review of advantages and concerns. J. Energy Resour. Technol. 140.
King, G.E., Valencia, R.L., 2014. Environmental risk and well integrity of plugged and abandoned wells. In: Paper Presented at the SPE Annual Technical Conference and Exhibition, Amsterdam, The Netherlands, 27-29 October, SPE-170949-MS.
Kiran, R., Teodoriu, C., Dadmohammadi, Y., Nygaard, R., Wood, D., Mokhtari, M., Salehi, S., 2017. Identification and evaluation of well integrity and causes of failure of well integrity barriers (A review). J. Nat. Gas Sci. Eng. 45, 511–526.
Kristiansen, T.G., Dyngeland, T., Kinn, S., Flatebø, R., Aarseth, N.A., 2018. Activating shale to form well barriers: theory and field examples. In: Paper Presented at the SPE Annual Technical Conference and Exhibition, Dallas, Texas, USA, 14-26 September, SPE-191607-MS.
Kutchko, B.G., Straziar, B.R., Dzombak, D.A., Lowry, G.V., Thaulow, N., 2007. Degradation of well cement by CO2 under geologic sequestration conditions. Environ. Sci. Technol. 41, 4787–4792.
Lecolier, E., Rivereau, A., Ferrer, N., Audibert, A., Longaygue, X., 2006. Durability of oilwell cement formulations aged in H2S-containing fluids. In: Paper Presented at the IADC/SPE Drilling Conference, Miami, Florida, USA, 21-23 February, IADC/SPE-99105-MS.
Lecolier, E., Rivereau, A., Le Saout, G., Audibert-Hayet, A., 2007. Durability of hardened Portland cement paste used for oilwell cementing. Oil & Gas Science and Technology – Rev. IFP 62 (3), 335–345.
Liu, X., Ramos, M., Nair, S.D., Lee, H., Espinoza, D.N., van Oort, E., 2017. True self-healing geopolymer cements for improved zonal isolation and well Abandonment. In: Paper Presented at the SPE/IADC Drilling Conference and Exhibition, the Hague, The Netherlands, 14-16 March, SPE-184675-MS.
Liversidge, D., Taoutaou, S., Agarwal, S., 2006. Permanent plug and abandonment solution for the North Sea. In: Paper Presented at SPE Asia Pacific Oil & Gas Conference and Exhibition, Adelaide, Australia, 11-13 September, SPE-100771-MS.
Malekmohammadi, S., Naccache, M.F., Frigaard, I.A., Martinez, D.M., 2010. Buoyancy driven slump flows of non-Newtonian fluids in pipes. J. Petrol. Sci. Eng. 72, 236–243.
McTiffen, D., Iversen, G.T., Smalley, M., Haq, M.A., 2017. Well Abandonment of offshore ageing gas fields using new section milling technology reduces time and costs to set a permanent barrier – a case study of section milling 100 ft of 13-3/8" casing to set cement plug. In: Paper Presented at the Abu Dhabi International Petroleum Exhibition & Conference, Abu Dhabi, UAE, 13-16 November, SPE-188976-MS.
Melder, J.E., Hartman, C.J., Hern, G., 2017. Change casing removal to a simple and dependable method. In: Paper Presented at the SPE/IATMI Asia Pacific Oil & Gas Conference and Exhibition, Jakarta, Indonesia, 17-19 October, SPE-186211-MS.
Moeinikia, F., Fjelde, K.K., Saasen, A., Vrålstad, T., 2014. An investigation of different approaches for probabilistic cost and time estimation of rigless P&A in subsea multiwell campaign. In: Paper Presented at the SPE Bergen One Day Seminar, Bergen, Norway, 2 April, SPE-169203-MS.
Moeinikia, F., Fjelde, K.K., Saasen, A., Vrålstad, T., Arild, Ø., 2015a. A probabilistic methodology to evaluate the cost efficiency of rigless technology for subsea multiwell Abandonment. SPE Prod. Oper. 30 (4), 270–282 SPE-167923-PA.
Moeinikia, F., Fjelde, K.K., Sørbø, J., Saasen, A., Vrålstad, T., 2015b. A study of possible solutions for cost efficient subsea well Abandonment. In: Paper OMAE2015-41261 Presented at the ASME 34th International Conference on Ocean, Offshore and Arctic Engineering, St. John's, Newfoundland, Canada. 31 May – 5 June.
Moeinikia, F., Fjelde, K.K., Saasen, A., Vrålstad, T., 2015c. Essential aspects in probabilistic cost and duration forecasting for subsea multi-well Abandonment: simplicity, industrial applicability and accuracy. In: Presented at the SPE Bergen One Day Seminar, Bergen, Norway, 22 April, SPE-173850-MS.
Munkerud, P.K., Inderberg, O., 2007. Riserless light well intervention. In: Paper Presented at the Offshore Technology Conference, Houston, Texas, USA, 30 April - 3 May, OTC-18746.
Nagelhout, A., Bosma, M.G.R., Mul, P., Krol, G., van Velzen, H., Joldersma, J., James, S.G., Dargaud, B., Schreuder, R., Théry, F., 2010. Laboratory and field validation of a sealant system for critical plug-and-abandon applications. SPE Drill. Complet. 25 (03) Paper SPE-97347-PA.
Nahm, J.J., Romero, R.N., Javanmardi, K., Wyant, R.E., 1995. Interfacial sealing properties of slag mix (Mud-to-Cement conversion technology): laboratory and field evaluation. In: Paper Presented at the 1995 SPE/IADC Drilling Conference, Amsterdam, 28 February – 2 March, SPE 29407-MS.
Nelson, E.B., Guillot, D. (Eds.), 2006. Well Cementing, second ed. Schlumberger, Sugar Land, Texas, USA.
Nelson, E.B., Michaux, M., Drochon, B., 2006. Cement additives and mechanism of action. In: second ed. In: Nelson, E.B., Guillot, D. (Eds.), Well Cementing, vol. 2006 Schlumberger, Sugar Land, Texas, USA.
Nelson, J.F., Jørpeland, J.-T., Schwartze, C., 2018. Case history: a new approach to section milling: leaving the swarf behind. In: Paper Presented at the Offshore Technology Conference, Houston, Texas, USA, 30 April – 3 May, OTC-28757.
Noik, C., Rivereau, A., 1999. Oilwell cement durability. In: Paper Presented at the SPE Annual Technical Conference and Exhibition Held in Houston, Texas, USA, 3-6 October, SPE-56538-MS.
NORSOK D-010, 2013. Well Integrity in Drilling and Well Operations Rev. 4. Lysaker: Standard Norge.
NPC, 2011. Plugging and Abandonment of Oil and Gas Wells. White Paper 2-25. Operations & Environmental task Group (Technology Subgroup), US DOE, Washington D.C 5 September.
Obodozie, I.E., Trahan, S.J., Joppe, L.C., 2016. Eliminating sustained casing pressure in well Abandonment. In: Paper Presented at the Offshore Technology Conference Asia, Kuala Lumpur, Malaysia, 22-25 March, OTC-26432.
Øia, T.M., Aarlott, M.M., Vrålstad, T., 2018. Innovative approaches for full subsea P&A create new opportunities and cost benefits. In: Paper Presented at the SPE Bergen One Day Seminar, Bergen, Norway, 18 April, SPE-191315-MS.
Oil & Gas UK, 2015BBa. Guidelines on Well Abandonment Cost Estimation, Issue 2, July 2015.
Oil & Gas UK, 2015BBb. Guidelines for the Abandonment of Wells, Issue 5, July 2015.
Oil & Gas UK, 2015BBc. Guidelines on Qualification of Materials for the Abandonment of Wells, Issue 2, July 2015.
Oil & Gas UK, 2016. Decommissioning Insight Report 2016. Oil & Gas UK.
Opedal, N., Corina, A.N., Vrålstad, T., 2018. Laboratory test on cement plug integrity. In: Paper OMAE2018-78347 Presented at the ASME 37th International Conference on Ocean, Offshore & Artic Engineering, June 17-22, Madrid, Spain.
Provis, J.L., van Deventer, J.S.J., 2009. Geopolymers: Structure, Processing, Properties and Industrial Applications, first ed. Published by Woodhead Publishing Limited and CRC Press LLC, Washington DC978-1-84569-638-2.
Rassenfoss, S., 2014. Permanently plugging deepwater wells challenges standard operating procedures. J. Petrol. Technol. 52–60 December 2014.
Rodriguez, F.J., Mat Isa, S., Forness, A., 2017. Field tests results for a subsea wireless annulus monitoring system. In: Paper Presented at the Offshore Technology Conference, Houston, Texas, USA, 1-4 May, OTC-27886.
Saasen, A., Salmelid, B., Blomberg, N., Hansen, K., Young, S.P., Justnes, H., 1994. The use of blast furnace slag in North Sea cementing applications. In: Paper Presented at the European Petroleum Conference Held in London, UK, 25-27 October, SPE-28821-MS.
Saasen, A., Godøy, R., Breivik, D.H., Solvang, S.A., Svindland, A., Gausel, E., Frøyland, K., 2004. Concentrated solid suspension as an alternative to cements for temporary abandonment applications in oil wells. In: Paper Presented at the SPE 2004 Technical Symposium, Dhahran, Saudi Arabia, 15-17 May, SPE SA-34.
Saasen, A., Wold, S., Ribesen, B.T., Tran, T.N., Huse, A., Rygg, V., Grannes, I., Svindland, A., 2011. Permanent abandonment of a North sea well using unconsolidated well plugging material. SPE Drill. Complet. 26, 371–375. https://doi.org/10.2118/133446-PA.
Saasen, A., Fjelde, K.K., Vrålstad, T., Raksagati, S., Moeinikia, F., 2013. Plug and abandonment of offshore exploration wells. In: Paper Presented at Offshore Technology Conference, Houston, Texas, 6–9 May, OTC-23909-MS.
Salehi, S., Khattak, M.J., Ali, N., 2016. Development of geopolymers-based cement slurries with enhanced thickening time, compressive strength and shear bond strength and durability. In: Paper Presented at IADC/SPE Drilling Conference and Exhibition, 1-3 March, Fort Worth, Texas, USA, IADC/SPE-178793-MS.
Salehi, S., Khattak, M.J., Ali, N., Ezeakacha, C., Saleh, F.K., 2017. Study and use of geopolymer mixtures for oil and gas cementing applications. J. Energy Resour. Technol. 140 (1) Paper no JERT-17-1290.
Sanabria, A.E., Knudsen, K., Leon, G.A., 2016. Thermal activated resin to repair casing leaks in the Middle East. In: Paper Presented at the Abu Dhabi International Petroleum Exhibition & Conference, Abu Dhabi, UAE, 7-10 November, SPE-182978-MS.
Scanlon, E., Garfield, G., Brobak, S., 2011. New technologies to enhance performance of section milling operations that reduces rig time for P&A campaign in Norway. In: Paper Presented at IADC/SPE Drilling Conference & Exhibition, Amsterdam, The Netherlands, 1-3 March, SPE-140277-MS.
Shadravan, A., Schubert, J., Amani, M., Teodoriu, C., 2015. Using fatigue-failure envelope for cement-sheath-integrity evaluation. SPE Drill. Complet. 30 (01) SPE-168321-PA.
Skorpa, R., Vrålstad, T., 2018. Visualization of fluid flow through cracks and microannuli in cement sheaths. SPE J. 23 (04) SPE-180019-PA.
Smith, I., Shu, D., 2013. A strategic shift in well abandonment services. Oil and Gas Facilities 19–21 February 2013.
Sørheim, O.I., Ribesen, B.T., Sivertsen, T.E., Saasen, A., Kanestrøm, Ø., 2011. Abandonment of offshore exploration wells using a vessel deployed system for cutting and retrieval of wellheads. In: Presented at the SPE Arctic and Extreme Environments Conference & Exhibition, Moscow, Russia, 18–20 October, SPE-148859-MS.

Stein, A., 2018. Verification of barriers in a suspension or abandonment phase. In: Paper Presented at the Offshore Technology Conference Asia, Kuala Lumpur, Malaysia, 20-23- March, OTC-28218.

Stokkeland, T.A., McNicol, J., McWilliam, G., 2017. Successful multi-well deployment of a new abandonment system for a major operator. In: Paper Presented at the SPE/IADC Drilling Conference and Exhibition, the Hague, Netherlands, 14-16 March, SPE/IADC-184716-MS.

Stowe, C., Ponder, A., 2011. Performance advance in section milling technology. In: Paper Presented at the SPE Annual Technical Conference and Exhibition, Denver, Colorado, USA, 30 October – 2 November, SPE-145957-MS.

Taghipour, A., Ytrehus, J.D., Stroisz, A., 2018. Casing Removal tests in laboratory setup. In: Paper OMAE2018-77875 Presented at the ASME 37th International Conference on Ocean, Offshore & Artic Engineering, June 17-22, Madrid, Spain.

Taylor, H.F.W., 1992. Cement Chemistry, 2nd printing. Academic Press, London, UK.

Therond, E., Bois, A.-P., Whaley, K., Murillo, R., 2017. Large-scale testing and modeling for cement zonal isolation in water-injection wells. SPE Drill. Complet. 32 (04) SPE-181428-PA.

Towler, B.F., Firouzi, M., Holl, H.-G., Gandhi, R., Thomas, A., 2016. Field trials of plugging oil and gas wells with hydrated bentonite. In: Paper Presented at the SPE Asia Pacific Oil & Gas Conference and Exhibition, 25-27 October, Perth, Australia, SPE-182199-MS.

Valdal, M.B.L., 2013. Plug and Abandonment Operations Performed Riserless Using a Light Well Intervention Vessel. Master thesis. University of Stavanger.

van der Kuip, M.D.C., Benedictus, T., Wildgust, N., Aiken, T., 2011. High-level integrity assessment of abandoned wells. Energy Procedia 4, 5320–5326.

van Eijden, J., Cornelissen, E., Ruckert, F., Wolterbeek, T., 2017. Development of experimental equipment and procedures to evaluate zonal isolation and well Abandonment materials. In: Paper Presented at SPE/IADC Drilling Conference and Exhibition, 14-16 March, the Hague, The Netherlands, SPE/IADC-184640-MS.

Varne, T., Jorgensen, E., Gjertsen, J., Osugo, L., Friedberg, R., Bjerkvik, O., Halvorsen, E.C., 2017a. Plug and abandonment campaigns from a riserless light well intervention vessel provide cost savings for subsea well Abandonments. In: Paper Presented at the SPE Bergen One Day Seminar, Bergen, Norway, 5 April, SPE-185891-MS.

Varne, T., Jorgensen, E., Gjertsen, J., Osugo, L., Friedberg, R., Halvorsen, E.C., 2017b. Sustained intervention campaigns over 10-year period with riserless light well intervention vessels enables North Sea operator to improve operational efficiency and increase recovery from its subsea fields. In: Paper Presented at the SPE Bergen One Day Seminar, Bergen, Norway, 5 April, SPE-185914-MS.

Vielstädte, L., Karstens, J., Haeckel, M., Schmidt, M., Linke, P., Reimann, S., Libetrau, V., McGinnis, D.F., Wallmann, K., 2015. Quantification of methane emissions at abandoned gas wells in the Central North Sea. Journal of Marine Petroleum Geology 68, 848–860.

Vignes, B., Aadnoy, B., 2010. Well integrity issues offshore Norway. SPE Prod. Oper. 25 (02) SPE-112535-PA.

Vrålstad, T., Skorpa, R., Opedal, N., De Andrade, J., 2015. Effect of thermal cycling on cement sheath integrity: realistic experimental tests and simulation of resulting leakages. In: Paper Presented at the SPE Thermal Well Integrity and Design Symposium, Alberta, Canada, November 23-25, SPE-178467-MS.

Vrålstad, T., Todorovic, J., Saasen, A., Godøy, R., 2016. Long-term integrity of well cements at downhole conditions. In: Paper Presented at SPE Bergen One Day Seminar, Bergen, Norway, 20 April, SPE-180058-MS.

Vrålstad, T., Skorpa, R., Saasen, A., 2018. Rheological properties of barite sediments in water-based drilling fluids. In: Paper OMAE2018-78695 Presented at the ASME 37th International Conference on Ocean, Offshore & Artic Engineering, June 17-22, Madrid, Spain.

Wang, H., Tao, G., Shang, X., 2016. Understanding acoustic methods for cement bond logging. J. Acoust. Soc. Am. 139 (5), 2407.

Watson, T.L., Bachu, S., 2009. Evaluation of the potential for gas and CO_2 leakage along wellbores. SPE Drilling Compl. (01), 24 SPE-106817-PA.

Williams, S., Carlsen, T., Constable, K., Guldahl, A., 2009. Identification and qualification of shale annular barriers using wireline logs during plug and abandonment operations. In: Paper Presented at the SPE/IADC Drilling Conference and Exhibition, 17-19 March, Amsterdam, The Netherlands, SPE/IADC-119321-MS.

Willson, S.M., Fossum, A.F., Fredrich, J.T., 2003. Assessment of salt loading on well casings. SPE Drill. Complet. 18 (01) SPE-81820-PA.

Zhang, M., Bachu, S., 2011. Review of integrity of existing wells in relation to CO_2 geological storage: what do we know? International Journal of Greenhouse Gas Control 5, 826–840.